

THE GLOBAL CLIMATE 2001 – 2010

A DECADE OF CLIMATE EXTREMES



**World
Meteorological
Organization**

Weather · Climate · Water

WMO-No. 1103

THE GLOBAL CLIMATE 2001–2010

A DECADE OF CLIMATE EXTREMES

WMO-No. 1103

© **World Meteorological Organization, 2013**

The right of publication in print, electronic and any other form and in any language is reserved by WMO. Short extracts from WMO publications may be reproduced without authorization, provided that the complete source is clearly indicated. Editorial correspondence and requests to publish, reproduce or translate this publication in part or in whole should be addressed to:

Chairperson, Publications Board
World Meteorological Organization (WMO)
7 bis, avenue de la Paix Tel.: +41 (0) 22 730 84 03
P.O. Box 2300 Fax: +41 (0) 22 730 80 40
CH-1211 Geneva 2, Switzerland E-mail: publications@wmo.int

ISBN 978-92-63-11103-6

Cover: Shutterstock.com

NOTE

The designations employed in WMO publications and the presentation of material in this publication do not imply the expression of any opinion whatsoever on the part of the Secretariat of WMO concerning the legal status of any country, territory, city or area, or of its authorities, or concerning the delimitation of its frontiers or boundaries.

Opinions expressed in WMO publications are those of the authors and do not necessarily reflect those of WMO. The mention of specific companies or products does not imply that they are endorsed or recommended by WMO in preference to others of a similar nature which are not mentioned or advertised.

The findings, interpretations and conclusions expressed in WMO publications with named authors are those of the authors alone and do not necessarily reflect those of WMO or its Members.

Contents

	<i>Page</i>
Foreword	6
Introduction	8
Chapter 1	10
1.1 Global temperature	
Feature article Assessment of global temperature based on reanalysis data	
1.2 Regional temperature	
1.3 Temperature assessment at country level	
1.3.1 General result	
1.3.2 Analysis by continent	
Chapter 2	18
2.1 Global precipitation	
2.2 Regional precipitation	
2.2.1 Decadal assessment summary	
2.2.2 Annual assessment summary	
Chapter 3	22
Large-scale climate variability modes and related oscillation indices	
Overview	
3.1 El Niño/Southern Oscillation	
3.2 Arctic Oscillation/North Atlantic Oscillation	
3.3 Indian Ocean Dipole	
3.4 Southern Annular Mode	
Chapter 4	27
4.1 Extreme events	
Impact assessment	
4.1.1 Data and methodology	
4.1.2 Comparison of 2001–2010 with 1991–2000	
4.1.3 Regional analysis	
4.1.4 Other aspects of impacts	
4.2 Exposure, vulnerability and attribution of climate extremes	32
4.2.1 Increased exposure and vulnerability to hydrometeorological events	
4.2.2 Attribution of climate extremes	
4.3 Summary statistics from country data	34
4.3.1 Most reported extreme events	
4.3.2 Country absolute records	
4.4 Worldwide summary of extreme climate conditions	37
4.4.1 Heatwaves and abnormally high temperature conditions	
Case study A1 Extreme heatwaves in Europe in 2003	
Case study A2 Extreme heatwave in the Russian Federation in 2010	
Case study A3 Exceptional heatwaves in Australia in 2009	
4.4.2 Cold waves, abnormally low temperature conditions and snowstorms	
Case Study B Extreme winter conditions over the northern hemisphere (2009/2010)	
4.4.3 Flooding and heavy precipitation	
Case study C The severe Pakistan flooding of 2010	

	<i>Page</i>
4.4.4 Droughts	
Case study D1 Long-term drought in Australia	
Case study D2 Long-term drought in the Amazon Basin	
Case study D3 Long-term drought in East Africa	
4.5 Severe storms	66
4.5.1 Tropical cyclones	
Case study E1 Hurricane <i>Katrina</i>	
Case study E2 Cyclone <i>Nargis</i>	
4.5.2 Extra-tropical cyclones and storms	
Case study F Extra-tropical windstorms in Europe	
Case study G Sand- and duststorms in the Arabian Peninsula	
4.5.3 Tornadoes	
Chapter 5	82
5.1 Climate and composition of the atmosphere	
Greenhouse gases and climate	
5.2 Stratospheric ozone depletion	
5.3 Climate and air quality	
Chapter 6	90
6.1 Cryosphere and sea level	
Cryosphere	
6.1.1 Sea ice	
6.1.2 Ice sheets	
6.1.3 Glaciers	
6.1.4 Snow cover	
6.1.5 Permafrost and frozen ground	
Feature article Effects of unseasonably mild conditions on the ice-road network and traditional lifestyles in northern Canada	
6.2 Sea level	
Conclusion	100
Acknowledgements	103
References and bibliography	104
Acronyms	108
Glossary	110
Annex 1. Source and methodology for global surface-temperature assessment	112
Annex 2. Country survey – general information	114
Annex 3. Country data submission to the WMO survey	115

Foreword

The goal of the WMO Climate System Monitoring is to deliver timely, authoritative information on the status of the atmosphere, ocean, cryosphere and biosphere at sub-monthly, monthly, annual and decadal to multi-decadal timescales. WMO Members have been collaborating on Climate System Monitoring over several decades to achieve improved monitoring and understanding of climate variability and climate change and related extreme weather and climate events.

Nowadays, with modern communication technology, WMO Members issue timely and regular reports on their websites, thus marking a fundamental shift in the way monitoring products are disseminated. These products have become crucial inputs to the various decision-making processes of user communities, in addition to their traditional scientific purpose.

Improved Climate System Monitoring today allows a quick analysis of monthly and seasonal climate drivers, such as El Niño/Southern Oscillation, the Arctic Oscillation and the North Atlantic Oscillation, among others. This information is increasingly being used to help foresee potential positive or negative impacts on sector activities such as agriculture, water resources, health, energy, tourism and fisheries.

In addition to the WMO Annual Statements on the Status of the Global Climate, which have been produced regularly since 1993, WMO produced, in 2003, a six-year climate review covering the period 1996–2001 with more comprehensive data and information. The main content of the review was based on the annual State of the Climate reports which are published by the National Oceanic and Atmospheric Administration-National Climatic Data Center of the United States of America in the Bulletin of the American Meteorological Society. In 2005, the WMO Commission for Climatology recommended discontinuing the multi-year climate review and agreed instead to publish a five-year climate summary to complement the WMO annual statements.

This publication covers the first decade of the 21st century and aims at providing a decadal perspective of climate variability and change and its observed impacts on different sectors.

The decade 2001–2010 was characterized by a record global temperature increase since sufficiently comprehensive global surface temperature measurements began in 1850. For global land-surface air temperatures, as well as for ocean-surface temperatures, this decade was the warmest on record.

Despite interannual variations in the global temperature, which are driven by large-scale variability in the ocean and the atmosphere, the underlying long-term trend is clearly an upward one.

Except for the year 2008, the nine remaining years of the decade, together with 1998, constitute the top 10 warmest years on record since 1850. The decade was also the warmest on land, over the oceans and in the northern and southern hemispheres when taken separately in the assessment.

Flooding was reported by the great majority of countries as the most significant extreme event they faced during the decade, followed by droughts, flash floods, heavy rainfall, heatwaves and severe storms. Twelve studies are provided in this report to illustrate a few of the most significant extreme weather and climate events which caused high human and economic losses.

Carbon-dioxide concentration had reached an average global value of 389 parts per million by the end of the decade, the highest value recorded for at least the past 10 000 years.

The dramatic and continuing sea-ice decline in the Arctic is one of the most prominent features of the changing state of the climate during the decade with the five lowest minimum sea-ice extents at the end of the melting season, all recorded in the second half of the decade, with the record being set in 2007.

I am confident that this publication will provide added value to the great collective efforts by Members to deliver useful climate services to governments, user communities, research, academia and the public at large.

I wish to thank all the Members that responded to the WMO survey with the aim of collecting climate data and information on the decade 2001–2010. I also extend WMO's thanks to the international centres which continuously maintain climate datasets to the highest possible scientific standards, as well as their useful global climate monitoring, the results of which are continuously updated on their websites.

Last but not least, I would like to thank the many experts from various nations and organizations and the UN partners that participated in the preparation of this publication.



(Michel Jarraud)
Secretary-General

Introduction

The international collaboration underpinning Climate System Monitoring (CSM) involves monitoring the present state of the global atmospheric, oceanic and terrestrial climate system. The monitoring covers many aspects of the atmospheric and ocean conditions, cryosphere, trace gases, etc. Data sources include in situ and space-based observations collected through various WMO and co-sponsored programmes and numerical objective analyses. These observations and analyses provide useful information for the interpretation of the present climate, including extreme events and long-term trends.

WMO CSM uses essential climate variables (ECVs) as defined by the Global Climate Observing System (GCOS). Some 50 ECVs have been identified as feasible for global observation. The present report incorporates assessments of the status of the global climate and the observed extremes detected using ECV data and products, including air temperature, precipitation, wind speed, greenhouse-gas concentration (atmospheric ECVs); snow cover, fire disturbance and river discharge (terrestrial ECVs); as well as sea ice, ice sheet and sea level (oceanographic ECVs).

Climate assessment on the decadal timescale offers the necessary data and information to enable robust understanding of the varying and changing climate and places climate monitoring in an extended historical time frame, such as is not possible with the annual climate monitoring. The Global Climate 2001–2010 is a new WMO publication summarizing the state of the climate for the decade 2001–2010 and its assessment in the historical context. It complements the annual WMO statements on the status of the global climate and the more comprehensive annual report State of the Climate, which is published regularly in the Bulletin of the American Meteorological Society (BAMS) by the National Oceanic and Atmospheric Administration-National Climate Data Center (NOAA-NCDC) of the United States of America (USA).

The data and information used in this publication are based on international datasets that are maintained by advanced climate data, monitoring and research centres which collaborate with WMO and the data and climate information collected directly from Member countries through a special WMO survey. The methodologies used for analysing the data and describing the results in various chapters were reviewed during a special two-day expert review meeting which was hosted by the University of Rovira i Virgili, Tortosa, Spain, 22-23 November 2011. Subsequent reviews were undertaken with other individual experts. Another review meeting focusing on impact data was undertaken with the participation of the Centre for Research on the Epidemiology of Disasters (CRED), the United Nations International Strategy for Disaster Risk Reduction (UNISDR) and the Food and Agriculture Organization of the United Nations (FAO) during a two-day expert meeting hosted by WMO in Geneva, Switzerland, 3–4 September 2012.

The first chapter focuses on surface temperature at global, regional and national scales, including analysis of temperature anomalies and trends. Interdecadal and interregional comparative analysis was performed and depicted using maps, charts and tables. The global temperature analysis is based on three international datasets maintained by the Met Office Hadley Centre and the Climatic Research Unit, University of East Anglia, in the United Kingdom (HadCRU); NOAA-NCDC; the National Aeronautics and Space Administration-Goddard Institute for Space Studies (NASA-GISS) in the USA and reanalysis data maintained by the European Centre for Medium-Range Weather Forecasts (ECMWF). The assessment of national temperature anomalies is based on the data collected directly from Members through the WMO survey. A descriptive

analysis was performed on data provided by the 139 countries which responded to the WMO survey.

The second chapter deals with precipitation. Global and decadal averages were used to depict general features decade by decade. A description of regional precipitation was also conducted with focus on the main anomaly features. Precipitation analysis is based on the NOAA-NCDC datasets and those of the Global Precipitation Climatology Centre (GPCC), Deutscher Wetterdienst (DWD), Germany. A global precipitation index provided by NOAA-NCDC based on global averaged precipitation analysis was used for performing an interdecadal comparison.

Chapter 3 describes the main atmospheric and oceanic oscillations which triggered major observed climate variability patterns on seasonal-to-interannual timescales, including El Niño/Southern Oscillation (ENSO), the Arctic Oscillation (AO), the North Atlantic Oscillation (NAO), the Indian Ocean Dipole (IOD) and the Southern Annular Mode (SAM). Analysis of indices pertaining to these oscillations is illustrated through time-series plots.

Chapter 4 focuses on extreme events. It starts with an impact assessment based on data provided by CRED, UNISDR, the United Nations Office for the Coordination of Humanitarian Affairs (OCHA), the Famine Early Warning System Network (FEWS-NET, US Agency for International Development) and Munich Reinsurance (MunichRe), as well as data collected by WMO from its Members and from available publications. It includes a section summarizing the occurrence in the past five decades of country absolute records of daily maximum and minimum temperature and 24-hour total precipitation. It also includes global maps referencing the location and timing of major heatwaves, cold waves, heavy precipitation, droughts and tropical cyclones, and a table describing the occurrence of major extreme events year by year. The second part of this chapter addresses severe storms, focusing mainly on tropical cyclones, with statistical data describing their occurrence at the decadal scale, globally and in the various ocean basins. A section on tornadoes in the USA is included, as well as 12 case studies focusing on some major observed extreme weather and climate events and the observed impacts on lives and goods.

Chapter 5 describes the connection between climate and atmosphere composition. The data used are provided by the measurement facilities of the WMO Global Atmosphere Watch (GAW).

Chapter 6 provides an analysis of the cryosphere and sea level. It describes the observed changes in these two critical components of the climate system, which are the most evident response variables to global warming. Trend analysis depicts the observed dramatic changes in Arctic sea ice, as well as the clear upward trend of sea level.

CHAPTER 1. TEMPERATURE ASSESSMENT

1.1 Global temperature

The decade 2001–2010 was the warmest decade since instrumental global average surface temperatures first became available in 1850 (Figure 1). Except for 2008, the remaining nine years of the decade were among the 10 warmest years on record, as warmer-than-average temperatures predominated across the globe. The global combined land air-surface and sea-surface mean temperature for 2001–2010 was estimated at $0.47^{\circ}\text{C} \pm 0.1^{\circ}\text{C}$ above the 1961–1990 average of 14.0°C . The mean global temperature of this decade has increased by 0.88°C since the first decade of the past century (1901–1910). The warmest year on record was 2010, closely followed by 2005, with a mean temperature anomaly estimated at $+0.54^{\circ}\text{C}$, and the least warm year was 2008, with an estimated anomaly of $+0.38^{\circ}\text{C}$ (Figure 2). While a trend is clearly confirmed at the decadal timescale, it is difficult to identify any clear trend within the decade due to the large interannual variability (Figure 2).

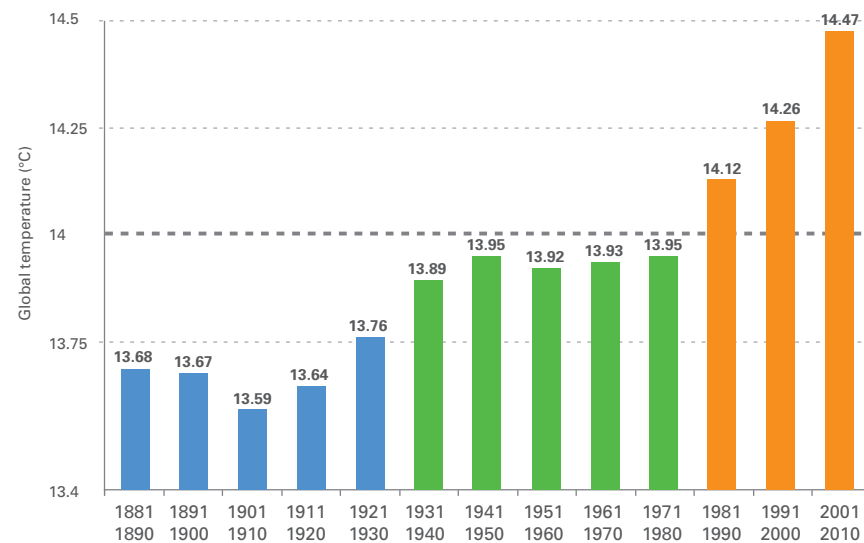


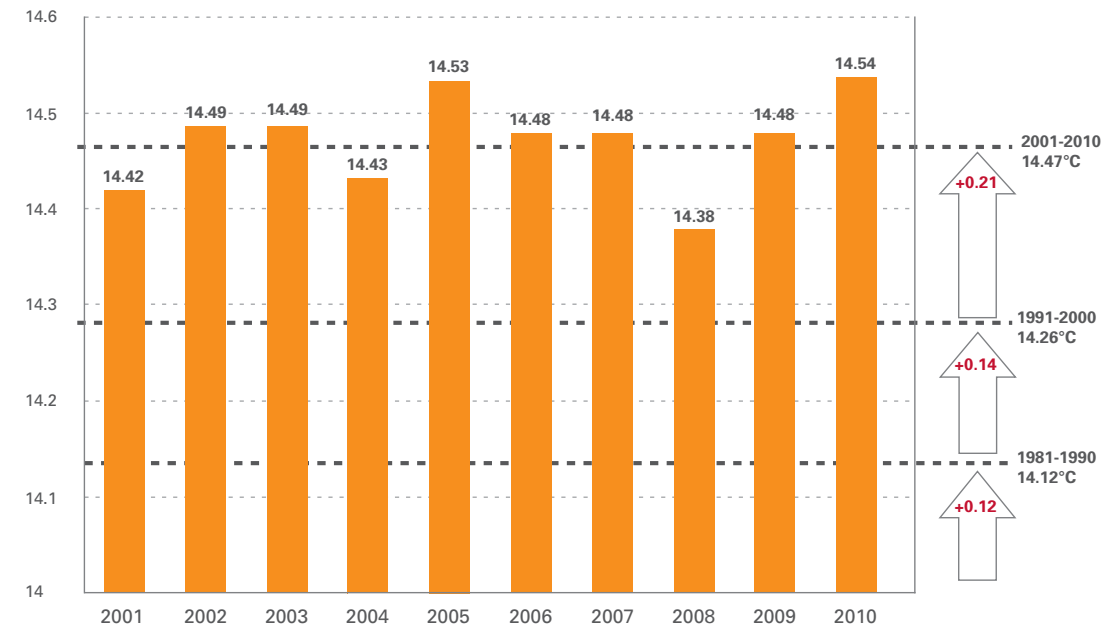
Figure 1. Decadal global combined surface-air temperature over land and sea-surface temperature ($^{\circ}\text{C}$) obtained from the average over the three independent datasets maintained by HadCRU, NOAA-NCDC and NASA-GISS. The horizontal grey line indicates the long-term average value (14.0°C) computed based on the 1961–1990 base period.

Note: The differences observed between the three datasets arise mainly from the way that the data are processed and the extent of extrapolation over data-sparse areas. Decadal averages are a more robust indicator of long-term change than annual values, avoiding uncertainties in individual annual values and short-term variability (for more information, see Annex 1).

Using reanalysis data covering the period 1979–2010, surface air-temperature anomalies computed using the reference period 1981–2010 (see feature article), show that the decade 2001–2010 exhibits the highest annual temperature anomaly values, except for the year 1998, which was characterized by a strong El Niño (Figures 4 and 5).

Figure 3 shows a sustained increase in the global temperature increase since the 1970s. In fact, the global temperature increased since 1971 at an average estimated rate of 0.17°C per decade compared with the average increase rate of 0.062°C per decade computed using linear fitting over the period 1880–2010. Furthermore, as can be deduced from Figure 2, the increase of 0.21°C in the average decadal temperature from 1991–2000 to 2001–2010 is larger than for any other two successive decades since the beginning of instrumental records.

The decade 2001–2010 was also the warmest on record for both land-only and ocean-only temperatures. The warmest year for worldwide land-only surface-air temperature was 2007, with a temperature anomaly of $+0.95^{\circ}\text{C}$ while, for the worldwide ocean-only surface temperature, the warmest year was 2003 with an anomaly of $+0.40^{\circ}\text{C}$ above the 1961–1990 average. Conversely, the least warm years during the decade 2001–2010 were 2004 and 2001 ($+0.68^{\circ}\text{C}$) for global land temperature and 2008 ($+0.26^{\circ}\text{C}$) for global ocean temperature.



The northern and southern hemispheres recorded their warmest decadal average land-surface air temperature on record with 0.90°C and 0.48°C above the 1961–1990 average, respectively (see Table 1). The northern hemisphere recorded its warmest year in 2007 with an anomaly of $+1.13^{\circ}\text{C}$, becoming the warmest year on record. Meanwhile, the least warm year during 2001–2010 was 2004, with an anomaly of $+0.76^{\circ}\text{C}$.

In the southern hemisphere, the warmest year over the land surface was 2005, with a mean air temperature of $+0.67^{\circ}\text{C}$ above the 1961–1990 average. The least warm year of the decade was 2001 with a temperature anomaly of $+0.34^{\circ}\text{C}$.

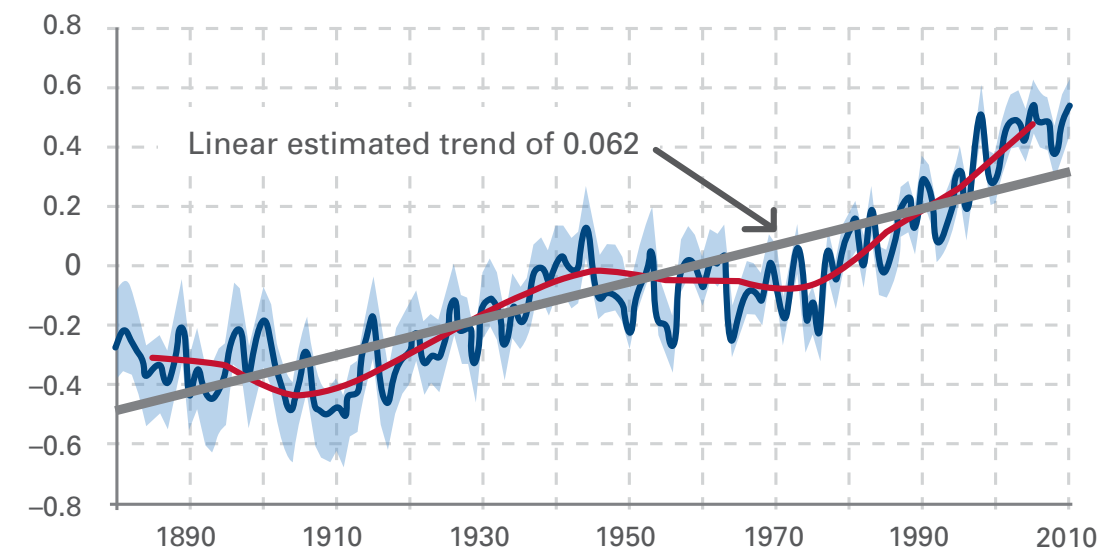


Figure 2. Annual global combined surface air temperature over land and sea-surface temperature ($^{\circ}\text{C}$) obtained from the average over the three datasets. Black horizontal lines refer to the decadal average temperature of the previous decades 1981–1990, 1991–2000 and 2001–2010. On the right, the values inside the two upper vertical arrows indicate departure of the decadal value from its counterpart in the previous decade. The value in the lower arrow is the temperature anomaly value of 1981–1990 with respect to the long-term average of 1961–1990 base period (data source: HadCRU, NOAA-NCDC and NASA-GISS).

Figure 3. Decadal global (red) combined surface air-temperature anomaly (computed using 1961–1990 base period) over land and sea and linear fitted trend (grey) over the whole period 1880–2010 and annual (dark blue) combined surface air-temperature anomaly over land and sea linear with the light blue area representing 95 percent uncertainty range (data source: HadCRU)

Table 1. Surface temperature anomalies with respect to 1961–1990 over the globe, northern hemisphere and southern hemispheres for 2001–2010 (A), annual extreme values for 2001–2010 (B) and decadal extreme values for 1881–2010 (C) (data source: UK Met Office and NOAA for global analysis combined; NOAA-NCDC for the northern and southern hemispheres)

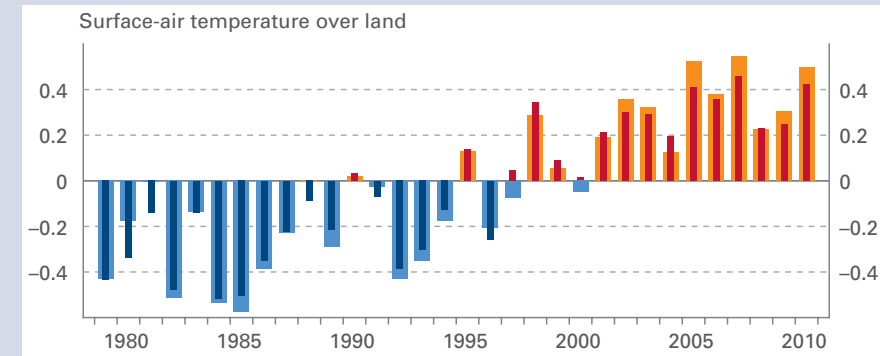
Domain		Temperature anomaly (°C)		
		2001–2010 (A)	Warmest/least warm year during 2001–2010 (B)	Warmest/coldest decade on record (C)
Global	Land	+0.79°C	2007 (+0.95°C) 2001 and 2004 (+0.68°C)	2001–2010 (+0.79°C) 1881–1890 (-0.51°C)
	Ocean	+0.35°C	2003 (+0.40°C) 2008 (+0.26°C)	2001–2010 (+0.35°C) 1901–1910 (-0.45°C)
	Land-ocean	+0.47°C	2010 (+0.54°C) 2008 (+0.35°C)	2001–2010 (+0.47°C) 1901–1910 (-0.45°C)
Northern hemisphere	Land	+0.90°C	2007 (+1.13°C) 2004 (+0.76°C)	2001–2010 (+0.90°C) 1881–1890 (-0.52°C)
	Ocean	+0.41°C	2005 (+0.47°C) 2008 (+0.33°C)	2001–2010 (+0.41°C) 1901–1910 (-0.39°C)
	Land-ocean	+0.60°C	2010 (+0.69°C) 2008 (+0.53°C)	2001–2010 (+0.60°C) 1901–1910 (-0.38°C)
Southern hemisphere	Land	+0.48°C	2005 (+0.67°C) 2001 (+0.34°C)	2001–2010 (+0.48°C) 1901–1910 (-0.53°C)
	Ocean	+0.29°C	2002 (+0.34°C) 2008 (+0.20°C)	2001–2010 (+0.29°C) 1901–1910 (-0.51°C)
	Land-ocean	+0.33°C	2009 (+0.38°C) 2008 (+0.24°C)	2001–2010 (+0.33°C) 1901–1910 (-0.51°C)

Assessment of global temperature based on reanalysis data

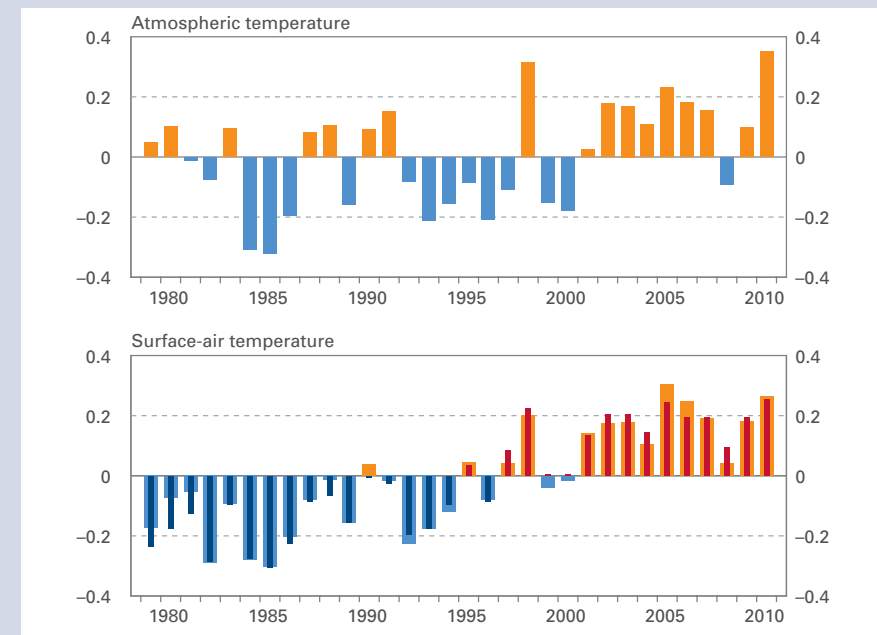
Reanalysis of past observations using the data-assimilation approach of modern weather-prediction systems complements the traditional climatological approach to estimating global climate variability and change. It confirms the warmth of the decade 2001–2010, provides further indications of the uncertainties inherent in the various global datasets and places warming at the Earth's surface in the context of change in the atmosphere and ocean as a whole.

The global reanalyses carried out by ECMWF and the Japan Meteorological Agency (JMA) estimate surface air temperature over land from synoptic surface observations of temperature made several times each day, using background information from processing many other types of surface and upper-air observation. This differs from the approach that forms the basis for figures presented elsewhere in this chapter, which uses carefully assembled but fewer monthly climatological temperature records over land. The two approaches are nevertheless in close agreement. In Figure 4, the small differences between the two estimates are known to be due mainly to differences in spatial sampling, with reanalysis detecting more warming due to its complete coverage of high northern latitudes where warming has been greatest. It shows more warming than the earlier figures for global temperature because warming over land has, in general, been greater than warming over sea since the late 1980s.

Comprehensive data from satellites, balloons and aircraft enable a quite complete picture to be built up of temperature variations throughout the troposphere and stratosphere over the past three decades, with highest reliability for the most recent years when observational quality and quantity are generally at their best. The reanalysis estimate of average atmospheric temperature (Figure 5) shows greater variability from year to



year than occurs at the surface. This is largely because variations in tropical sea-surface temperature lead to intermittent warming or cooling of a particularly deep layer of the atmosphere. 2010 stands out as the warmest year of the decade for the atmosphere as a whole, matching and probably exceeding 1998, when there was an unusually strong shift from El Niño to La Niña conditions. At the surface, the reanalysis identifies 2005 as globally warmer than 2010, but significance should not be attached to the difference in ranking compared to the combined dataset because of the small temperature difference.



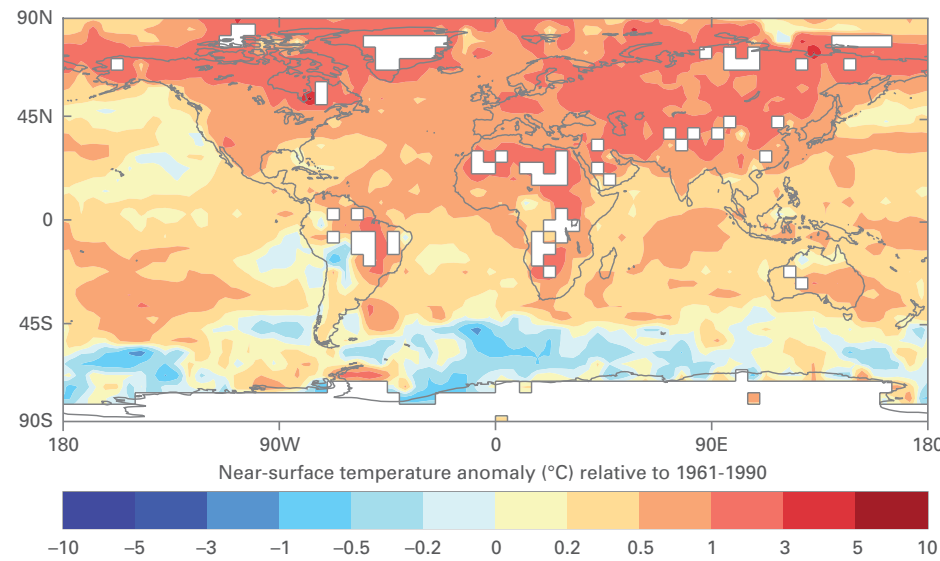
Estimating the multi-decadal state of the ocean using data assimilation is emerging as a valuable tool for documenting and understanding the heat content of the upper ocean and the transfer of heat to the deeper ocean. Improvement in ocean observation, in particular the establishment during the decade 2001–2010 of a network of more than 3 000 drifting Argo floats that regularly profile the upper 2 000 m of the ocean, has been a key factor in reducing uncertainty in ocean reanalyses. Variability in the ocean is influenced by and is an influence on atmospheric variability, and development of coupled systems has become a priority for advancing global reanalysis. Parallel developments are coupling atmosphere with land and incorporating key trace species and their chemical interactions. This is paving the way to comprehensive analysis and reanalysis of the climate system, to enhanced monitoring, support for model development and starting points for predictions.

Figure 4. Annual global anomaly with reference to 1981–2010 for surface air temperature over land (°C) from the ERA-Interim reanalysis (broader, lighter coloured bars) (source: ECMWF) and CRUTEM4 (narrower, darker coloured bars) (source: CRU)

Figure 5. Annual global temperature anomaly with reference to 1981–2010 (°C), for the atmosphere as a whole from the ERA-Interim reanalysis and for surface air from both ERA-Interim (broader, lighter coloured bars) (source: ECMWF) and the combined dataset (narrower, darker coloured bars) (source: HadCRU, NASA-GISS, NOAA-NCDC). The average for the atmosphere as a whole is mass-weighted and in essence proportional to the thermal energy of the atmosphere.

1.2 Regional temperature

Above-average temperatures were observed over most parts of the globe during the decade (Figure 6). The largest anomalies were recorded in the northern hemisphere over land and ocean areas. Continental average temperatures were above the 1961–1990 normal in every year of the decade for every continent, except for Australia in 2001. Most parts of Canada, Alaska (USA), Greenland, Asia and northern Africa recorded temperature anomalies for the decade ranging between 1°C and 3°C above the long-term average (Figure 6). In the southern hemisphere, the most remarkable positive anomalies over land areas were observed over north-eastern South America, parts of central and southern Africa and the interior of Australia. The only extended part of the globe where below-normal temperatures were recorded was in the southern hemisphere over the ocean and south of 45°S latitude (Figure 6).



Between 2001 and 2009, above-normal temperatures were remarkably predominant over Europe with 2007 being the warmest year on record for large parts of the region. The exception to this pattern was 2010, when normal to below-normal annual temperatures were recorded in some parts of central and northern Europe. The normal to below-normal temperatures were mainly due to the extreme cold conditions experienced at the beginning and end of the year. Europe as a whole was still warmer than normal in 2010, however, driven largely by conditions in the Mediterranean and Russian Federation.

Most parts of Asia also broke annual historic record highs in 2007. By contrast, in the same year, southern and western South America was the only extended land-surface region to record below-normal temperatures, due mostly to the extreme cold winter conditions. Africa, Canada and Greenland experienced warmer-than-normal conditions in every year of the decade; 2010 was exceptionally warm across most parts of these regions with records broken by nearly +1°C in some places.

Ocean-surface temperatures, as well as the combined land-ocean surface temperatures, reached their lowest value of the decade in 2008, due mostly to the moderate-to-strong La Niña event which lasted from the second half of 2007 until the beginning of 2009.

Figure 6. Global combined surface air temperature over land and sea-surface temperature anomaly (°C) for 2001–2010, relative to 1961–1990 base period. Grid areas without sufficient data are left blank (source: HadCRU).

Continental area	Warmest year (anomaly)	Least warm year (anomaly)
Globe	2010 (+0.53°C)	2008 (+0.38°C)
Europe	2007 (+1.42°C)	2010 (+0.68°C)
Asia	2007 (+1.39°C)	2009 (+0.73°C)
Africa	2010 (+1.29°C)	2001 (+0.66°C)
North America	2006 (+1.09°C)	2008 (+0.16°C)
South America	2005 (+0.49°C)	2007 (+0.17°C)
Australia	2005 (+1.06°C)	2001 (-0.13°C)
Antarctic	2007 (+0.81°C)	2005 (+0.27°C)

Despite the cooling effects of La Niña, Figure 7 shows that global temperature kept increasing with 2008 being the warmest La Niña year on record. On the other hand, it shows the influence of El Niño in exacerbating global positive temperature anomalies. This indicates that, despite interannual variations in the global temperature, which are driven by large-scale interannual variability in the ocean and the atmosphere, the underlying long-term trend is clearly in the upward direction, despite the cooling of La Niña, for instance.

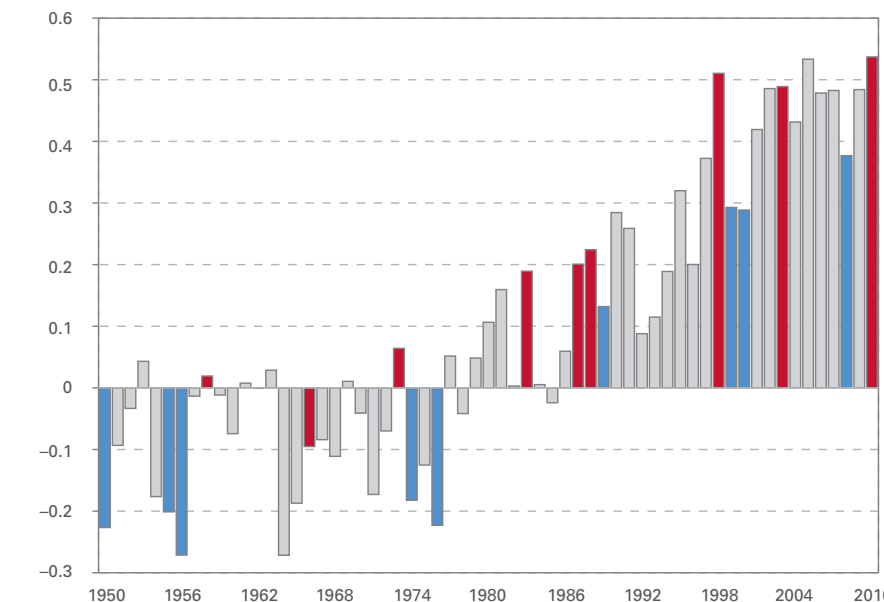


Table 2. Warmest and coldest years of the decade for global and continental areas (data source: HadCRU)

Figure 7. Annual global surface temperature anomaly for 1950–2010 with reference to 1961–1990 base period, indicating years with La Niña events (blue) and years with El Niño events (red) (data source: HadCRU, NOAA-NCDC and NASA-GISS)

1.3 Temperature assessment at country level

1.3.1 General result

Temperature assessment at country level was based on countries' climate data and information collected by WMO through a special survey (see Annex 2).

The survey collected information on country-wide temperature anomalies (based on stations' temperature data on a yearly basis and averaged over the decades), information indicating national absolute records for daily maximum temperature, daily minimum temperature and 24-hour total precipitation, as well as information describing the most significant extreme weather and climate events observed during the decade 2001–2010.

The number of countries providing decadal temperature anomaly data for the last decade in the survey (118) was slightly below the total number of 139 countries which participated in the survey. Out of 118 countries, 109 provided data for at least the last three decades. The statistical analysis shown below is therefore based on the actual data sample.

Out of the 118 countries that reported temperature anomalies for 2001–2010 with respect to 1961–1990, 55 countries (47 per cent) had a decadal national average temperature ranging between +0.51 and +1°C above normal. An anomaly of +0.51°C or higher was reported by 94 countries (80 per cent) and an anomaly higher than +1°C was reported by 39 countries (33 per cent); large countries – in terms of surface area – such as Canada, China, Denmark (including Greenland), the Russian Federation, and most of the rest of Europe are part of this last category. The warmest decade for 103 out of 110 countries (nearly 94 per cent) was 2001–2010. The warmest decade for the large countries listed above was also 2001–2010.

Greenland temperature anomaly	
Year	Anomaly (with reference to 1961–1990 base period)
2001	+1.03
2002	+1.46
2003	+2.29
2004	+1.51
2005	+2.35
2006	+1.41
2007	+1.53
2008	+1.11
2009	+1.18
2010	+3.20
2001–2010	+1.71

The rate of increase was particularly high in the northern latitudes of the northern hemisphere. Greenland recorded the largest decadal mean temperature anomaly of +1.71°C, with the warming being particularly pronounced during the warmest year, 2010, with a temperature anomaly of +3.2°C.

Consistent with the clear warming trend observed globally, the number of countries reporting decadal negative temperature anomalies decreased with time until they ceased in the last decade. For instance, 15 per cent of the countries reported a negative anomaly in the decade 1981–1990; only 6 per cent reported a negative anomaly in 1991–2000; and no country reported any negative anomaly in 2001–2010.

1.3.2 Analysis by continent

The analysis based on the WMO survey was also grouped by continent. The results are summarized in the following key features:

- Europe shows a steady temperature increase with consistently positive temperature anomalies during the last two decades. Europe’s median temperature anomaly of +1.0°C for the decade is higher than the whole dataset median value (+0.85°C);

- In Asia, a consistent temperature increase was recorded, with dominating positive decadal temperature anomalies. The median value of the country decadal temperature anomalies in Asia was +0.84°C, slightly less than the whole dataset median value (+0.85°C). The Russian Federation, China, Mongolia and the Islamic Republic of Iran, constituting a greater portion of Asia surface area, each had a temperature anomaly exceeding +1°C;
- In Africa, the majority of the country anomalies of the last three decades were positive. The median anomaly value of +0.7°C for the decade 2001–2010 was slightly less than the median for the whole country dataset median value (+0.85°C). Most African countries north of the Equator have the highest temperature anomalies of the continent. Several countries in this part of Africa recorded temperature anomalies either close to or exceeding +1°C. Burkina Faso, Chad, Morocco, Niger and Tunisia exceeded the +1°C temperature anomaly. South of the Equator, Angola, Botswana, Madagascar, Namibia, South Africa and Zimbabwe showed temperature anomalies exceeding 0.5°C, with values close to +1°C for Angola and Namibia.
- In South America, the same warming trend for the decadal temperature was clear in the data sample. The median value of the temperature anomalies started to turn positive in 1981–1990 and reached +0.60°C in the decade 2001–2010. Brazil, the largest country of the region, had the highest temperature anomaly value of +0.74 °C, with the decade as the warmest on record;
- In North and Central America, positive decadal anomalies were reported for the last three decades. During 2001–2010, Canada and the contiguous USA and Alaska, constituting the largest land mass of the region, recorded a temperature anomaly greater than +0.5°C. Canada recorded the highest anomaly value in this region with +1.3 °C anomaly and 2001-2010 as the warmest decade.
- In Oceania, Australia, French Polynesia, New Caledonia, New Zealand and Tonga – which participated in the WMO survey – reported positive temperature anomalies at least in the last two decades with a median value of +0.34°C for the last decade. The warmest decade for Australia, the largest country of the region, was 2001–2010, with an anomaly value of +0.48°C.

Table 3. Greenland temperature anomaly (data source: Danish Meteorological Institute)

CHAPTER 2. PRECIPITATION ASSESSMENT

2.1 Global precipitation

Global land surface precipitation averaged over 2001–2010 (Figure 8) was above the 1961–1990 average. According to this analysis, 2001–2010 was the first decade to record above-global-average precipitation since 1971–1980, a decade which came at the end of the only 30-year period with precipitation consistently above the 1961–1990 average. Within the decade 2001–2010 (Figure 9), only three years experienced less-than-global average precipitation (2001, 2002 and 2009), while the other years recorded above-average values, with the exception of 2003, which recorded a near-average value. Globally, 2010 was the wettest year on record, not only for the decade but also for all time. The previous highest values were recorded in 1956 and 2000, coinciding with strong La Niña events. On the other hand, 2002 had the least average global precipitation in the decade but was well short of the lowest recorded values in 1902 and, more recently, in 1992.

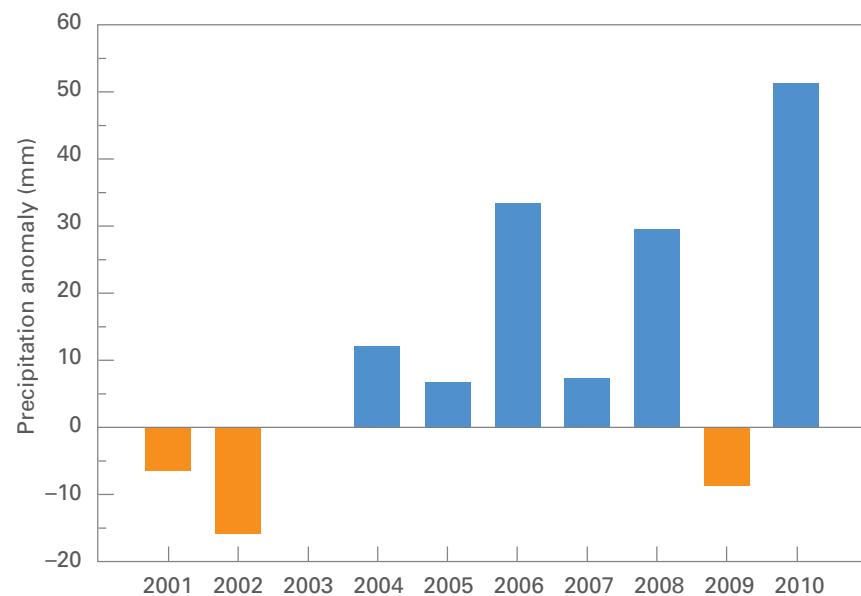
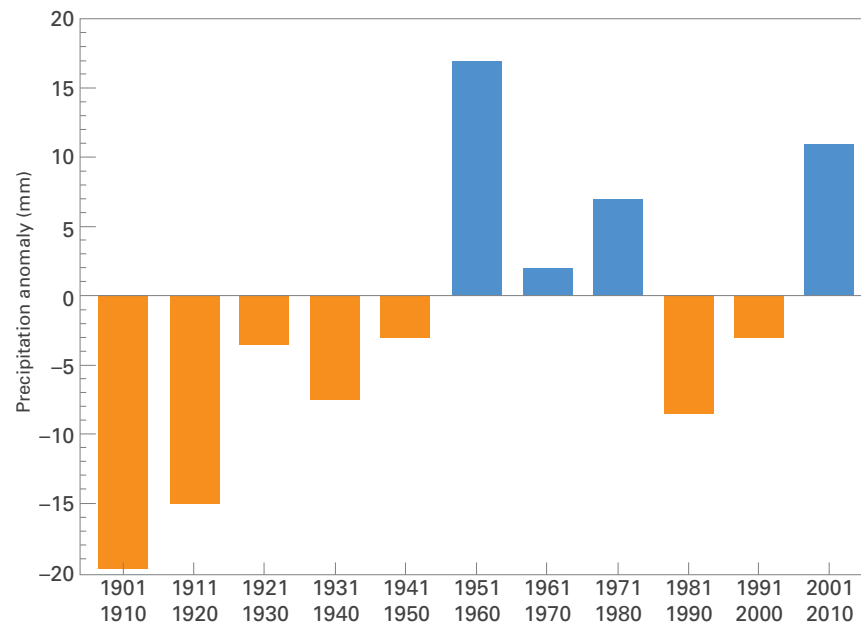


Figure 8. Decadal global precipitation anomalies (mm) relative to the 1961–1990 WMO standard normal (source: NOAA-NCDC)

Figure 9. Annual global precipitation anomalies (mm) relative to the 1961–1990 WMO standard normal (source: NOAA-NCDC)

The assessment of global average precipitation anomalies is the simplest means for global precipitation analysis. By whichever global precipitation pattern (above or below average) the year is classified, numerous weather and climate extremes related to precipitation affected almost every part of the globe on a yearly basis due to the interannual variability in various regions as summarized in the following section.

2.2 Regional precipitation

2.2.1 Decadal assessment summary

The decade 2001–2010 was characterized by above-normal precipitation across most parts of the globe (Figure 10). Large parts of the northern hemisphere recorded wetter-than-average conditions. The eastern USA, northern and eastern Canada and many parts of Europe and central Asia were particularly wet. In South America, Colombia, parts of northern and southern Brazil, Uruguay and north-eastern Argentina experienced wetter-than-average conditions. Most parts of southern Africa, Indonesia and northern Australia also recorded, on average, above-normal precipitation. In contrast, other regions experienced, on average, below-normal precipitation. Western USA, south-western Canada, Alaska, most parts of southern and western Europe, most parts of southern Asia, central Africa, central South America, and eastern and south-eastern Australia were the most affected.

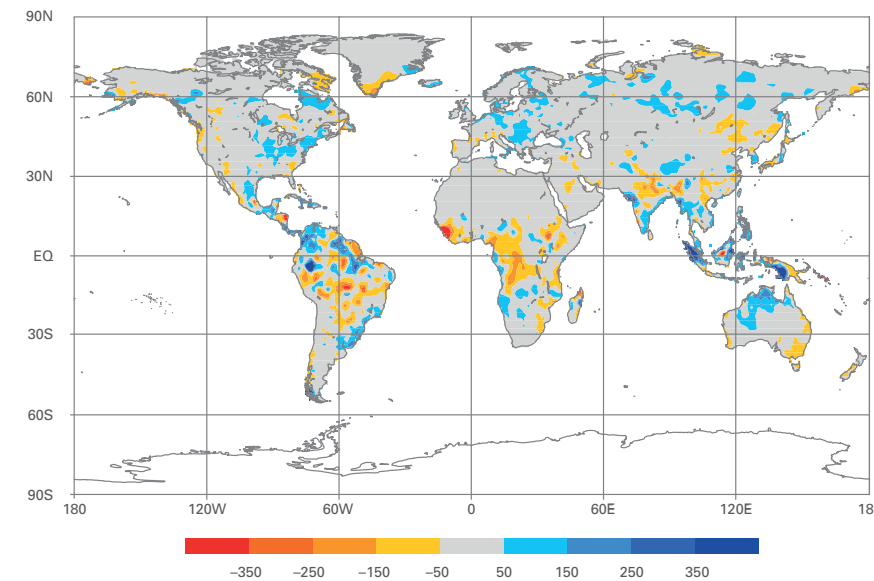


Figure 10. Decadal precipitation anomalies for global land areas for 2001–2010; gridded 1° raingauge-based analysis as normalized departures in mm/year from averages computed using 1951–2000 base period (source: GPCP-DWD)

2.2.2 Annual assessment summary

During 2001, most southern hemisphere land areas experienced above-average precipitation. Southern South America, South Africa and central and western Australia were the most affected regions. In contrast, large parts of the northern hemisphere recorded below-normal precipitation, such as northern Africa and the Arabian Peninsula, large parts of central and southern Asia, southern Europe and western North America.

In 2002, southern South America continued in a wetter-than-normal pattern, while parts of South Africa and Australia recorded significantly drier conditions than in the previous year. Most parts of central Europe recorded above-average precipitation, as did central

Asia. On the other hand, large parts of south-western Asia and the Arabian Peninsula were affected by a drier-than-normal year. As previously stated, the year 2002 was, on average, the driest year of the decade.

Wetter-than-normal conditions predominated in West Africa and most parts of Asia during 2003 but, in large parts of South Africa, southern and western North America and central Europe, below-normal precipitation was observed.

In 2004, wetter-than-normal conditions were predominant across the globe, especially in southern and eastern South America, western and northern Australia, the Greater Horn of Africa region, northern North America and Greenland.

In 2005, western Europe was affected by dry conditions, as were parts of central Africa, East Africa and eastern Australia. On the other hand, south-eastern Europe, central and northern North America, eastern South America, northern Africa, the Arabian Peninsula and southern Asia recorded above-normal precipitation.

Most parts of the African continent recorded a wetter-than-normal 2006. Central and south-eastern parts of Australia were affected by drier-than-normal conditions, but the northern and western areas presented the opposite pattern, together with Indonesia and southern Asia. Greenland and northern Canada also experienced above-average annual precipitation.

In 2007, large parts of Europe and Asia recorded above-normal precipitation. This pattern extended to the Pacific islands and northern Australia. Below-normal precipitation was also observed in parts of eastern and southern South America, south-western and south-eastern North America and across the Arabian Peninsula.

South-eastern South America experienced a dry 2008, as did the Arabian Peninsula and south-western Australia. Conversely, precipitation was well above normal in some regions, including northern Australia, the Pacific islands and southern Asia. Northern South America, Central America and eastern North America also recorded above-normal precipitation.

In 2009, central and southern Australia recorded below-normal precipitation, as did

large parts of southern South America, south-western North America, Greenland and some parts of central Asia. In contrast, north-western and southern Africa, most parts of central and north-eastern South America and south-eastern North America experienced above-average precipitation.

The year 2010 was the wettest on record globally (Figure 11). Only a few regions experienced significantly below-normal precipitation: parts of Greenland, south-western Western Australia, some parts of central and southern South America and south-western Asia. Most parts of central, northern and eastern Australia, southern and eastern Asia, north-western South America, Central America, most parts of North America, western Africa (including the Sahel) and central and southern Europe were affected by above-normal precipitation in 2010.

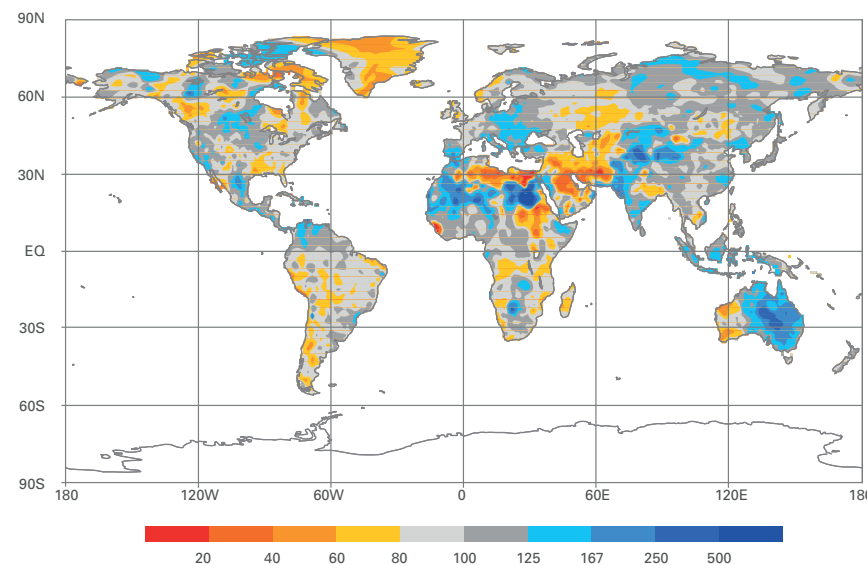


Figure 11. 2010 precipitation anomalies over land areas: gridded 1° raingauge-based analysis as percentage of normal computed using 1951–2000 base period (source: GPCC-DWD)

CHAPTER 3. LARGE-SCALE CLIMATE VARIABILITY MODES AND RELATED OSCILLATION INDICES

Overview

Natural climate variability operates on multiple scales at all times and can affect global and regional atmospheric and oceanic circulations. Many of these variations are recurrent and are usually recognized as well-known climatic patterns, such as warming or cooling of sea-surface temperature (SST) in the tropical oceans, ENSO, NAO, the Madden-Julian Oscillation and the strengthening or weakening of the upper-level jets, and are often characterized in terms of climate indices (for example, ENSO or NAO indices). These indices can correlate significantly with regional climate anomalies at monthly, seasonal and interannual timescales. In fact, some of these indices provide good indicators of a possible onset of many extreme weather and climate events which have direct or indirect impacts on human life, goods, property and the well-being of societies. Droughts, heatwaves, cold waves, flooding, extreme windstorms, landslides, bush and forest fires and coastal erosion are just a few of the impacts that can be triggered by one or more such anomalies (Climate Sense, WMO 2009).

3.1 El Niño/Southern Oscillation

El Niño/Southern Oscillation is a quasi-periodic climate pattern that occurs across the tropical Pacific Ocean. It is characterized by variations in the temperature of the surface of the tropical eastern Pacific Ocean – warming or cooling known as El Niño and La Niña, respectively – and in the air-surface pressure in the tropical western Pacific – the Southern Oscillation. The two variations are coupled: the warm oceanic phase, El Niño, accompanies high air-surface pressure in the western Pacific, while the cold phase, La Niña, accompanies low air-surface pressure in the western Pacific. El Niño and La Niña phases each occur two to three times a decade on average, but the period between individual events is highly variable. There are also periods of a decade or more where one phase is dominant; for example, the 1950s and 1970s saw numerous La Niña events and few El Niño events, whereas El Niño predominated over La Niña for most of the 1980s and 1990s.

ENSO influences climate in a wide range of ways over large parts of the world. El Niño is associated with a high risk of drier-than-normal conditions in areas such as the eastern half of Australia, the Indonesian region, India, southern Africa, the Caribbean and north-eastern Brazil. Conversely, El Niño years tend to be wetter than normal on the west coast of South America, north-eastern Argentina and Uruguay, equatorial east Africa, the islands of the central tropical Pacific and the southern USA. They are also associated with above-normal temperatures over much of South-East Asia, and, in winter, north-western North America and the north-eastern USA. El Niño also influences tropical cyclone formation. Moreover, there is a marked tendency for global temperatures to be higher than the preceding and following years when El Niño conditions are in place at the start of the year.

In general, the effects of La Niña are the reverse of those of El Niño: for example, an increased risk of heavy rain and flooding in Australia, the Indian subcontinent and southern Africa, and an increased risk of drought in the southern USA. La Niña years are typically relatively cool on the global scale.

A number of indicators are used to monitor ENSO. The most common are the Niño 3 and Niño 3.4 indices, an average of SST anomalies over the eastern and east-central equatorial Pacific respectively, and the Southern Oscillation Index (SOI) – an index of air-

pressure differences between Darwin (Australia) and Tahiti. The oceanic indices are more stable but only extend back to 1950, whereas SOI data have been available since 1876.

The long-running La Niña episode that began in mid-1998 ended in early 2001. Assessing ENSO variability during the decade 2001–2010, Figure 12 illustrates a new episode of El Niño which developed in 2002 and lasted throughout the first half of 2003. Neutral conditions then prevailed for most of the next three years until mid-2006, although conditions approached marginal El Niño conditions in late 2004 and early 2005 (which were recognized as a weak El Niño by some agencies) and La Niña thresholds were approached in early 2006.

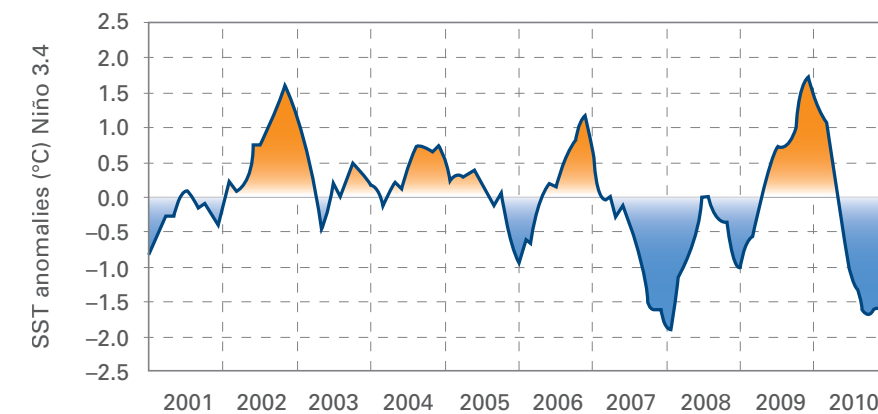


Figure 12. Monthly time series of area-averaged SST anomaly (°C) in the El Niño region 3.4 (5°N–5°S; 170°W–120°W) for 2001–2010 with respect to the 1971–2000 base period (data source: CPC/National Center for Environmental Prediction (NCEP), NOAA)

A moderate El Niño event developed in the second half of 2006, but quickly dissipated in January 2007. La Niña conditions then became well-established across the central and eastern equatorial Pacific in the latter half of 2007. This event peaked in February 2008 as an event of moderate to strong intensity. The event weakened through the first half of 2008 but then showed some redevelopment, approaching marginal La Niña thresholds in late 2008 and early 2009.

A new El Niño event started in June 2009. It rapidly intensified to moderate levels during October, reaching the peak of the mature phase in December. In the middle months of 2010, a new La Niña episode quickly developed, following the dissipation of the 2009/2010 El Niño in April. The event was moderate to strong from August onwards and became, by some measures, the strongest since at least the mid-1970s. The atmospheric response was especially strong, with the SOI reaching its highest monthly values since 1973 in September 2010 (25.0) and December 2010 (27.1), while its six-month mean from September 2010 to February 2011 was the highest since 1917. This La Niña event was near its peak at the end of 2010 and declined during the early months of 2011.

3.2 Arctic Oscillation/North Atlantic Oscillation

The Arctic Oscillation and North Atlantic Oscillation are two closely related modes of variability in the atmospheric circulation at middle and higher latitudes of the northern hemisphere. In the positive mode, the subtropical high-pressure ridge is stronger than normal, as there are areas of low pressure at higher latitudes (such as the “Icelandic” and “Aleutian” lows), resulting in enhanced westerly circulation through mid-latitudes. In the negative mode, the reverse is true, with a weakened subtropical ridge, weakened higher-latitude low-pressure areas and anomalous easterly flow through the mid-latitudes. As

the name implies, NAO describes this mode of variability over the North Atlantic sector only; AO describes the mode over the entire northern hemisphere.

The principal effects of AO and NAO on climate occur in the colder months. When these oscillations are in their positive mode, there tend to be more numerous and stronger storms over the North Atlantic. This results typically in warmer and wetter winters in northern and central Europe and the eastern USA, drier winters in the Mediterranean and cold, dry conditions over northern Canada and Greenland. These relationships are reversed in negative mode; in particular, negative modes of NAO are strongly associated with below-average winter temperatures in northern and central Europe.

A number of indices exist to describe NAO and AO. The longest-running indices of NAO, with records dating back to about 1860, are based on differences in mean sea-level pressure between mid-latitude and subtropical latitudes in the North Atlantic sector. More recently, indices of both NAO and AO have been developed which use principal component analysis to characterize pressure patterns throughout the full North Atlantic sector (for NAO) or full northern hemisphere (for AO).

According to the series of these atmospheric circulation indices, a positive phase has generally predominated since the 1990s (Figure 13). In the winter of 2009/2010, however, extremely strong negative phases of both NAO and AO occurred, reaching record or near-record levels. This winter was cooler than average in northern Europe and the south-eastern USA. Greenland and parts of northern Canada were exceptionally warm. This temperature pattern was strongly influenced by AO and NAO.

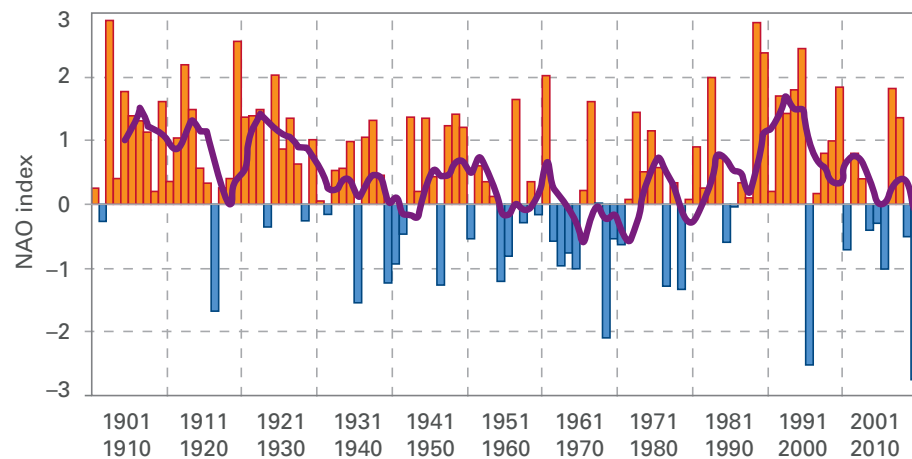


Figure 13. December–January–February–March NAO index from 1901 to 2010: the index is calculated as a difference between normalized sea-level pressure over Gibraltar and normalized sea-level pressure over south-western Iceland. The smooth purple curve is a five-year filtered average (data source: CRU).

The northern hemisphere winters of 2001/2002, 2006/2007 and 2007/2008, however, showed strong positive modes of AO and NAO. The most strongly positive modes of AO and NAO during this decade were recorded in 2007, a year with record warmth in large parts of Europe and Asia.

3.3 Indian Ocean Dipole

The Indian Ocean Dipole (IOD) is a coupled ocean-atmosphere phenomenon in the Indian Ocean. It is normally characterized by anomalous cooling of SST in the eastern

equatorial Indian Ocean, south of the Indonesian islands of Java and Sumatra and anomalous warming of SST in the western equatorial Indian Ocean. Associated with these changes, the normal convection situated over the eastern Indian Ocean warm pool shifts to the west. A positive IOD phase sees greater-than-average SST and greater precipitation in the western Indian Ocean region, with a corresponding cooling of waters in the eastern Indian Ocean – which tends to cause droughts in adjacent land areas of Indonesia and Australia. The negative phase of IOD brings about the opposite conditions, with warmer water in the eastern Indian Ocean, wet conditions in Indonesia and Australia and dry conditions in East Africa. IOD also affects the strength of monsoons over the Indian subcontinent and is one aspect of the general cycle of global climate, interacting with other, similar phenomena such as ENSO in the Pacific Ocean. There is a correlation – but not a one-to-one correspondence – between IOD and ENSO. Positive IOD events are more likely to occur in El Niño years, and negative IOD events in La Niña years, but recent example of this relationship breaking down occurred in 2007, the only clear-cut case in the last 40 years of a positive IOD event coinciding with La Niña. Significant positive IOD events occurred in 2006 and 2007, while the one clear-cut negative IOD event was in 2010.

The most commonly used indicator of IOD is the difference in SST anomalies between the western equatorial Indian Ocean (50°E–70°E and 10°S–10°N) and the eastern equatorial Indian Ocean (90°E–110°E and 10°S–EQ). This index is known as the Dipole Mode Index (DMI). Values of DMI over the 2001–2010 decade are shown in Figure 14.

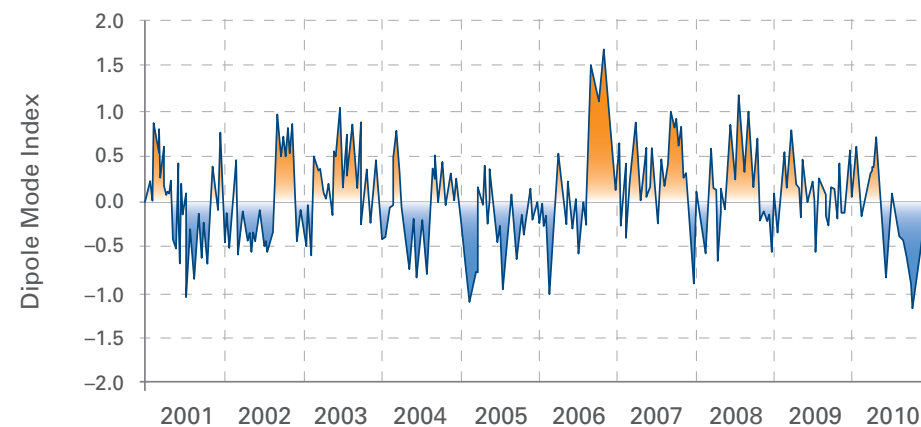


Figure 14. Weekly DMI from January 2001 to December 2010 (data source: Japan Agency for Marine-Earth Science and Technology)

3.4 Southern Annular Mode

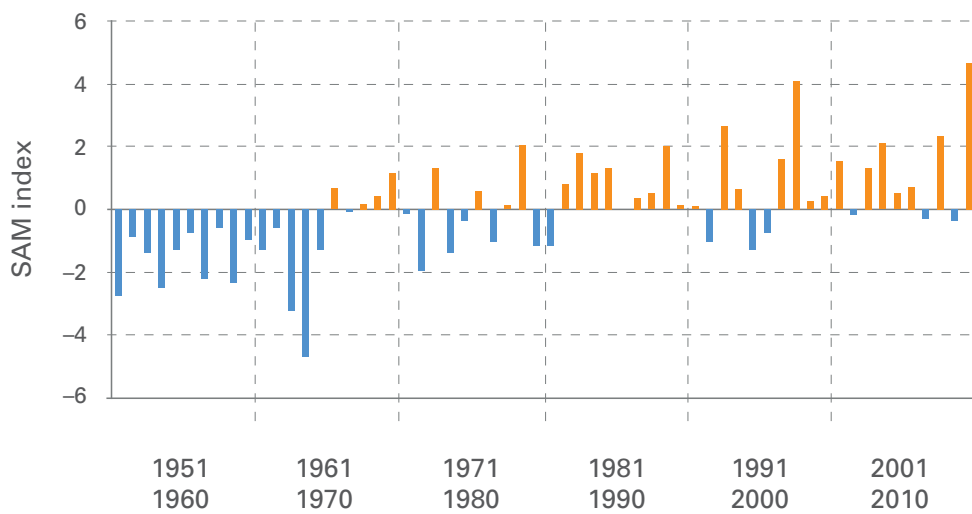
The Southern Annular Mode, also known as the Antarctic Oscillation (AAO), is the southern hemisphere analogue of the AO and indices describing it are constructed in a similar way; as for AO, positive modes of SAM are indicative of a stronger subtropical ridge and a stronger Antarctic circumpolar trough and enhanced westerly flow between them. (Because of the lack of land areas at high southern latitudes, the Antarctic circumpolar trough is more continuous and consistent than its northern hemisphere counterpart. It is strongly influenced by the Antarctic ozone hole (for more information, see Chapter 5).

The enhanced westerly flow in a positive phase of SAM has only a limited effect on land areas because the only land areas in the latitude range where flow occurs are in southern South America, the Antarctic Peninsula and the southernmost parts

of New Zealand, all of which tend to be warmer than normal during periods with a positive SAM mode. Of more significance to climate on land is the strengthening of the subtropical high-pressure belt in a positive SAM phase, which is typically associated with below-average precipitation in southern Australia (especially the south-west) and southern New Zealand.

During the first three decades of the period 1951–2010, negative phases of SAM predominated, while positive phases predominated the last three decades, 1981–2010 (Figure 15).

Figure 15. SAM index for June–July–August 1951–2010: the SAM index is defined as the difference in the normalized monthly zonal mean sea-level pressure between 40°S and 70°S. The anomalies are calculated as departures from 1958–2000 long-term average (*data source: State Key Laboratory of Numerical Modelling for Atmospheric Sciences and Geophysical Fluid Dynamics, China*).



CHAPTER 4. EXTREME EVENTS

4.1 Impact assessment

4.1.1 Data and methodology

Impact data used in this chapter are taken from two major sources of disaster-related global data. The Emergency Events Database (EM-DAT) maintained by CRED at the Catholic University of Louvain in Brussels, Belgium (<http://www.emdat.be>) is a comprehensive record of natural hazards, documenting more than 12 500 events by type and country of occurrence over the last century. The NatCatSERVICE database, maintained by MunichRe in Munich, Germany (<http://www.munichre.com>), provides information about major natural and technological catastrophes that have occurred around the world since 1965.

For a disaster to be entered into the database of EM-DAT/CRED, at least one of the following criteria must be fulfilled:

- Ten or more people reported killed;
- One hundred or more people reported affected;
- Declaration of a state of emergency;
- Call for international assistance.

For a disaster to be entered into the database of MunichRe at least one of the following criteria must be fulfilled:

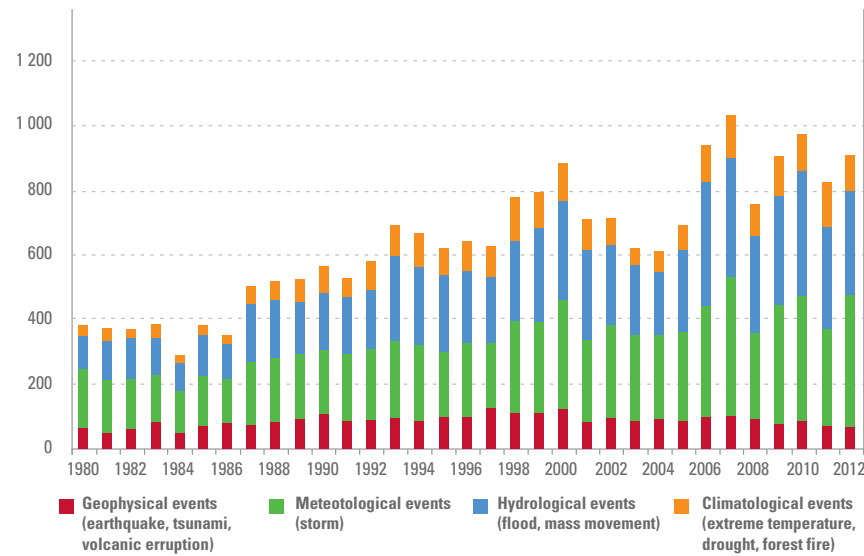
- Property damaged;
- People killed;
- People injured.

According to EM-DAT/CRED, more than 226 million people are affected on average by natural disasters every year. Over the decade 2001–2010, nearly 400 natural disasters accounted for a total death toll of more than one million people. Weather-related disasters represented about 88 per cent of all events, causing 72 per cent of all economic losses and 36 per cent of fatalities. Figure 16 shows the annual occurrence of natural disasters of various causes – geophysical, meteorological, hydrological and climatological – over the period 1980–2010.

At the global scale, meteorological and hydrological disasters comprise the prevailing part of total natural disasters.

Damage in the past two decades was significantly greater than in earlier decades (Figure 16). This could be due to greater exposure or better reporting – or even both. Rich countries (USA, in Europe, and increasingly in Asia) incur greater absolute damage as the value of their infrastructure is higher. For example, the 2005 Indian Ocean tsunami cost US\$ 10 billion, whereas hurricane *Katrina* cost more than US\$ 130 billion in the USA. The average cost of a disaster in a highly developed nation is US\$ 636 million, in a medium-developed nation US\$ 209 million and in a low-income nation US\$ 79 million. In Africa, the damage is least, where the poor possess little but, in the mean time, poor people are the ones who suffer the greatest long-term consequences of disasters as they have no insurance nor the means to recover quickly (EM-DAT/CRED).

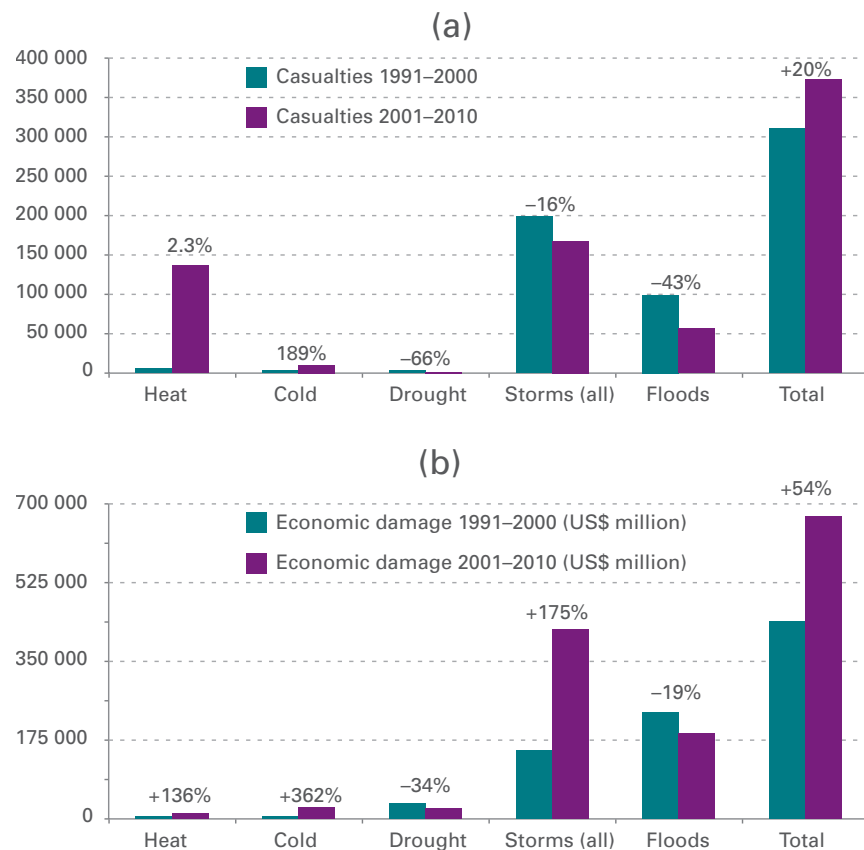
Figure 16. Number of natural disasters, 1980–2010 (source: MunichRe NatCatSERVICE)



4.1.2 Comparison of 2001–2010 with 1991–2000

Figure 17 (a) shows that, during the decade 2001–2010, more than 370 000 lives were lost owing to extreme climate conditions, including heat, cold, drought, storms and floods, marking an overall increase of +20 per cent with respect to the previous decade, 1991–2000. This increase is due mainly to the dramatic increase in the total reported deaths arising from heatwaves in 2003 and 2010. In fact, in 1991–2000, total

Figure 17. Impact of extreme events during 2001–2010 compared with 1991–2000: (a) total number of lives lost; and (b) economic losses in millions of US\$. The percentages above the bars indicate the change in losses during 2001–2010 compared to 1991–2000 (data source: EM-DAT/CRED).



deaths due to heatwaves were less than 6 000, while, in 2001–2010, the toll exceeded 136 000 – an increase of more than 2 000 per cent. On the other hand, it is noticeable that storms (both tropical and extra-tropical) rank as the major cause of loss of life in 2001–2010, with a total number exceeding 167 000, despite a decrease of 16 per cent compared to 1991–2000. Loss of life due to flooding stands as the third major cause of loss of life in 2001–2010, marking a substantial decrease (–43 per cent) compared with the previous decade, 1991–2000. Deaths caused by cold also increased by nearly +190 per cent, due mainly to a few but intense and large-scale extreme winter conditions which affected the northern hemisphere during the decade, such as those in 2009/2010 (WMO/TD-No 1550, 2010).

Economic losses (Figure 17(b)), amounting to an estimated US\$ 660 billion arising from hydrometeorological events were reported, marking an increase of 54 per cent compared to 1991–2000. Damage of more than US\$ 400 billion was caused by devastating tropical cyclones and nearly US\$ 200 billion caused by floods. It is noticeable that the large economic damage caused by storms increased by 175 per cent in 2001–2010 compared to 1991–2000. On the other hand, there was a decrease of nearly 20 per cent in the amount of economic losses owing to floods and 34 per cent to drought. Cold and heat conditions caused the least economic damage at nearly US\$ 25 billion and US\$ 13 billion, respectively. The increase with respect to the previous decade, 1991–2000, however, was 362 per cent and 136 per cent, respectively.

4.1.3 Regional analysis

Figure 18 shows the percentage of each category of loss from meteorological, hydrological and climatological events (see section 4.1.1 on data and methodology) and the percentage of fatalities and losses due to each category during the decade 2001–2010, by continent. The three lower histograms in the same figure provide the distribution by continent of the number of events (all three categories combined) and the resulting impacts in terms of fatalities and overall economic losses.

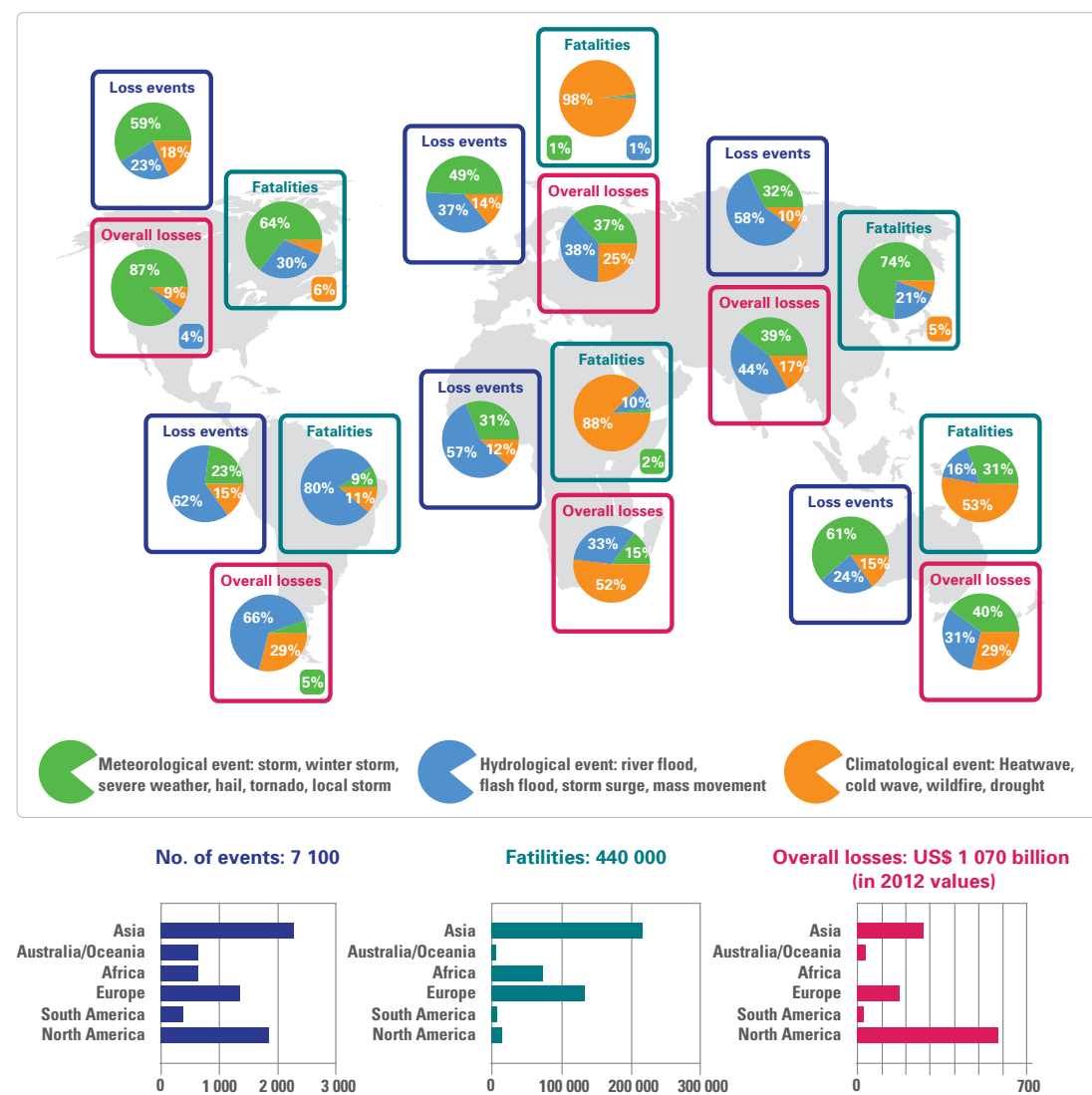
Globally, during the decade 2001–2010, a total number of 7 100 hydrometeorological disasters of various types was recorded, causing 440 000 fatalities and overall losses of more than US\$ 1 trillion.

In Europe, Australia and Africa, the main cause of fatalities were climatological events, mainly heatwaves for Europe and Australia, and drought for Africa. For South America, hydrological events such as floods, flash floods and storm surges were the main cause of fatalities. In Asia and North America, meteorological events such as tropical storms and severe weather conditions were the main causes of the fatalities.

On the other hand, meteorological and hydrological events constituted the main causes of overall losses, except for Africa, where the overall losses (in economic terms) were due mainly (52 per cent) to climatological events.

Asia was the continent most often hit by natural disasters. More than 32 per cent of all hydrometeorological disasters were reported in Asia, resulting in 215 000 victims, i.e. 49 per cent of total deaths caused by hydrometeorological disasters worldwide (MunichRe). The deadliest disaster of the decade 2001–2010 was tropical cyclone *Nargis* in Myanmar in April/May 2008, which killed some 138 500 people.

Figure 18. World map of hydrometeorological disasters, broken down by continent, 2001–2010 (data source: MunichRe)



In North America during the decade 2001–2010, most of the disasters reported in the USA were of meteorological origin: numerous devastating storms and hurricanes accounted for the majority of natural disaster damage, amounting to more than US\$ 502 billion. These were followed by climatological disasters (US\$ 52 billion) and hydrological disasters (US\$ 23 billion).

It is difficult to conduct a statistically significant analysis for Africa, due to the fact that damage and fatalities arising from natural disasters remain poorly reported or data are lacking. The available data show that 88 per cent of all fatalities in Africa were related to climatological disasters, although only 12 per cent of all the events were reported in this category.

In South America, 80 per cent of the fatalities and 66 per cent of economic losses were related to hydrological events.

In Europe, disasters of hydrometeorological origin caused some 16 per cent of total economic damage and around 19 per cent of fatalities reported worldwide. However, the severe heatwaves of 2003 and 2010 were the most remarkable hydrometeorological

disasters in terms of fatalities, causing together more than 100 000 excess deaths (source: EM-DAT/CRED).

Oceania was less affected than Africa with regard to economic damage. Nevertheless, 70 400 events were reported during the decade 2001–2010. Economic damage was around 3 per cent of global damage and related fatalities were less than 1 per cent.

4.1.4 Other aspects of impacts

Population displacement

One of the major consequences of natural disasters is the displacement of thousands or even millions of people in the area affected. The United Nations Guiding Principles on Internal Displacement identified natural disasters as one of the main causes of internal displacement. Global databases do not, however, collect the data on displacement. In order to begin addressing this issue, OCHA, in partnership with the Internal Displacement Monitoring Centre (IDMC), developed a methodology for this purpose and started to monitor and estimate forced displacement as a result of natural disasters in 2008.

According to these estimates, climate-related disasters were the trigger for the displacement of nearly 20 million people worldwide, representing 56 per cent of the total number of people displaced in that year. The figure increased to 88 per cent in 2009 and 93 per cent in 2010. Floods and storms formed the vast majority of events, causing the displacement of more than 15 million people in 2009 and more than 38 million in 2010. Floods in China and Pakistan in 2010 caused the displacement of at least 15 million and 11 million people, respectively.

Indirect impacts on health

While the stress of a natural disaster is felt immediately by the victims, the impacts upon their health take days to weeks to become noticeable. Millions of people have suffered injuries, disease and long-term disabilities, as well as emotional torment from the loss of loved ones and the memories of traumatic events. In the weeks and months following a disaster event, many people suffer from psychological ailments such as post-traumatic stress disorder or general anxiety disorder: the statistics cannot reflect the full health impact or the depths of human suffering endured.

For instance, floods and cyclones may directly and indirectly affect health in many ways. The greatest risk of mortality from a flood is drowning and blunt trauma. However, these devastating events also trigger widespread health problems, such as faecal-oral diseases (e.g. diarrhoea and typhoid), mosquito-borne and other infections (e.g. malaria, leptospirosis and respiratory infection), especially in least developed countries. A recent study on children exposed and not exposed to floods (mortality, diarrhoea, respiratory infection) in Bangladesh in 2004 (Milojevic et al., 2012) shows a moderate elevation in risk of acute respiratory infection in children during the subsequent 18 months. Results of another study (Rodriguez-Llanes et al., 2011) for rural communities in Orissa (India) show that children exposed to floods during their first year of life presented higher levels of chronic malnutrition. Long-term malnutrition prevention programmes after floods should, therefore, be implemented in flood-prone areas.

According to the WMO/WHO Atlas of Health and Climate (WMO-No. 1098, 2012), droughts also have acute and long-lasting impacts on health, such as malnutrition and

dehydration owing to the decreased availability of food; increased risk of communicable diseases arising from acute malnutrition; inadequate or unsafe water for consumption and sanitation; and increased crowding among displaced populations; psycho-social stress and mental health disorders; overall increase of population displacement; and disruption of local health services due to a lack of water supplies and/or health-care workers being forced to leave local areas.

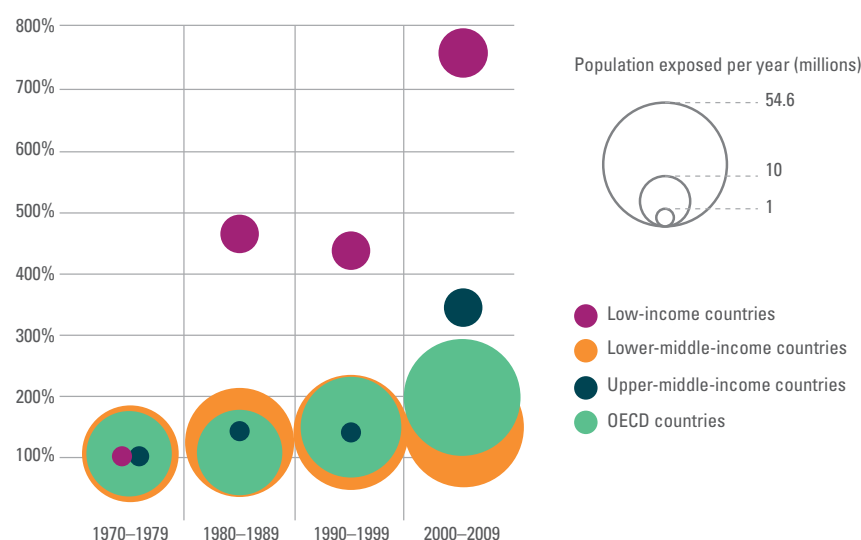
4.2 Exposure, vulnerability and attribution of climate extremes

4.2.1 Increased exposure and vulnerability to hydrometeorological events

On 2 and 3 May 2008, Category-3 Cyclone *Nargis* struck the coast of Myanmar and moved inland across the Ayeyarwady Delta and southern Yangon Division, causing more than 100 000 deaths (the official death toll stood at 84 537 with 53 836 missing), destroying livelihoods and disrupting economic activities and social conditions. *Nargis* is listed as the third most destructive cyclone on record and the worst disaster in Myanmar (PONJA, 2008).

It has been calculated that more than eight million people were exposed to the storm and its enormous impact brought to the fore the extreme vulnerability, in particular of the country's coastal regions, to such low-frequency but high-impact natural hazards.

Figure 19 shows an increase in tropical cyclone exposure in the past four decades for different categories of countries based on their income (World Bank, 2011). The dramatic increase of exposure for developing countries in the most recent decade covered by the study (2000–2009) – even the upper-middle-income countries – is evident. A steady increase in the exposure of OECD countries is also clear.



When looking at extreme events, it is essential to keep in mind that disaster risk is driven not only by the occurrence of a natural phenomenon (hazard) but also – and especially – by its impacts on a highly vulnerable, exposed population. Extreme events will continue becoming extreme disasters in those areas where exposure or vulnerability, or both, are high.

As the Global Assessment Report 2011 (GAR, 2011) revealed, the average population exposed to flooding every year increased by 114 per cent globally (from 32.5 million to 69.4 million annually) between 1970 and 2010, a period in which the world's population increased by 87 per cent (from 3.7 billion to 6.9 billion). Even more dramatic exposure growth is occurring in cyclone-prone areas, where exposure almost tripled (increasing by 192 per cent) in the same period.

Nevertheless, mortality vulnerability to tropical cyclones has decreased in all regions since 2000 (GAR, 2011), reducing overall mortality risk worldwide. Even though the vulnerability of low-income countries in 2010 was about 20 per cent lower than in 1980, it was still 225 times higher than in industrialized countries.

While mortality risk and vulnerability have improved, thanks to various factors, including better early warning systems, more preparedness and undoubtedly less physical vulnerability, economic risk is definitely on the rise. Improvements have failed to offset the increase in exposure fuelled by rapid economic growth and, therefore, the economic impact of disasters – and especially extreme disasters – is growing exponentially. The IPCC report *Managing the Risks of Extreme Events and Disasters to Advance Climate Change Adaptation* (IPCC, 2012) indicated that physical exposure to flooding will increase in the next two decades, in particular in Asia and Africa, compared to the situation in 1970 (Figure 20).

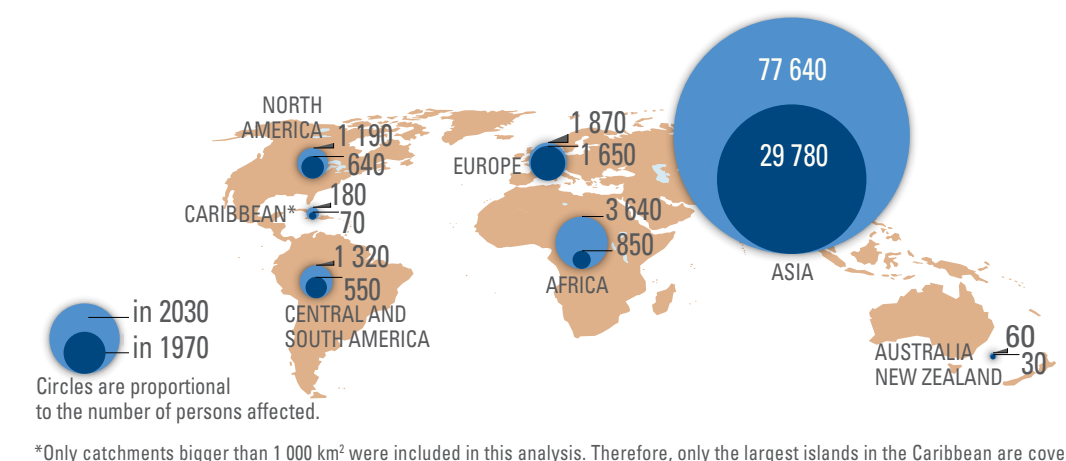


Figure 20. Average physical exposure to flooding, assuming constant hazard in thousands of people per year (source: *Intergovernmental Panel on Climate Change (IPCC), 2012*)

Better measures to protect lives in many cases do not immediately reduce the vulnerability of existing fixed assets such as buildings and infrastructure, which are often constructed below minimum standards, used beyond their expected lifespan and located in hazard-prone areas, particularly in rapidly urbanizing areas.

The case of the floods in Thailand from September to December 2011 demonstrated this global economic vulnerability, with a relatively low toll on human life – a total of 815 deaths were reported – but with a staggering US\$ 1.425 billion in economic losses as reported by the World Bank and with disruptions to manufacturing supply chains which affected industries regionally and globally in ways difficult to evaluate.

It is important to note that economic loss risk is increasing faster in industrialized and high-income countries than in other geographic and income regions, where it is growing

faster than GDP per capita. As the 2011 floods in Australia and Germany illustrate, even high-income countries struggle to manage increasing exposure, making this a global issue, not just concerning developing countries.

4.2.2 Attribution of climate extremes

Extreme climate events, as well as climate anomalies with significant impact on societies and economies, are of great public concern and interest. Several such events and anomalies are documented in this decadal report. Governments worldwide increasingly act to mandate and enable NMHSs and other key players to correctly monitor, document and – where possible – predict such events and anomalies and their related impacts.

The occurrence patterns of climate extremes and high-impact events and anomalies can be influenced by human-induced climate change and it is likely that the number and intensity of at least some of these types of events are consequently increasing. Owing to the naturally high internal variability of the climate system, however, it is still difficult to assess in a systematic way the degree and amount of climate-change influence on a single observed event. In an attempt to reduce the uncertainty of such an assessment, recent studies have led to the emergence of science-based methodologies to conclude with more confidence whether the risk of a given individual extreme event or anomaly has increased or whether such an extreme event might have occurred in a different way in the absence of human-induced climate change.

Applying such methodologies to the recent most extreme heatwaves shows that the 2003 European heatwave, for example, is considered to be among those events for which human influence had probably substantially increased the likelihood of its occurrence. On the other hand, natural climate variability can also be important in some cases. For example, the extreme magnitude of the 2010 Russian Federation heatwave demonstrates the important effects of natural climate processes in amplifying some climate extremes. The science of attribution requires carefully calibrated, physically based assessments of observed weather and climate-related events, including comparisons of ensemble-based model simulations where particular climate drivers (e.g. concentrations of greenhouse gases) are excluded. The underlying global and regional climate conditions are then objectively considered to assess the extent to which the likelihood of occurrence of individual climate extremes might have changed had such climate drivers been absent. Subsequent statistical analyses provide probability expressions for a climate threshold to be exceeded (e.g. positive temperature anomalies associated with a heatwave) and what fraction of the risk of exceeding the threshold is attributable to a particular influence (climate driver). Attribution science is still a matter for extensive research.

Based on the encouraging results from this research, climate assessment and related services will be further enhanced in the years to come to include information on the influence of global warming on individual extremes.

4.3 Summary statistics from country data

4.3.1 Most reported extreme events

The WMO survey requested Member States to list the most significant events which had occurred in their territories during the decade. A total number of 81 countries provided data on extreme weather and climate events which occurred in the decade

2001–2010. A list of 10 types of weather and climate extremes was provided as a basis for collecting information in the survey. The results of the analysis show that the most reported events in the country data sample were flooding, droughts, flash floods, heavy rain, severe storms and heatwaves. Up to 60 per cent of the countries reported at least one of these events. Up to 30 per cent reported they had been affected by one or more of the following extreme events: cold waves, bush or forest fires, tropical cyclones or snowstorms. A more detailed summary on the occurrence of these extremes during 2001-2010 decade is provided in Section 4.4

4.3.2 Country absolute records

An assessment of the absolute country records since 1961 for the daily maximum temperature, daily minimum temperature and 24-hour total precipitation was conducted based on the WMO survey. The occurrence of these records in one of the previous five decades was then established. The assessment focuses on the five decades starting with 1961–1970 as there was nearly 100 per cent data coverage in the country data sample. The result of the assessment is summarized below and depicted in Figure 21. A total of 128 countries provided data on these records out of the total number of 139 participating countries.

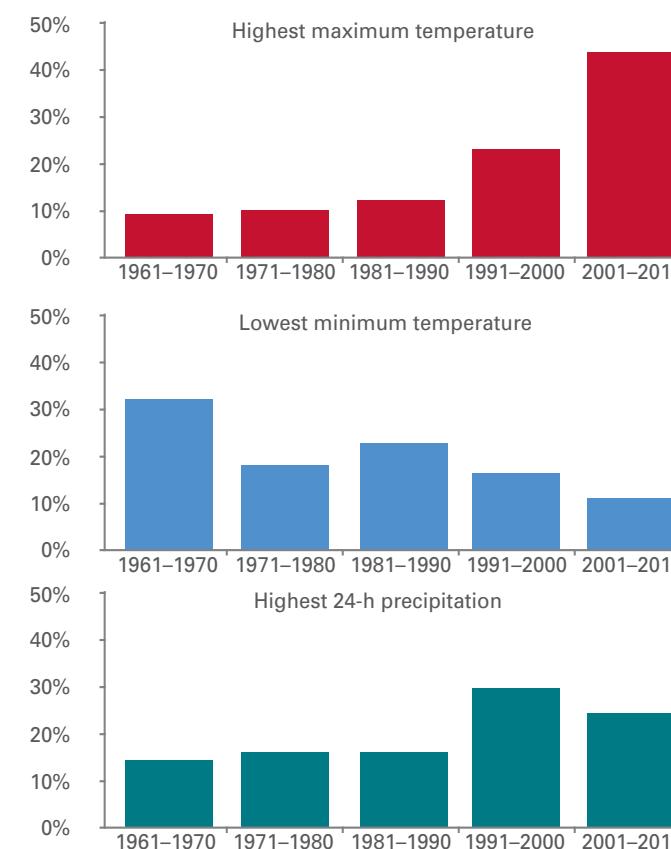


Figure 21. Absolute country records of the daily maximum and minimum temperature and 24-hour total precipitation in the last five decades (source: WMO survey)

A total of 56 countries (44 per cent) reported their highest absolute daily maximum temperature record being observed in 2001–2010, compared to 24 per cent in 1991–2000, with the remaining 32 per cent spread over the earlier three decades.

Conversely, 11 per cent (14 out of 128) of the countries reported their absolute daily minimum temperature record being observed in 2001–2010, compared to 32 per cent in 1961–1970 and around 20 per cent in each of the intermediate decades. These trends fit well with the IPCC conclusions on increasing warm days and nights and decreasing cold days and nights (IPCC, 2012).

The last two decades collected most of the country 24-hour total precipitation country absolute records, with 2001–2010 (24 per cent of the countries) lagging slightly behind 1991–2000 (30 per cent). The three preceding decades each collected some 15 per cent of the country absolute records. This fits also with the IPCC finding that positive trends in heavy precipitation events were assessed in some regions (IPCC, 2012).

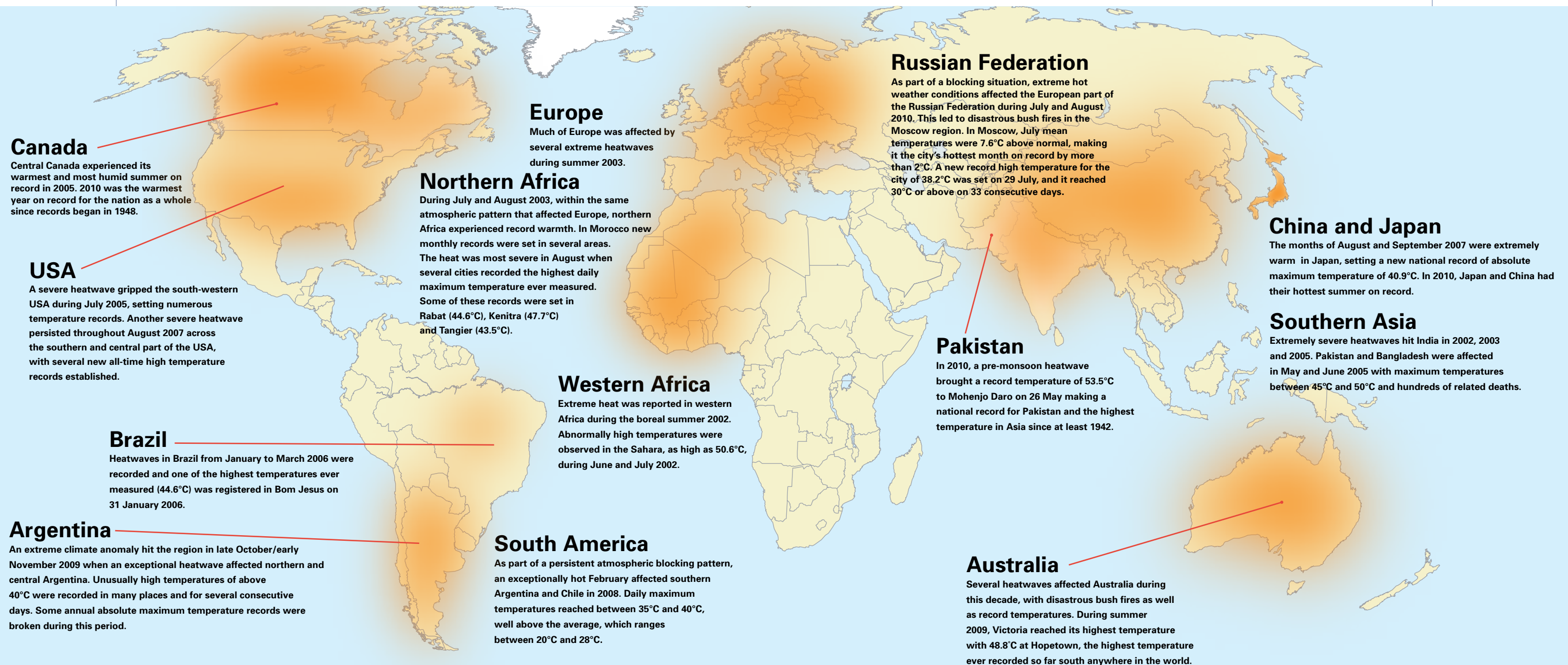
4.4 Worldwide summary of extreme climate conditions

In this section, the assessment focuses on weather and climate conditions that are related to the extreme manifestation of temperature and precipitation parameters. Section 4.5 is devoted to the extreme manifestation of the wind parameter which characterizes severe storms, including tropical cyclones, extra-tropical cyclones and tornadoes.

4.4.1 Heatwaves and abnormally high temperature conditions

Anomalously warm weather that lasts for several days or weeks and has a severe impact on society is often referred to as a heatwave.

Figure 22. Most significant heatwaves and abnormally high-temperature conditions reported during 2001–2010 (source: NOAA-NCDC)



Three examples of major heatwaves which occurred in Europe in summer 2003, the Russian Federation in 2010 and Australia in 2009 are described in special case studies later on in this section.

Figure 22 shows the most significant heatwaves and abnormally high-temperature conditions reported to WMO during the decade 2001–2010. The year-by-year occurrence of this category of extremes is given in Table 4 below with a more detailed list of events. Additional information on impacts caused by heatwaves and extreme high temperatures was communicated to WMO in the previous annual statements, which are summarized below.

India was affected twice at the beginning of the decade in 2002 and 2003, when severe heatwaves caused more than 1 000 deaths each year. In 2003, much of Europe was affected by an extreme heatwave causing more than 66 000 deaths in France, Germany, Italy, Portugal and Spain, together. At the end of the decade, in 2010, the Russian Federation was affected by an exceptionally intense and long-lasting heatwave in July and August, causing more than 55 000 related deaths (EM-DAT/CRED).

Table 4. Significant abnormally high temperature conditions and heatwave events during the decade 2001–2010 (source: WMO Statements on the Status of the Global Climate)

2001	<ul style="list-style-type: none"> • 33.2°C was the highest minimum temperature for the decade in Spain, recorded in Almería on 31 July. • High temperature record of 18.4°C observed in December in Iceland • Near-record warmth in some parts of Canada and the USA between November and December • Warm anomalies between +2°C to +5°C in May across Kazakhstan
2002	<ul style="list-style-type: none"> • Record warmth in summer 2002 experienced in Norway and Sweden • Higher-than-average temperatures occurred across much of central and south-eastern Brazil, especially during the austral winter. Warm and dry conditions exacerbated the occurrence of wildfires in the region. • A prolonged heatwave was observed in India during April-May. • Extreme heat was reported in western Africa during the boreal summer. Abnormally high temperature was observed in Sahara (as high as 50.6°C) during June and July.
2003	<ul style="list-style-type: none"> • Much of Europe affected by extreme heatwaves during the summer • Parts of northern and eastern South America had temperatures in the highest percentile range. • India experienced a severe heatwave from the last week of May to the first week of June. • Northern Africa experienced record warmth. The heat was most severe in August with cities recording their highest daily maximum temperatures ever measured, such as 47.7°C in Kenitra, Morocco.
2004	<ul style="list-style-type: none"> • In June and July, heatwaves with near-record temperatures affected Portugal, Romania and southern Spain. • An unusual heatwave affected parts of Iceland in August. • Record summer heat observed on the west coast of Canada • Above-normal temperatures predominated between September and November in large parts of Brazil. • In Japan, extremely hot conditions persisted during the summer with record-breaking maximum temperatures. • An exceptional heatwave hit eastern Australia during February, with temperatures around 45°C in many areas.

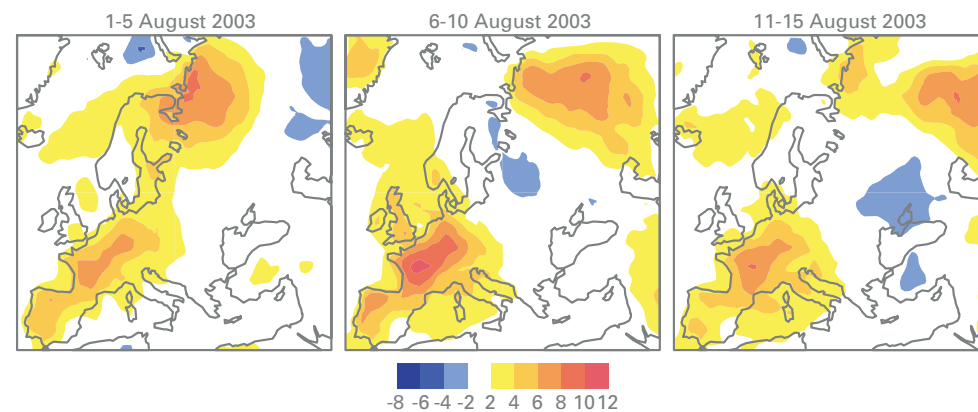
2005	<ul style="list-style-type: none"> • During July, southern Europe was affected by severe heatwave conditions. • A severe heatwave gripped the south-western USA in July. • Central Canada experienced its warmest and most humid summer on record. • In Bangladesh, India and Pakistan, extremely harsh heatwaves in May and June brought maximum temperatures of between 45°C and 50°C. • Hottest year on record for Australia • A severe heatwave affected Morocco and Algeria in July.
2006	<ul style="list-style-type: none"> • Warmest year in the 352 years of the central England temperature series • Warmest spring for Canada as a whole • Heatwaves recorded in Brazil from January to March: one of the highest temperatures ever measured (44.6°C) was registered in Bom Jesus on 31 January.
2007	<ul style="list-style-type: none"> • One of the warmest winter and spring seasons ever recorded in large parts of Europe • Two extreme heatwaves affected south-eastern Europe in June and July with daily maximum temperatures exceeding 40°C. • A severe heatwave affected parts of southern and central USA in August, with several new all-time high temperature records established. • The Russian Federation recorded its warmest year on record. • The months of August and September were extremely warm in Japan, setting a new absolute national record of 40.9°C.
2008	<ul style="list-style-type: none"> • A remarkably mild winter (December 2007/February 2008) was observed in most parts of Scandinavia and Finland, resulting in new seasonal records in Norway, Sweden and Finland. • Southern Argentina and Chile were exceptionally hot in February, with daily maximum temperatures between 35°C and 40°C, well above the average. • A severe prolonged heatwave affected much of southern Australia in March 2008. Adelaide had 15 consecutive days of maximum temperatures above 35°C, breaking the previous record of eight days.
2009	<ul style="list-style-type: none"> • April was extremely warm in large parts of central Europe with temperature anomalies of more than +5°C. • In July, records of daily maximum temperature were set in some areas of Canada, such as the 35.0°C recorded in Victoria on 29 July. • Argentina recorded its warmest year on record in five decades. • Australia was marked by three exceptional heatwaves: one in January/February, affecting the south-eastern region; another in November across the same area; and the third in August, affecting the subtropical eastern part of the country
2010	<ul style="list-style-type: none"> • As part of a blocking situation, the persistence of extreme hot-weather conditions affected the western Russian Federation during July and August 2010. • Canada had its warmest winter (December 2009–February 2010) on record, with national temperatures 4.0°C above the long-term average. • December brought extreme high temperatures across central Argentina. Several locations recorded between five and 12 consecutive days with maximum temperatures above the 90th percentile. • Exceptional pre-monsoon heat in southern Asia brought an absolute maximum temperature record of 53.5°C at Mohenjo Daro, Pakistan, the highest temperature in Asia since at least 1942. • Extreme heat affected the Middle East during summer, with notable readings: 52.0°C in Jeddah, Saudi Arabia. Jordan recorded +2.8 °C annual temperature anomaly with 1961–1990 base period. • Extreme heat affected northern Africa during summer, with noteworthy readings (47.7°C at Taroudant, Morocco).

Case study A1. Extreme heatwaves in Europe in 2003

Most of Europe was affected by an extreme heatwave during boreal summer 2003 (June, July and August). These conditions were part of a prolonged warm and dry spell that began in April in response to a persistent upper-level ridge of high pressure centred over the continent. Surface temperatures were well above average across Europe from April to August, with the largest mean departures exceeding +2.5°C across central Europe and +1.5°C across northern Europe. Precipitation totals were also well below average during this period, with deficits of 75-100 mm observed throughout central Europe. Record high values of sunshine duration were also observed. These conditions were associated with a larger-scale anomalous circulation characterized by below-average geopotential heights at high latitudes from Canada to the United Kingdom and above-average geopotential heights in the middle latitudes from the north-eastern USA to eastern Europe, as well as in the subtropics. The extremely hot conditions had an immense socio-economic impact, especially on human health, agriculture and an increase in forest fires.

Austria, France, Germany, Italy, Portugal, Spain and Switzerland were the most affected by the extreme heat. From southern Spain to central France, maximum temperatures exceeded 34°C on 30–50 days during the season, which was approximately 20 days above average. In central and northern France 10-30 days with maximum temperatures above 34°C were observed, which was well above the mean of five days or less.

The peak of the heatwave was reached between 6 and 15 August (Figure 23) with mean temperatures ranging between 6°C and 12°C above the long-term average. Two distinct periods of exceptional heat occurred during the season, the first in June and the second during the first half of August. The August heatwave was the more serious of the two, because it coincided with the normal summer peak and was accompanied



by an almost complete absence of precipitation. Daily maximum temperature during this period averaged more than 40°C across most of interior Spain, 36°C–38°C across southern and central France and 32°C–36°C across northern France. For the country average temperature in Germany, both June and August were the warmest months since the beginning of the 20th century. Thus, the summer (June, July, August) became the hottest in Germany since 1901. During this heatwave, many records were broken.

In the United Kingdom, the national record was broken when 38.5°C was recorded at Faversham (Kent) on 10 August. In Switzerland, Grono recorded the highest temperature

ever measured for the whole country, reaching 41.5°C on 11 August. In Portugal, Amaraleja recorded 47.4°C, reaching another new high national record. Another indicator of this kind of climate extreme is to count the number of hot days during a period. A hot day is considered to have occurred when the maximum temperature is in the top 10 per cent for the local climate for that season. In summer, the normal total of hot days is around nine but, in this unprecedented summer, the total of hot days reached the highest values on record for several locations in central Europe. More than 50 hot days were observed, for example, in Austria, central and southern France, southern Germany, northern Italy and Switzerland.

Tens of thousands of deaths were reported that were associated with this exceptional and prolonged heatwave. According to EM-DAT/CRED, more than 66 000 heat-related deaths were reported between late July and mid-August in the five countries most affected in Europe. These deaths resulted not only from the extreme daily heat, but also from the frequency of extremely hot and dry days in areas not accustomed to such conditions.

The 2003 heatwave ranges from second to sixth place regarding the 10 most important extreme temperature disasters sorted by the number of people killed at the country level. The number of deaths compared with normal summer conditions revealed a total of more than 66 700 excess deaths that were attributed to the heatwave. Italy (>20 000), followed by France (>19 000), Spain (>15 000), Germany (>9 300) and Portugal (>2 600) were the most severely affected European countries. Regarding the induced economic damage at country level, the 2003 heatwave affected France and Italy most with a loss of nearly US\$ 4.5 billion each, followed by Germany with nearly US\$ 1.7 billion.

Case study A2. Extreme heatwave in the Russian Federation in 2010

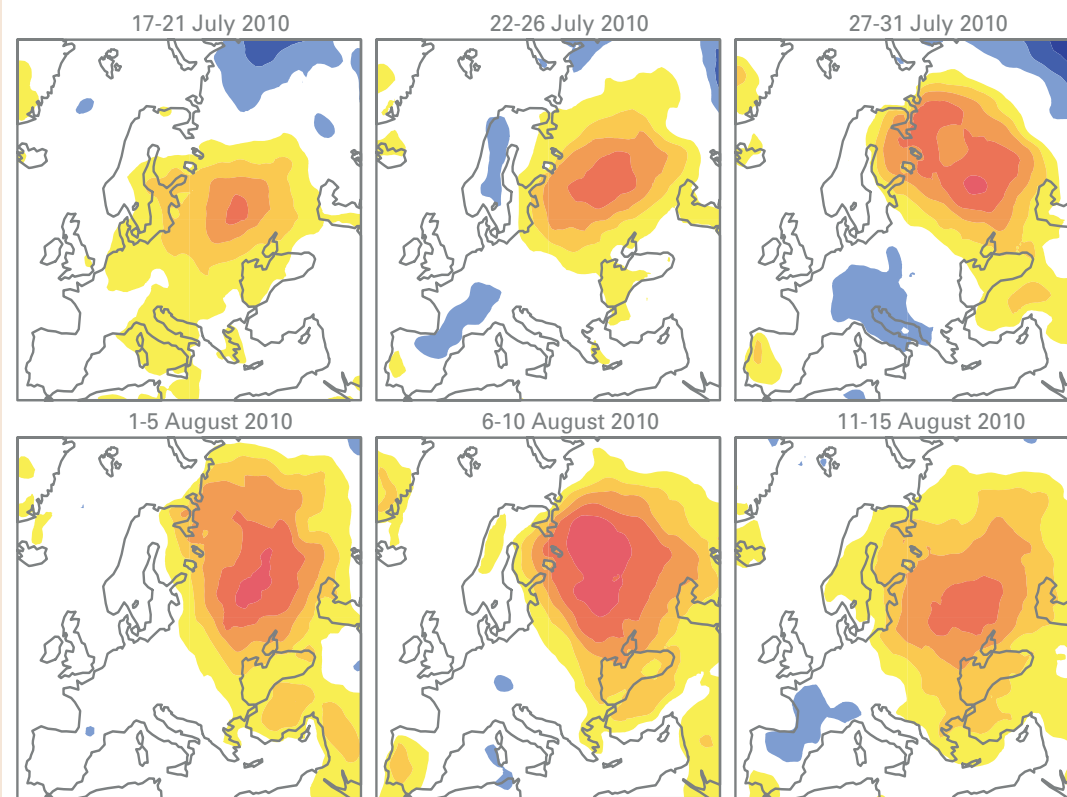
The summer of 2010 recorded very hot conditions which affected several parts of Eurasia with exceptional heat in July and August. The most extreme heat was centred over the western Russian Federation, with the peak extending from early July to mid-August (Figure 24), although temperatures were well above average from May onwards. In Moscow, July mean temperatures were 7.6°C above normal, making it the city's hottest month on record by more than 2°C. Similar anomalies continued until cooler conditions developed in the last 10 days of August. A new record high temperature for the city of 38.2°C was set on 29 July and 30°C or above was reached on 33 consecutive days. Parts of the central European Russian Federation had average temperatures of more than 5°C above normal for the summer. Nearby countries, such as Belarus and Finland, were also affected by a hot summer during the same period with their highest temperatures on record.

In each of these periods, the mean temperature was well above average, recording always positive anomalies above +6°C in some areas. The peak of this heatwave was observed during the first 10 days of August 2010, when temperature anomalies exceeded +12°C in some locations and also coincided with the normal peak of temperatures in a normal year. From this analysis it can be estimated that this prolonged heatwave had a duration of approximately one month.

The extreme heatwave of 2010 caused more than 55 000 excess deaths. According to EM-DAT/CRED, the heatwave was the deadliest natural disaster ever in the country.

Figure 23. Five-day mean surface air temperature anomaly (°C) for August 2003, relative to 1991–2010 from the ERA-Interim reanalysis (source: ECMWF)

Figure 24. Five-day mean surface air-temperature anomaly (°C) for July and August 2003, relative to 1991–2010 from the ERA-Interim reanalysis (source: ECMWF)



On the other hand, a combination of abnormally hot weather and substantial precipitation deficit (4 per cent–40 per cent of monthly normal) observed in many regions of the Russian Federation resulted in severe agriculture damage. Over 20 per cent of crops growing on some 9 million hectares of farmland were destroyed. There were more than 600 wildfires and some 950 forest fires in 18 regions at the beginning of August, with thousands of people made homeless. The wildfires are listed as the costliest natural disaster of the country since 1900, with an estimated economic damage of US\$ 1.8 billion.

Other severe impacts included dense smog which wrapped Moscow, Ryazan and other cities in early August. A fire that engulfed the roads and led to zero visibility brought a severe disruption in road traffic and rail movement.

Case study A3. Exceptional heatwaves in Australia in 2009

The annual number of record hot days across Australia has doubled since 1960. The increase is most prominent in the last decade (Figure 25).

During the severe heatwaves reported in 2009 in south-eastern Australia, Melbourne experienced three consecutive days and Adelaide four consecutive days with maximum temperature at or above 43°C in late January. This had a large impact on human health, infrastructure, agriculture and other activities. A week later, on 7 February, temperatures reached 46.4°C in Melbourne and 48.8°C at Hopetoun, north-western Victoria. The extreme heat, combined with strong winds and very low humidity, contributed to some of the most extreme wildfires ever experienced in Australia that resulted in 173 deaths and the destruction of more than 2 000 buildings.

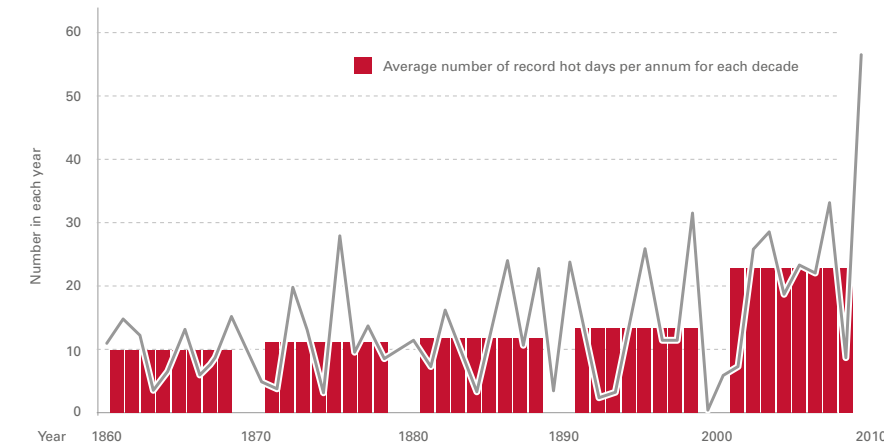


Figure 25. Number of record hot day maximums at Australian climate reference stations (source: Bureau of Meteorology, Australia)

Over the last decade, severe heatwaves around Australia resulted in deaths and in increased hospital admissions for heart attacks, strokes, kidney disease and acute renal failure. In total, there were 980 deaths in Melbourne during this period, 374 more than would have occurred on average at that time of year.

The prolonged extreme heat in Melbourne in January/February 2009 caused substantial damage to infrastructure, including energy transmission and rail transportation. The demand for electricity increased substantially while, in addition, faults to the transmission systems made the entire grid vulnerable to collapse. The Basslink electricity cable between Tasmania and Victoria reached maximum operating temperature and was automatically shut down for safety reasons. The shutdown of this transmission source, combined with faults at a number of transformers, caused widespread blackouts across Melbourne. On the evening of 30 January 2009, an estimated 500 000 residents were without power (Queensland University of Technology (QUT), 2010). Melbourne's train and tram networks also suffered widespread failures, caused by faults in air-conditioning systems and rail lines buckling in the extreme heat. Approximately one quarter of train services did not run (QUT, 2010). Financial losses from the heatwave, estimated at US\$ 800 million, were caused mainly by the power outages and disruptions to the transport system (Chhetri et al., 2010). This amount does not include losses associated with fires.

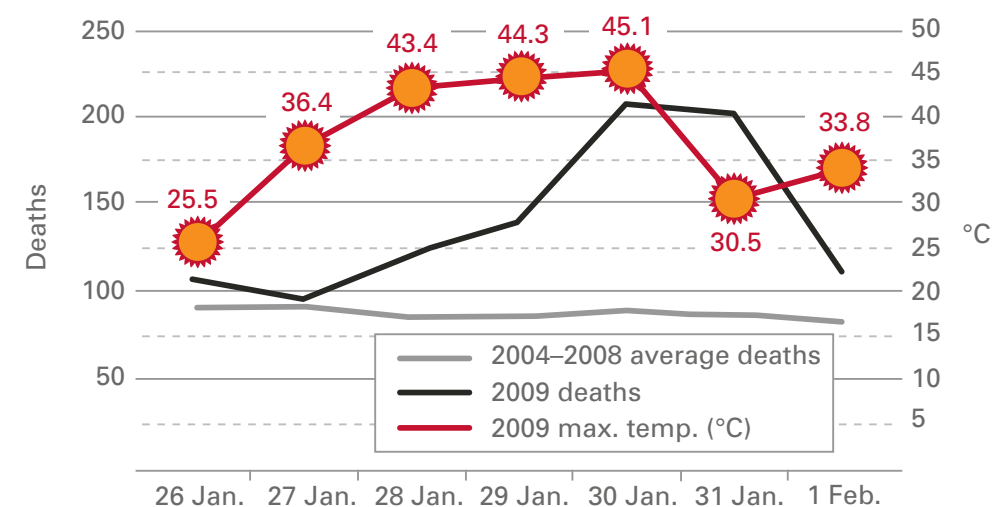


Figure 26. Daily temperature and mortality during the 2009 heatwave in Melbourne (source: Department of Human Services, Australia, 2009)

4.4.2 Cold waves, abnormally low temperature conditions and snowstorms

Figure 27 shows the most significant extreme low-temperature and snowfall conditions which were reported to WMO for the decade 2001–2010. The year-by-year occurrence of this category of extremes is given in Table 5 with a more detailed list of events.

A case study reflecting exceptional cold conditions which occurred during the northern hemisphere winter 2009/2010 is also given. The case study describes strong negative temperature anomalies and prolonged snow conditions which occurred over Europe, where it resulted in more than 450 casualties, the Russian Federation, parts of North America – particularly the USA – and Asia.

Figure 27. Most significant cold waves, abnormally low temperature conditions and snowfall events which were reported for the decade 2001–2010 (source: NOAA-NCDC)

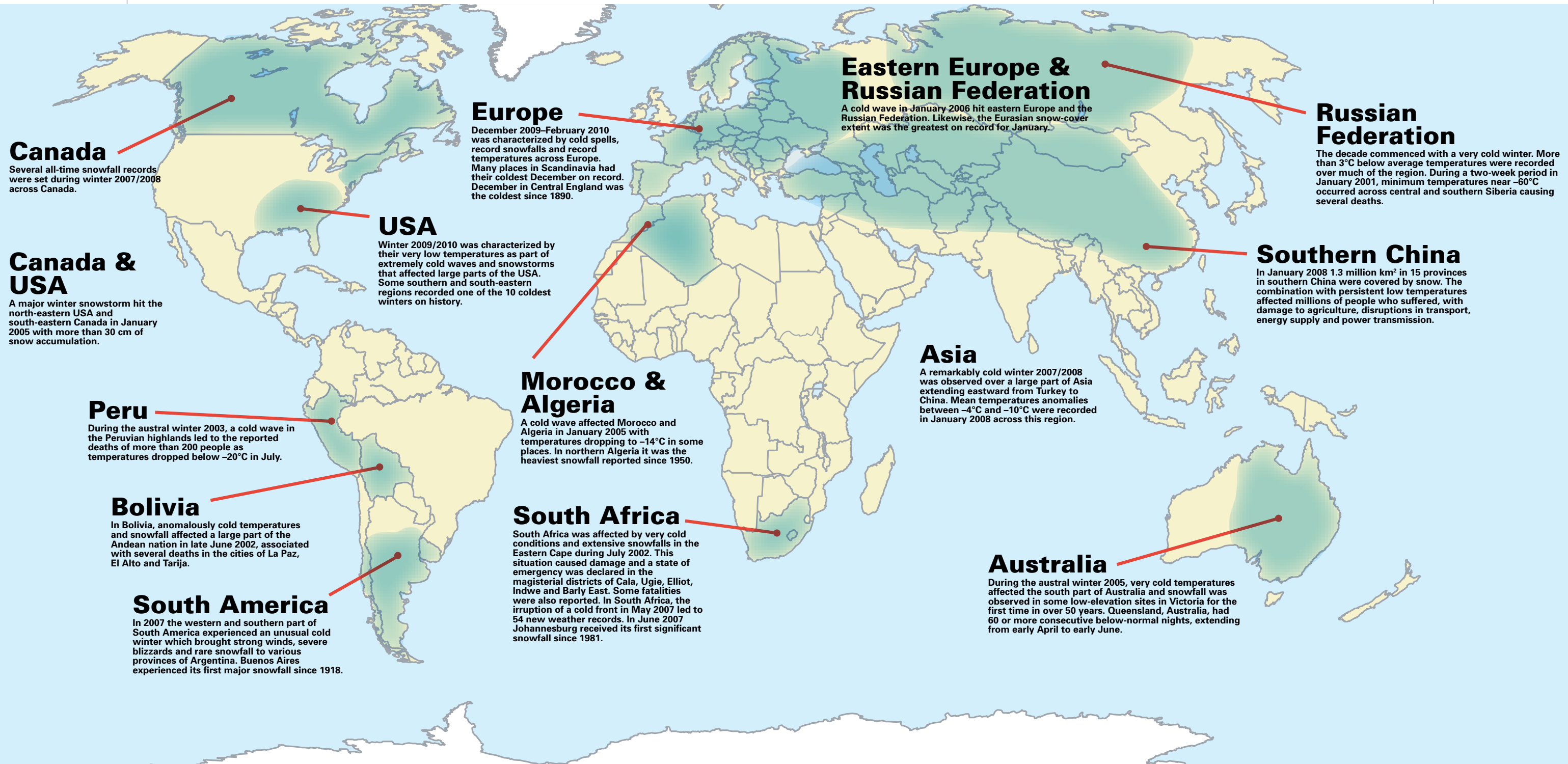


Table 5. Significant cold waves, abnormally low temperature conditions and snowfall events during the decade 2001–2010 (source: WMO Statements on the Status of the Global Climate)

2001	<ul style="list-style-type: none"> • Exceptionally low temperatures affected central and northern parts of Greece in December. • Cold winter temperatures affected a large part of the USA and eastern Canada. • A very cold winter (December 2000–February 2001) across the Russian Federation: during a two-week period in January; minimum temperatures reached -60°C across central and southern Siberia.
2002	<ul style="list-style-type: none"> • The three-month period from October to December was the coldest since 1981 in Norway. • Anomalously cold temperatures and snowfall affected a large part of the Plurinational State of Bolivia in late June. • December was exceptionally cold and snowy in Armenia. The monthly temperature anomalies were generally around -4°C. • South Africa was affected by very cold conditions and extensive snowfall in the Eastern Cape during July.
2003	<ul style="list-style-type: none"> • Extremely cold weather conditions and snowstorms were observed in some parts of Europe during the first half of January. France, Hungary and Slovenia were the worst affected. • In February, snowstorms brought numerous new snowfall records to the eastern USA. • During the austral winter (June–August), a cold wave hit the highlands of Peru and temperatures dropped below -20°C in July. • Northern India experienced a very cold January and December with maximum temperatures ranging from 4°C to 5°C below normal.
2004	<ul style="list-style-type: none"> • In February, widespread winter storms affected Greece and Turkey. • Record-breaking snowfalls and blizzard conditions were experienced in Canada in February. • Severe cold and snow occurred in June and July in Peru, southern Chile and the central Patagonian region of Argentina. • Parts of South Asia experienced very cold episodes during winter 2003/2004.
2005	<ul style="list-style-type: none"> • In Bulgaria, a 50-year-old minimum temperature record was broken, with temperatures dropping to -34°C. • A major snowstorm hit the north-eastern USA and south-eastern Canada in January. • Record-breaking heavy snowfall occurred in parts of Japan during December. • A cold wave affected Algeria and Morocco in January, with temperatures dropping to -14°C in some places. Northern Algeria experienced its heaviest snowfall since 1950.
2006	<ul style="list-style-type: none"> • Record-breaking fresh-snow amounts fell within one day (4/5 March) in a large part of the plateau region of Switzerland. • In the USA, a major snowfall hit New York City in February and Buffalo, New York state, in October. • During January, record-breaking frosts persisted for a long time in the central Krasnoyarsk Territory and in south-western Siberia: for more than 20 days, air temperature did not rise above -30°.

2007	<ul style="list-style-type: none"> • Severe winter storms and freezing rain hit the mid-western states of the USA in the second week of December, covering large areas with a thick layer of ice. • An unusual cold winter (June–August) in western and southern South America with strong winds, severe blizzards and rare snowfall in various provinces of Argentina. Buenos-Aires experienced its first major snowfall since 1918. • Australia recorded its coldest June in history with the mean temperature 1.5°C below normal and record low daytime temperatures in large parts of the tropics. • In South Africa, the passage of a cold front in May led to 54 new temperature records. In June, Johannesburg received its first significant snowfall since 1981.
2008	<ul style="list-style-type: none"> • Several all-time snowfall records were set during winter 2007/2008 across Canada. • An early Antarctic air mass outbreak in May affected central and northern Argentina, where the minimum temperature dropped below -6°C in some locations, breaking annual absolute minimum temperature records. • A remarkably cold winter 2007/2008 was observed over a large part of Asia, including major snowfall across China. • Parts of northern Australia had 60 or more consecutive nights with below-normal temperatures, extending from April to early June. • An eight-day extreme cold spell affected northern Saudi Arabia in January. • A severe cold wave with temperatures ranging between -5°C and -2°C affected Israel for at least one week in January.
2009	<ul style="list-style-type: none"> • A cold October was reported in the Scandinavia region with mean temperature anomalies ranging from -2°C to -4°C. • A very cold October 2009 was observed across the USA. For the nation as a whole, October ranked as the fourth coldest October on record with a mean temperature anomaly of -2.0°C. • An extremely cold November affected the south of Argentina. Late snowfalls broke frequency records in some locations where between four and 11 days with snow were reported. • China experienced very low temperatures in the first half of November as part of an early cold wave which brought a record snowstorm one month earlier than would normally be expected.
2010	<ul style="list-style-type: none"> • The winter was characterized by extreme cold weather conditions over most of Europe. Cold spells, record extended snowfalls and record temperatures were observed. • Winter 2009/2010 was characterized by very low temperatures and snowstorms that affected large parts of the USA. • A cold wave in July affected southern South America. Several snowfalls across Argentina were observed, reaching the northern provinces with unusual intensity. Lima, Peru, recorded its lowest temperature (8°C) in 46 years. • A very heavy snowstorm in January raged for six days in southern Taymir in the Russian Federation. • A severe snowstorm hit New Zealand on 18 September.

Case study B. Extreme winter conditions over the northern hemisphere (2009/2010)

During the boreal winter 2009/2010, i.e. the period from December 2009 to February 2010, extreme conditions were recorded in many places across the northern hemisphere. Strong negative temperature anomalies (Figure 28) and prolonged snowfall events occurred over Europe, the Russian Federation, parts of North America, particularly the USA, and Asia, while many other larger areas registered above-normal temperatures for this season. Despite this large-scale cold spell, the northern hemisphere surface temperature anomaly for the winter remained positive – around +0.52°C above the long-term average.

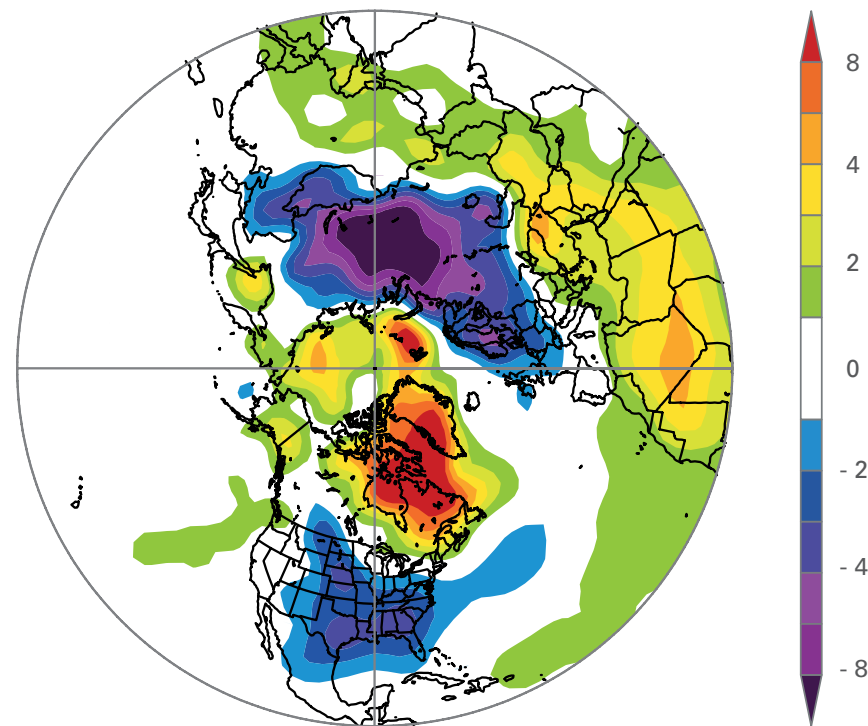


Figure 28. Northern hemisphere winter 2009/2010 temperature anomaly in °C for December–January–February at 1 000 hPa based on NCEP-NCAR reanalysis, with 1981–2010 as reference period (source: NOAA, ESRL-PSD)

During this winter, several places in the northern hemisphere recorded extended cold spells associated with very low temperatures and heavy and prolonged snowfall. In Europe, the United Kingdom experienced its most prolonged spell of freezing temperatures and snowfall since the winter of 1981/1982. Ireland and Scotland had their coldest winter since 1962/1963. In the second half of December, Germany reported daily minimum temperatures ranging between -10°C and -25°C with several locations experiencing their lowest minimum temperatures for at least six decades. In late January, central and eastern Europe were severely hit by an extremely cold weather episode affecting Hungary, Poland, Romania, Turkey and Ukraine. Some 12 stations in the European part of the Russian Federation and Siberia registered new absolute temperature minima for this time of year. Most of north-eastern China experienced very cold conditions. Some stations recorded temperatures as low as -32°C and low temperature records were broken at 26 meteorological stations. During the period 2–17 January, the mean maximum daily temperature dropped 4°C below normal over many parts of northern India.

Hundreds of records of daily minimum temperatures were broken across the eastern two-thirds of the USA. In Key West, Florida, the thermometer dipped to 6°C on 11 January. This was the second lowest temperature ever recorded at the southernmost weather station in the contiguous USA.

The extent and duration of snow events were unusual in several places in Europe, including southern locations in Italy and Spain. Based on the frequency of snowfall in France, this was probably one of the country's snowiest winters in the past 30 years. Similarly, many places in Germany experienced their longest period of snow in at least 30 years. In the USA, the meteorological station at the Ronald Reagan Washington National Airport in Arlington, Virginia, reported 142 cm of snow accumulation during the winter (Figure 29), breaking the record set in 1898. In Seoul, Republic of Korea, 28 cm of snow fell on 3 January, marking the greatest snowfall amount for the city since records began in 1937.

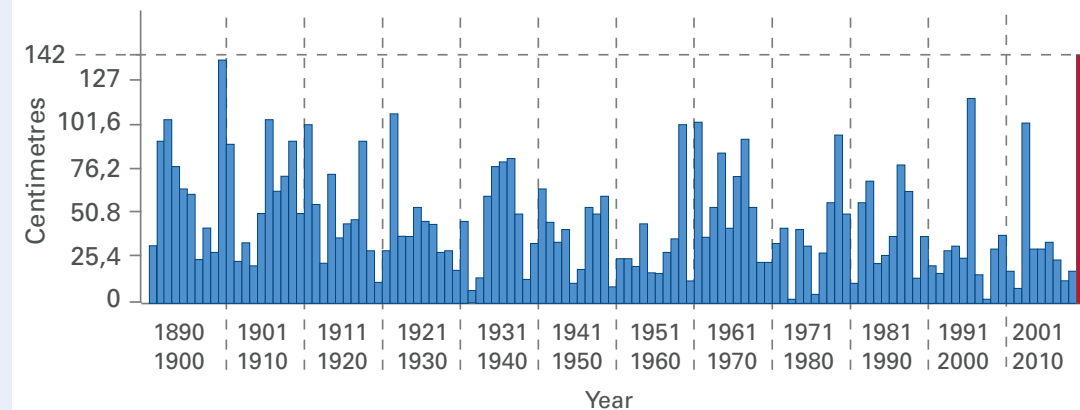


Figure 29. Annual snowfall at the Ronald Reagan Washington National Airport meteorological station for 1888/1889 to 2009/2010. The red bar shows the ~142 cm accumulated snow until 11 February 2010 that broke the previous record from 1898/1899 (source: NOAA National Weather Service).

According to the Arctic Report Card: Update for 2010 (Richter-Menge, Overland, 2010), the boreal winter 2009/2010 showed a new connectivity between mid-latitude extreme cold and snowy weather events on the one hand and changes in the wind patterns of the Arctic on the other. This so-called warm Arctic-cold continents pattern has happened previously only three times in the last 160 years. Higher pressures over the central Arctic allowed cold air from the region to break southward, setting highly contrasted temperature conditions and record-setting snowfalls at lower latitudes.

The cold spells in late January caused at least 450 casualties in Europe. Daily life was affected; air, rail and road transport links were disrupted, schools and many other public services were closed and crops were damaged by frost. Combined with these cold conditions, heavy snowfall in many places caused severe disturbances to ground and air traffic.

Figure 30. Most significant flooding and heavy rainfall reported during 2001–2010 (source: NOAA-NCDC)

4.4.3 Flooding and heavy precipitation

This section provides a summary of the most significant flooding and heavy precipitation events reported to WMO for the period 2001–2010 (Figure 30). A special case study is devoted in this section to the large-scale flooding event which occurred in Pakistan in

July 2010, which affected more than 20 million people and claimed some 2 000 casualties. Elsewhere, numerous other high-impact flooding and heavy precipitation events were recorded during the decade. Table 6 provides a year-by-year detailed list of extreme events related to precipitation and flooding reported during the decade.

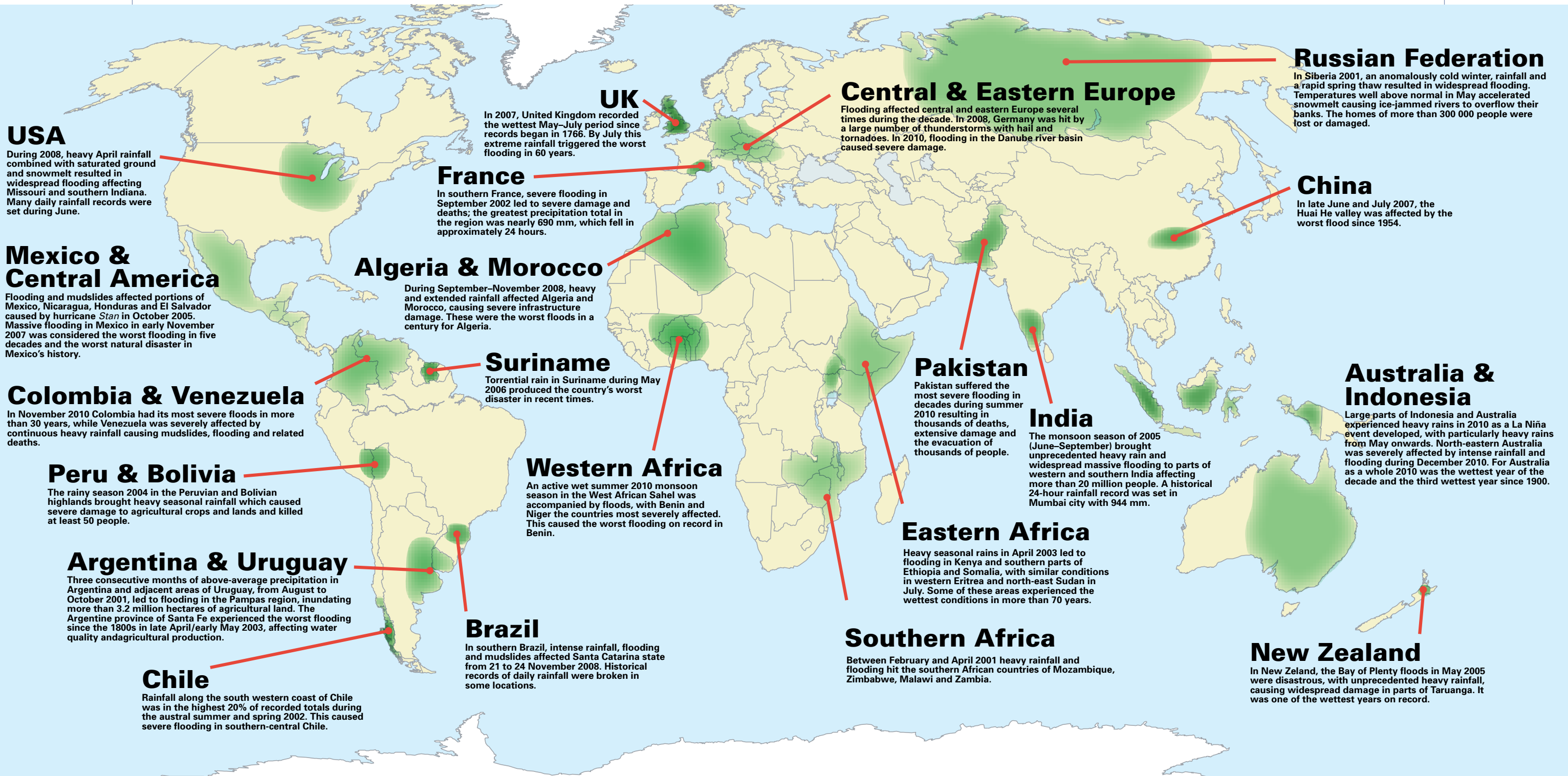


Table 6. Significant flood and precipitation extreme events during the decade 2001–2010 (source: WMO Statements on the Status of the Global Climate)

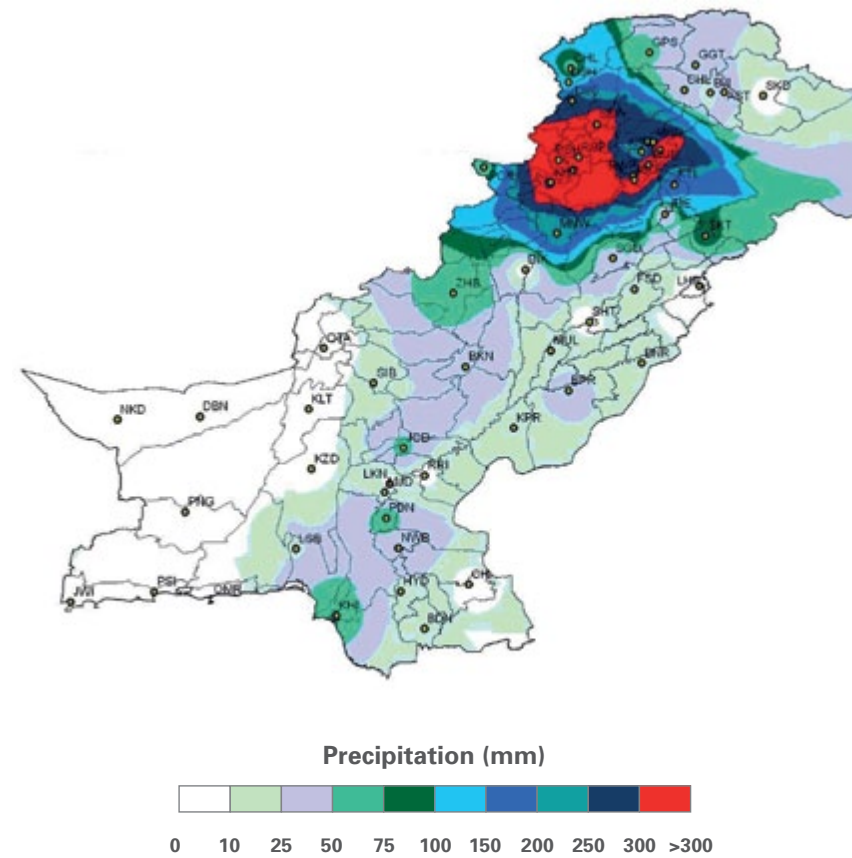
2001	<ul style="list-style-type: none"> • In July, severe floods struck parts of Eastern Europe for the third consecutive year, with Poland being the worst affected. • During November, southern parts of the USA were affected by severe thunderstorms and a daily total rainfall of 250 mm. • Three consecutive months of above-average precipitation in Argentina and adjacent areas of Uruguay, from August to October, led to flooding in the Pampas region. • Rainfall and a rapid spring thaw resulted in widespread flooding in Siberia, Russian Federation. • Because of the dominant influence of La Niña in early 2001, northern and central Australia were affected by above-average precipitation. • Between February and April, heavy rainfall and flooding hit the southern African countries of Malawi, Mozambique, Zambia and Zimbabwe.
2002	<ul style="list-style-type: none"> • Exceptionally heavy rain affected parts of central Europe during the first two weeks of August and led to widespread flooding. • In southern France, severe flooding was recorded in September. The highest precipitation in the region was nearly 690 mm in 24 hours. • Flooding in June produced hundred of millions of US dollars in damage and crop losses in the northern USA, particularly in Minnesota and North Dakota. • Rainfall along the south-western coast of Chile was one of the highest ever recorded during the austral summer and spring and caused severe flooding in southern-central parts. • Heavy rains and amplified mountain glacier meltwater caused flooding in the whole north Caucasus region in June. The flooding on the Terek and nearby rivers exceeded all levels recorded since 1900. • In East Africa, flooding was observed in the southern United Republic of Tanzania in January and in Kenya and Uganda from March to May, when some locations recorded their wettest conditions since 1961.
2003	<ul style="list-style-type: none"> • Severe weather with abundant rainfall and snow caused flooding in many countries across Europe in January, with the largest impact in the Czech Republic. South-eastern France was hit by flooding in early December. • In November, rainfall records were set in portions of coastal British Columbia, Canada, as up to 470 mm of rain in a six-day period caused the worst flooding in a century. • The Argentine province of Santa Fe experienced the worst flooding since the 1800s in late April/early May, which affected water quality and agricultural production. • The monsoon season brought heavy rain and flooding to parts of Pakistan, northern India, Nepal and Bangladesh. The Ganges River reached its highest level since 1975. • Heavy seasonal rains in April led to flooding in Kenya and southern parts of Ethiopia and Somalia, with similar conditions in western Eritrea and north-eastern Sudan in July. Some of these areas experienced the wettest conditions in more than 70 years.

2004	<ul style="list-style-type: none"> • In the Former Yugoslav Republic of Macedonia, heavy rains during 4-7 June produced flooding along the Pena, Vardar, Anska Reka, Trkajna and Turija Rivers. • In April, a storm brought heavy rain to the south-western USA and adjoining Mexico, causing one of the worst flash floods in the region. • Heavy rains triggered mudslides and floods in part of Brazil during January and early February. • The Asian summer monsoon brought heavy rain and flooding to parts of Bangladesh, eastern and southern China, northern India, Nepal and Thailand. • Heavy rains from mid-January to March in areas of Angola produced flooding along the river system, which flows into neighbouring Botswana, Namibia and Zambia.
2005	<ul style="list-style-type: none"> • Heavy rain during May-August led to destructive flooding in Eastern Europe. • Flooding and mudslides, triggered by hurricane <i>Stan</i> in October, affected parts of El Salvador, Honduras, Mexico and Nicaragua. • Heavy January and February rainfall triggered massive flooding in the area of Georgetown, Guyana. • In February, at least two weeks of torrential downpours in Colombia and the Bolivarian Republic of Venezuela caused river flooding and landslides. • Torrential rain during March caused severe flooding across Angola. • The monsoon season brought heavy rain and widespread massive flooding to parts of India. A historical 24-hour rainfall record was set in the city of Mumbai with 944 mm. • In Saudi Arabia, heavy rains during January produced some of the worst flooding in 20 years in the city of Medina.
2006	<ul style="list-style-type: none"> • Heavy rainfall and snowmelt produced extensive flooding along the Danube River in April and the river reached its highest level in more than a century. • Across the mid-Atlantic and north-eastern USA, exceptionally heavy rainfall occurred in June and caused widespread flooding. • Heavy rainfall in the Plurinational State of Bolivia and Ecuador in the first months of the year caused severe flooding and landslides. • Torrential rain in Suriname during May produced the country's worst natural disaster in recent times. • After 500 mm of torrential rainfall during a five-day period in February, a large-scale landslide occurred in Leyte Island, Philippines. • Severe flooding struck Algeria and Morocco. Devastating floods also affected Ethiopia, Kenya and Somalia. Between October and December the Greater Horn of Africa countries experienced heavy rainfall and associated severe flooding.

2007	<ul style="list-style-type: none"> • The United Kingdom recorded the wettest May–July period since records began in 1766. By July, this extreme rainfall had triggered the worst flooding in 60 years. • Heavy rain and flooding during October prompted a deadly mudslide in Costa Rica, resulting in one of the worst weather disasters ever recorded in the country. • Extreme flooding affected the littoral region of Argentina in late March/early April. • In early May, Uruguay was hit by heavy rain and its worst flooding since 1959. • In late June and July, the region of the Huai He valley in China was affected by its worst flood since 1954. Intense monsoon rainfall events caused the worst flooding in years in parts of South Asia. • Flooding continued affecting many African countries as part of summer heavy rainfall. Burkina Faso, Sudan and Uganda suffered the most damage.
2008	<ul style="list-style-type: none"> • Heavy April rainfall combined with saturated ground and snowmelt resulted in widespread flooding affecting Missouri and southern Indiana in the USA. • In southern Brazil, intense rainfall, flooding and mudslides affected Santa Catarina state from 21 to 24 November, when historical records of daily rainfall were broken in some locations. • In South Asia, heavy monsoon rains and torrential downpours produced flash floods. • Australia was hit by widespread flooding in north-eastern parts during January and February. • The worst ever recorded flooding in Zimbabwe occurred in January. • During September–November, heavy and extended rainfall affected Algeria and Morocco. Rainfall amounts up to 200 mm in less than six hours were observed. Algeria had its worst flooding in a century.
2009	<ul style="list-style-type: none"> • In late spring and summer a large number of thunderstorms with heavy rain, hail and tornadoes caused local flooding and significant damage across Germany and in Istanbul, Turkey. • During November, continuous heavy and intense rainfall in north-eastern Argentina, southern Brazil and Uruguay caused flooding in many places. Monthly precipitation records were broken with rainfall exceeding 500 mm in many locations. • Local flooding due to heavy monsoon rains affected north-eastern Australia in January and early February. • Record flooding hit western Africa during September with 263 mm being recorded in less than 12 hours in Burkina Faso, breaking a 90-year record. • Heavy rainfall (70 mm) was recorded on 25 November in Jeddah, Saudi Arabia, causing extreme flash floods and damage.

2010	<ul style="list-style-type: none"> • Central Europe was affected by major flooding during May, particularly in eastern Germany, Poland and Slovakia. • Several north-eastern states of the USA had their wettest March on record and historic flooding in April. • In April, localized flash floods caused severe damage in Rio de Janeiro, Brazil. • In November, Colombia had its most severe flooding in more than 30 years, while the Bolivarian Republic of Venezuela was severely affected by continuous heavy rainfall, causing mudslides and flooding. • Large parts of Australia and Indonesia experienced heavy rains when a La Niña event developed in May. • In Pakistan, heavy monsoon rainfall in June caused the worst flooding since 1929 across parts of the country. • An active wet summer monsoon season in the West African Sahel was accompanied by floods, with Benin and Niger most severely affected. It was the Sahel's wettest year since the mid-1970s.
------	--

Case study C. The severe Pakistan flooding of 2010



Pakistan experienced one of the worst cases of flooding in its history as a result of exceptionally heavy monsoon rains. The event occurred from 26 to 29 July, when four-day rainfall totals exceeded 300 mm over a large area of northern Pakistan. A record-breaking 274 mm of rain fell in Peshawar during 24 hours. Some of the discharge levels were comparable to those seen during the historical flooding events of 1988, 1995 and 1997. In early August, the heaviest flooding moved southward along the Indus River from the northern regions toward western Punjab.

According to EM-DAT/CRED, the Pakistan flood in 2010 was among the 10 most important flood-related disasters worldwide since 1900, sorted by economic damage costs at country level, of US\$ 9.5 billion. The event caused some 2 000 casualties and affected more than 20 million people.

Agriculture was also severely damaged with more than 570 000 ha of cropland destroyed in Punjab (cotton, sugarcane, rice, pulses, tobacco and animal fodder were the most severely impacted agriculture production).

4.4.4 Droughts

Definition of droughts

Meteorological drought is usually defined by a precipitation deficiency threshold over a predetermined period of time. The threshold chosen and duration period will vary by location, according to user needs or applications. Meteorological drought is a natural event and results from multiple causes which differ from region to region.

Agricultural drought is defined more commonly by the availability of soil water to support crop and forage growth than by the departure of normal precipitation over some specified period of time. There is no direct relationship between precipitation and infiltration of precipitation into the soil. Infiltration rates vary, depending on antecedent moisture conditions, slope, soil type and the intensity of the precipitation event. Soil characteristics also differ: some soils have a high water-holding capacity while others do not. The latter are more prone to agricultural drought.

Hydrological drought is even further removed from precipitation deficiency since it is normally defined by the departure of surface- and subsurface-water supplies from some average condition at various points in time. Like agricultural drought, there is no direct relationship between precipitation amounts and the status of surface- and subsurface-water supplies in lakes, reservoirs, aquifers and streams because these hydrological system components are used for multiple and competing purposes, such as irrigation, recreation, tourism, flood control, transportation, hydroelectric power production, domestic water supply, protection of endangered species and environmental and ecosystem management and preservation. There is also a considerable time lag between departures of precipitation and the point at which these deficiencies become evident in surface and subsurface components of the hydrological system. Recovery of these components is slow because of long recharge periods for surface- and subsurface-water supplies.

Socio-economic drought differs markedly from the other types of drought because it reflects the relationship between the supply and demand for some commodity or economic good, such as water, livestock forage or hydroelectric power, which is dependent on precipitation. Supply varies annually as a function of precipitation or water availability. Demand also fluctuates and is often associated with a positive trend as a result of increasing population, development or other factors.

Agricultural, hydrological and socio-economic droughts occur less frequently than meteorological drought, because impacts in these sectors are related to the availability of surface- and subsurface-water supplies. It usually takes several weeks before precipitation deficiencies begin to produce soil-moisture deficiencies leading to stress on crops, pastures and rangeland. Continued dry conditions for several months at a time bring about a decline in streamflow, reduced reservoir and lake levels and, potentially, a lowering of the groundwater table. When drought conditions persist for a period of time, agricultural, hydrological and socio-economic drought occurs, producing associated impacts. During drought, not only are inflows to recharge surface- and subsurface-water supplies reduced but demand for these resources also increases dramatically.

Figure 31. Rainfall over Pakistan during the period 26–29 July 2010 (source: Pakistan Meteorological Department)

Figure 32. Most significant droughts reported during 2001–2010 (source: NOAA-NCDC)

An assessment of the most significant droughts which occurred in different parts of the world is provided in this section with a map locating the severe droughts during the decade (Figure 32) and a summary of drought conditions which were reported to WMO on an annual basis (Table 7). Three special case studies which are included at the end

of the section illustrate examples of long-term, high-impact droughts which occurred in Africa, South America and Australia. The three case studies reflect the type of impacts in these regions on water resources, food production, food security, nutrition and the environment.

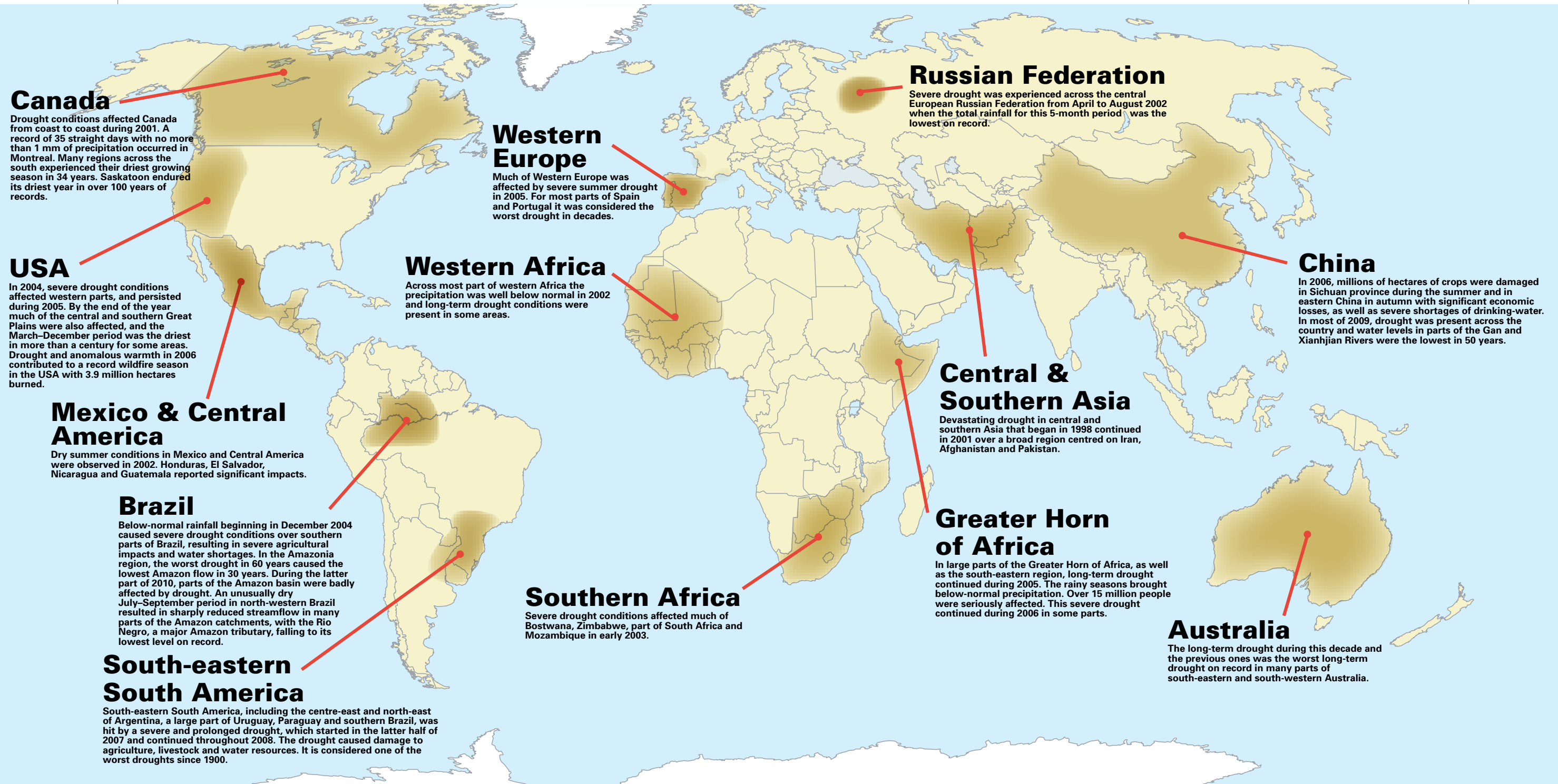


Table 7. Significant droughts during the decade 2001–2010 (source: WMO *Statements on the Status of the Global Climate*)

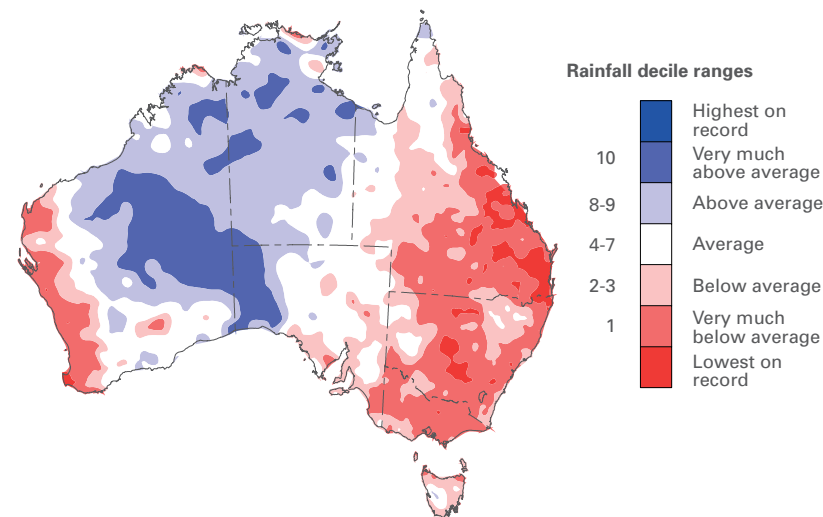
2001	<ul style="list-style-type: none"> • Drought conditions affected Canada, where a record of 35 consecutive days with no more than 1 mm of precipitation occurred in Montreal. Many regions in the south experienced their driest growing season in more than 30 years. • Very dry conditions were prevalent during the austral summer and autumn over much of Brazil. • Devastating drought in central and southern Asia that began in 1998 continued in 2001 over a broad region centered on Afghanistan, the Islamic Republic of Iran and Pakistan. • Persistent drought during 2001–2002 affected Jordan, causing serious impacts on crop production and drinking-water. • Drought in parts of Kenya and neighbouring countries in the Greater Horn of Africa continued. • The long-season rains (March–May) were well below normal in some parts of north-eastern Kenya which experienced one of their driest months of May since 1961.
2002	<ul style="list-style-type: none"> • The central European Russian Federation experienced a period of severe drought from April to August, resulting in one of the lowest total precipitations for this five-month period on record. • Dry summer conditions in Mexico and Central America were observed. El Salvador, Guatemala, Honduras and Nicaragua reported significant agricultural impacts. • Dryness persisted in north-eastern Brazil, especially during the normal rainy season (December–May). • Across most parts of western Africa, the precipitation was well below normal and long-term drought conditions were present in some areas.
2003	<ul style="list-style-type: none"> • Severe drought in Europe adversely affected agriculture, electricity and water supply. France, Portugal, Spain and countries in central and Eastern Europe also suffered from fierce forest fires. • Near the end of the year, about 37 per cent of the USA was classified as having a moderate-to-extreme drought. • Australia was affected by dry conditions and record warmth. This combination led to devastating wildfires in the south-east in January and February. • Severe drought conditions affected much of Botswana, parts of South Africa and Mozambique and Zimbabwe in the early months.
2004	<ul style="list-style-type: none"> • The fifth year in a row with severe drought conditions in some areas of the western USA. • A prolonged drought affected and severely threatened food security and health in the south-eastern El Chaco region of the Plurinational State of Bolivia. • The north-eastern part of China was affected by severe drought during spring, while the southern provinces were affected during autumn. • At the beginning of the year, drought conditions continued to affect parts of Lesotho, Mozambique, eastern South Africa and Swaziland. • Across parts of the Greater Horn of Africa, precipitation during both rainy seasons was well below normal, resulting in the continuation of the multi-seasonal drought.

2005	<ul style="list-style-type: none"> • Much of western Europe was affected by severe summer drought. In most parts of Portugal and Spain, it was considered the worst drought in decades. Dry conditions also aggravated wildfires in the region. • By the end of the year, much of central USA was severely affected by drought and the March–December period was reported as the driest in more than a century for some areas. • Severe drought conditions starting in December led to severe agricultural impacts and water shortages in southern Brazil. • In the Amazonas region, the worst drought in 60 years caused the lowest Amazon flow in 30 years. • The period January–May was exceptionally dry for much of Australia with 44 per cent of the continent experiencing precipitation in the lowest decile. • In large parts of the Greater Horn of Africa, as well as the south-eastern region, long-term drought continued during the year.
2006	<ul style="list-style-type: none"> • Dry conditions in combination with anomalous warmth contributed to a record wildfire season in the USA. • Drought conditions in southern Brazil persisted in the early part of the year. • Because of droughts, millions of hectares of crops were damaged in Sichuan province during the summer and in eastern China in autumn. • Long-term drought continued in parts of the Greater Horn of Africa, including parts of Burundi, Djibouti, Eritrea, Ethiopia, Kenya, Somalia and the United Republic of Tanzania.
2007	<ul style="list-style-type: none"> • A strong drought combined with a persistent heatwave hit Romania in the summer and was its most severe since 1945/1946. • Severe-to-extreme drought was present across large parts of the western USA and the upper mid-west, as well as southern Ontario, Canada. • South-eastern South America, including the central-east and north-east of Argentina, large parts of Paraguay, Uruguay and southern Brazil were hit by a severe and prolonged drought, starting in the latter half of the year. • Six consecutive years (2002–2007) of drought in the Australian Murray-Darling Basin constituted one of the worst long-term droughts in the nation's history. These conditions persisted in some areas until 2009.
2008	<ul style="list-style-type: none"> • Portugal and Spain experienced their worst winter drought in decades. • In Canada, southern British Columbia experienced one of the driest periods in more than six decades. • The continuous dry conditions across northern and central California, USA, resulted in numerous large wildfires. • Drought continued in south-eastern South America throughout the year and is considered one of the worst droughts since 1900.
2009	<ul style="list-style-type: none"> • Mexico experienced severe-to-exceptional drought conditions. • In central Argentina, dry conditions persisted during most of the year. • Drought was present across China and water levels in parts of the Gan and Xianhjian Rivers were the lowest in 50 years.
2010	<ul style="list-style-type: none"> • Extreme warmth across the Russian Federation exacerbated drought conditions, resulting in the worst drought since 1972. • The United Kingdom had its driest January–June period since 1929. • The driest winter (December 2009–February 2010) in Canada on record. • An unusually dry July–September period in north-western Brazil resulted in sharply reduced streamflow in many parts of the Amazon catchments. • The driest monsoon season for Bangladesh since 1994. • The south-west of Australia had its driest year on record. • Dry conditions developed during the later months in parts of East Africa, particularly in equatorial regions of Kenya and the United Republic of Tanzania.

Case study D1. Long-term drought in Australia

Dry periods are a natural part of life in Australia, particularly in the marginal areas away from the coast and ranges. Lying directly under the subtropical belt of high pressure, much of Australia experiences low, but highly variable precipitation, and years with well-below-normal rain are to be expected.

Several major droughts affected Australia during the 19th and 20th centuries, underlining that this is part of climate variability in this region. The long-term drought observed during this decade (and late in the previous decade in places), however, was the worst on record in many parts of south-eastern and south-western Australia (Figure 33). According to the analysis made by the Australian Bureau of Meteorology, this long-lasting dry period commenced in the late 1990s and extended throughout the 2000s. Long-term dry conditions first became established in the south-west and south-east in 1997.



During 2000 and early 2001, much of Australia experienced wet weather brought by a strong La Niña episode which influenced weather patterns, but these rains largely missed the south-west, as well as the east coast from Brisbane southwards. By 2002, precipitation over the continent dropped to very low amounts and widespread dry conditions resulted in one of the driest years on record. Near-normal precipitation was observed in most areas during 2003 and 2004 but recovery from the precipitation deficiencies that had accumulated during the severe 2002/2003 El Niño-related drought was slow and patchy. Well-above-normal temperatures also limited the potential for a full recovery.

The early months of 2005 were very warm and dry and, despite near- to above-normal precipitation during the second half of the year, the lack of sustained above-normal precipitation led to the continuation of multi-year droughts in parts of Australia, particularly in the south-east. The exceptionally dry year of 2006 was the driest on record for many parts of south-western and south-eastern Australia, reinforcing the long-term drought conditions there. Above-normal precipitation along the east coast and the subtropical eastern inland during 2007 and 2008 eased this long-term drought,

Figure 33. Australian rainfall deciles for the period 1 June 2001 to 31 May 2007; deciles are calculated relative to the period 1900–2010, based on gridded data (source: Bureau of Meteorology, Australia).

particularly in the Sydney and Brisbane area, but conditions continued unabated in other parts of the south-east and south-west, with Melbourne experiencing 13 consecutive years of below-average precipitation from 1997 to 2009. During this period, South-east Australia was deprived of the equivalent of more than an average year's precipitation, making the current drought one of Australia's most severe on record – comparable in terms of precipitation deficiencies with the federation drought (1895–1903) and that of 1938–1946. The latest drought, however, was notable for its record high temperatures and record low inflows to water storages, especially in the agriculturally important Murray-Darling Basin, which experienced the lowest inflows in its history. The long-term drought in eastern Australia was finally broken, except in a few small parts of southern Victoria, in the second half of 2010, as a result of prolonged heavy rains associated with a strong La Niña event. It intensified in the south-west, however, where 2010 was the driest year on record.

Agricultural production was severely affected. Australia's cotton production dropped with the smallest area planted in 20 years. The crop was almost half its usual size for several years. Water use by the industry fell by 37 per cent in 2000–2001 and 2004–2005. There were also severe restrictions on water use in all the major cities of mainland eastern Australia at the peak of the drought.

Case study D2. Long-term drought in the Amazon Basin

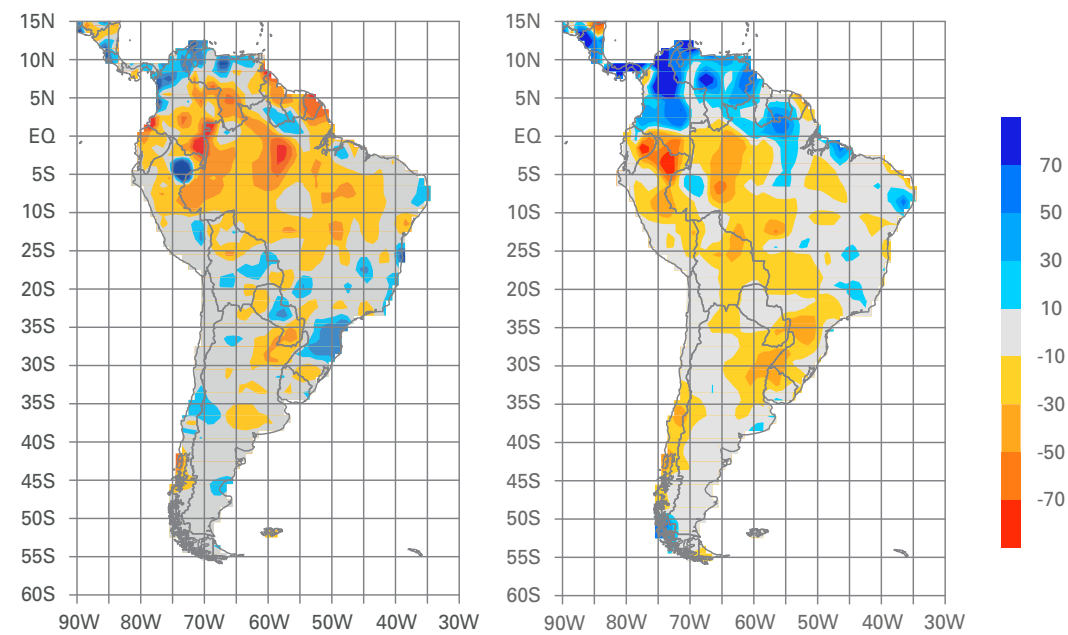
The Amazon Basin is the part of South America drained by the Amazon River and its tributaries, covering an area of nearly 7 million km², or roughly 40 per cent of South America. It is located in Bolivia (Plurinational State of), Brazil, Colombia, Ecuador, Guyana, Peru and Venezuela (Bolivarian Republic of).

The Amazon Basin is bounded by the Guiana Highlands to the north and the Brazilian Highlands to the south. The Amazon, which rises in the Andes Mountains at the west of the basin, is the second longest river in the world. It covers a distance of about 6 400 km before draining into the Atlantic Ocean. The Amazon and its tributaries form the largest volume of water of any river system in the world, accounting for about 20 per cent of the total water carried to the oceans by rivers. Some of the Amazon Basin has been deforested because of a growing interest in hardwood products. The Amazon River Basin has a low-water season, from May to November, and a wet season, from December to April, during which the rivers flood adjacent low-lying forests.

During the decade 2001–2010, large parts of this basin were affected by prolonged droughts with severe regional impacts. The most significant precipitation anomalies occurred during 2005 and 2010 (Figure 34), with the 2010 drought having the more severe impact on streamflow. An unusually dry July–September period in north-western Brazil resulted in sharply reduced streamflow in many parts of the Amazon catchments, with the Rio Negro, a major Amazon tributary, falling to its lowest level since record-keeping began in 1902.

Following the 2005 severe drought, scientists were able to study the impact on trees and to estimate the relationship between rainfall loss and the release of carbon. In an average year, the basin absorbs some 1.5 billion tonnes of CO₂ from the atmosphere.

Figure 34. Precipitation anomaly for South America in June–November 2005 (left) and June–November 2010 (right); gridded 1° raingauge-based analysis. The map shows normalized departures in mm/year from the 1951–2000 period average (source: GPCC-DWD)



Analysing the impact of the severe Amazon drought of 2005, a team of 68 researchers from 13 countries found evidence that rainfall-starved tropical forests lose massive amounts of carbon because of reduced plant growth and dying trees. The 2005 drought – triggered by warming in the tropical North Atlantic – resulted in a net flux of 5 billion tons of CO₂ into the atmosphere – more than the combined annual emissions of Japan and Europe – relative to normal years, when the Amazon is a net sink for 2 billion tons of CO₂ (R.A. Butler).

Case study D3. Long-term drought in East Africa

Drought in Africa in general, and sub-Saharan Africa in particular, strongly affects socio-economic conditions. It leads to severe consequences for agriculture, food supply and employment. East Africa has two rainy seasons: the short rainy season extending from October to December and the long rainy season extending from March to June.

During the current decade, severe and prolonged droughts were recorded in the Greater Horn of Africa, a region consisting of nine East African nations: Djibouti, Eritrea, Ethiopia, Kenya, Somalia, Sudan, South Sudan, Uganda and the United Republic of Tanzania, as well as in the southern part of the continent.

During 2004 and 2005, southern Somalia, eastern Kenya, south-eastern Ethiopia, north-eastern United Republic of Tanzania and Djibouti recorded below-normal precipitation in both rainy seasons, resulting in a continuation of a multi-season drought.

In 2004–2005, over 11 million people in Ethiopia, Djibouti, Somalia and Kenya were at risk of starvation due to the effects of the prolonged drought. Further south, the drought caused serious shortfalls in the cereal harvest in Angola, Malawi, Mozambique and Zimbabwe. At least 5 million people in Malawi were threatened with hunger as a result of one of the worst droughts in more than 10 years (source: WMO Statements on the Status of the Global Climate).

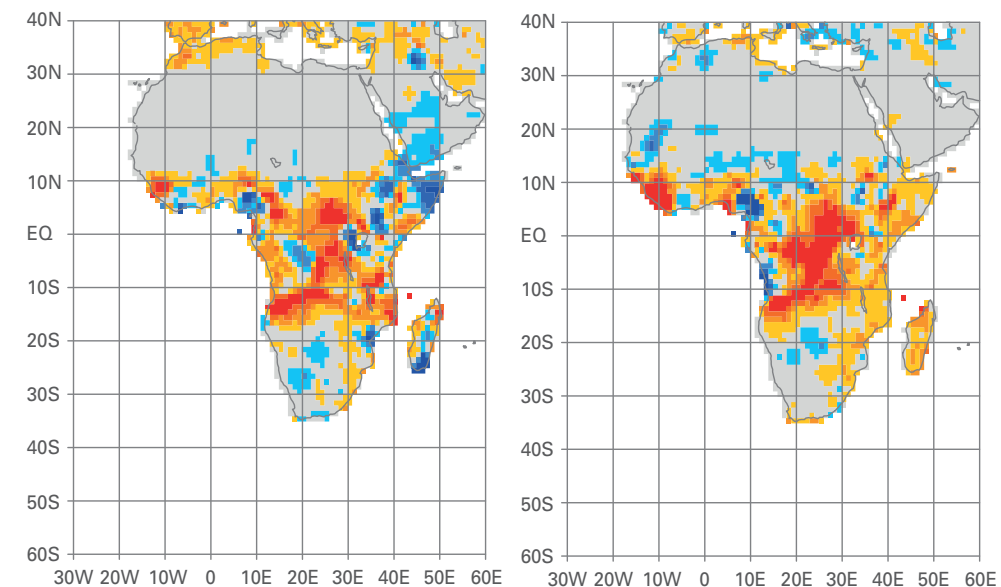
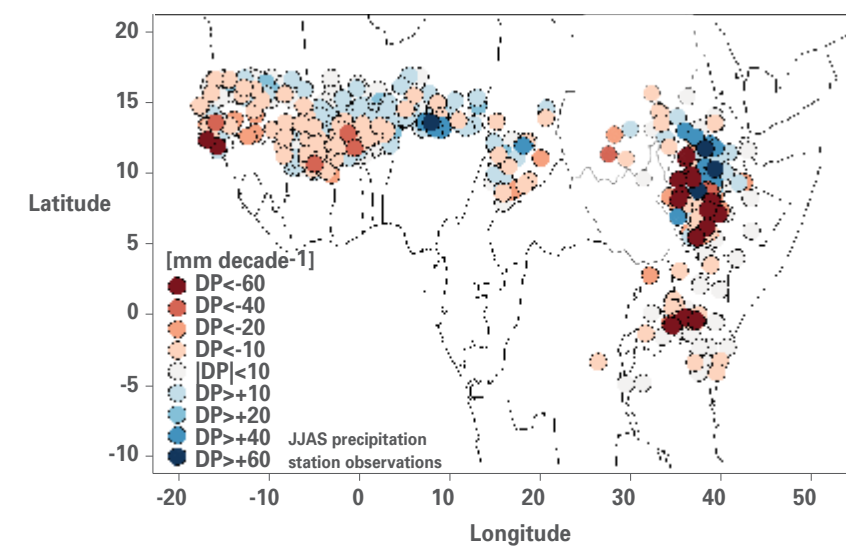
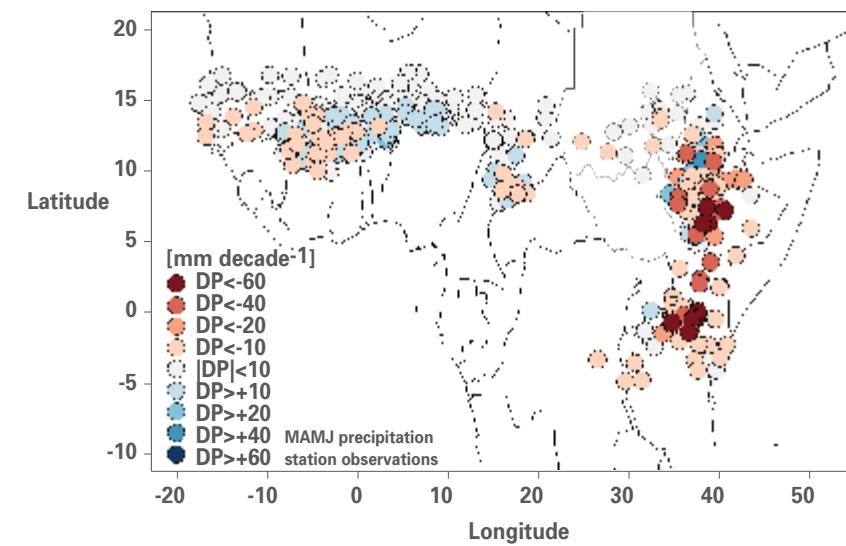


Figure 35. Station observations of differences in precipitation (DP) between the 1960–1989 average and the 2000–2009 average for March to June (above) and June to September (below) (source: US Geological Survey, Famine Early Warning System, 2011)

Figure 36. Observed 2004–2005 precipitation anomalies in Africa: March–May 2005 (left) and September–November 2005 (right), gridded 1° raingauge-based analysis as normalized departures in mm/month based on 1951–2000 base period (source: GPCC-DWD)

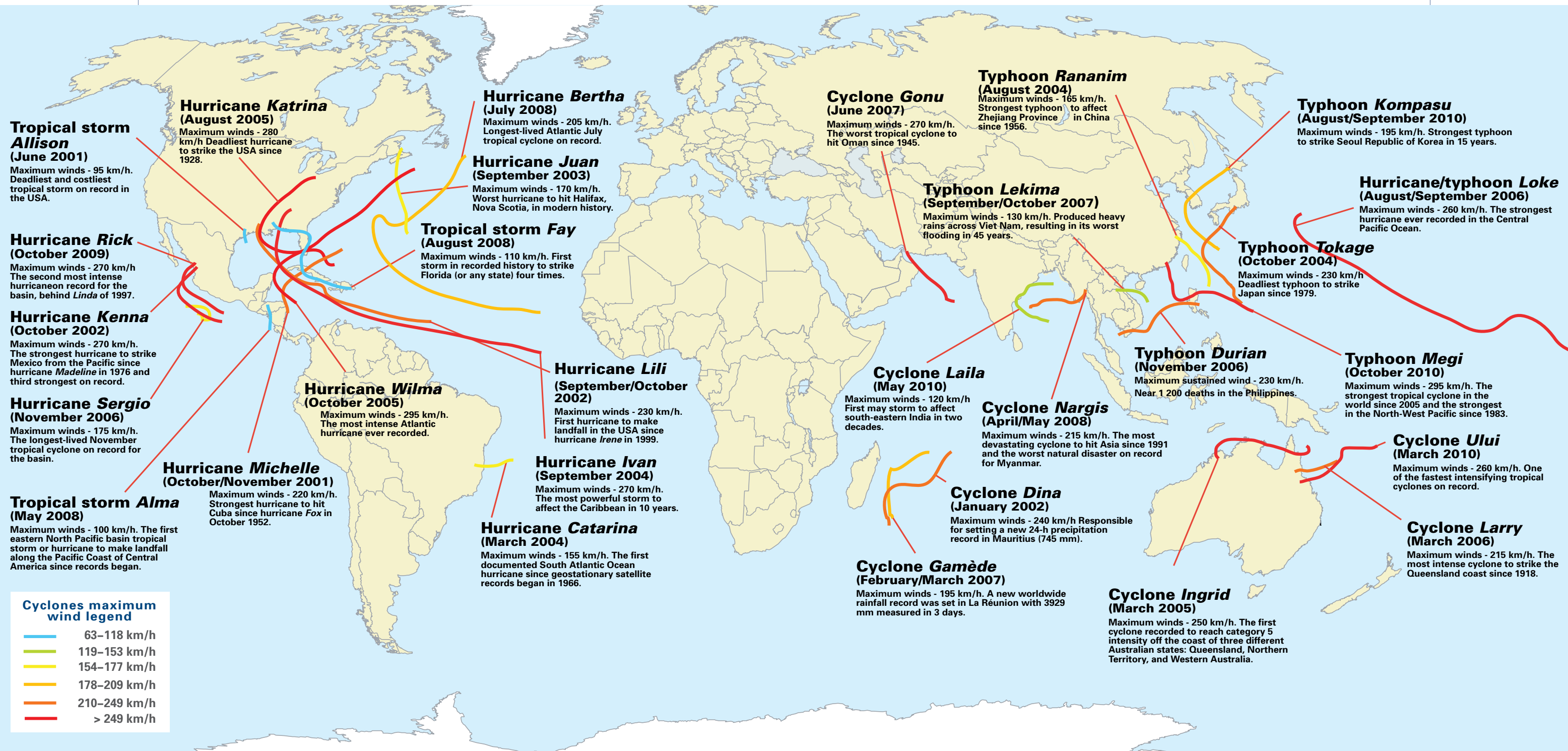
Figure 37. Most significant tropical cyclones recorded during 2001–2010 (source: NOAA-NCDC).

4.5 Severe storms

4.5.1 Tropical cyclones

Figure 37 provides the geographical and main meteorological characteristics of the most significant tropical cyclones recorded during the decade 2001–2010. A historical context is also provided, when available.

Two special case studies in this section are devoted to the two most devastating tropical cyclones which occurred in the decade 2001–2020: hurricane *Katrina*, which struck the USA in August 2005, was the costliest and one of the five deadliest hurricanes ever to strike the USA; and tropical cyclone *Nargis*, which affected Myanmar in April/May, leaving more than 80 000 casualties.



This section provides statistical details on tropical cyclone activities during the decade in the five oceanic basins: North Atlantic; Eastern North Pacific; North-West Pacific; South-West Indian Ocean; and Australia and South-West Pacific. During the decade, the North Atlantic basin recorded above-average tropical cyclone activity, while other basins recorded near- or below-average activity (Figure 38).

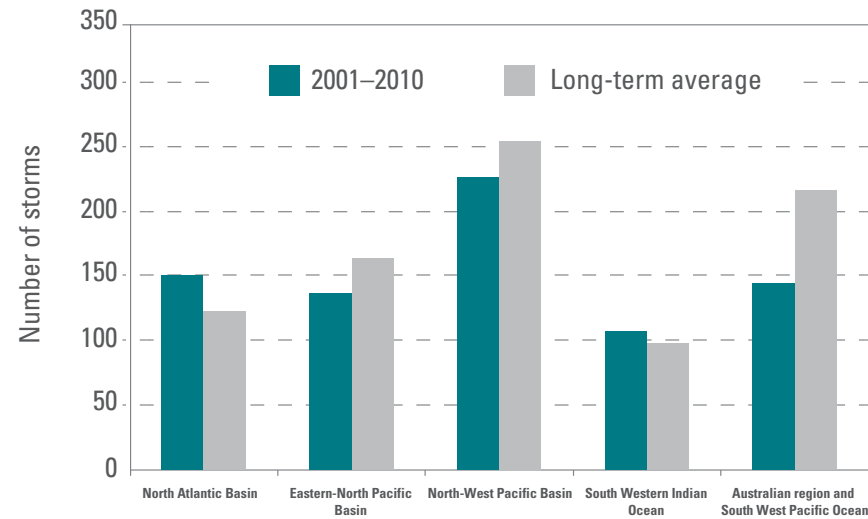


Figure 38. Total number of named tropical storms during 2001–2010 by basin compared to the long-term average of the 1981–2010 base period (data source: NOAA-NCDC)

North Atlantic basin

According to NOAA’s NCDC database, 2001–2010 was the most active decade since 1855 in terms of tropical cyclone activity. An average of 15 named storms per year was recorded, well above the 1981–2010 long-term average of 12 named storms per year. Only 2006 and 2009 recorded slightly below-average numbers of storms. On an annual basis (Figure 39), the most active season ever recorded was 2005, with a total of 27 named storms, of which 15 reached hurricane intensity and seven were classified as major hurricanes (Category-3 or higher). The 2005 hurricane season broke the previous record for named storms (21 in 1933) and hurricanes (12 in 1969). The year 2005 ranked as second on record for the highest number of major hurricanes behind 1950, which

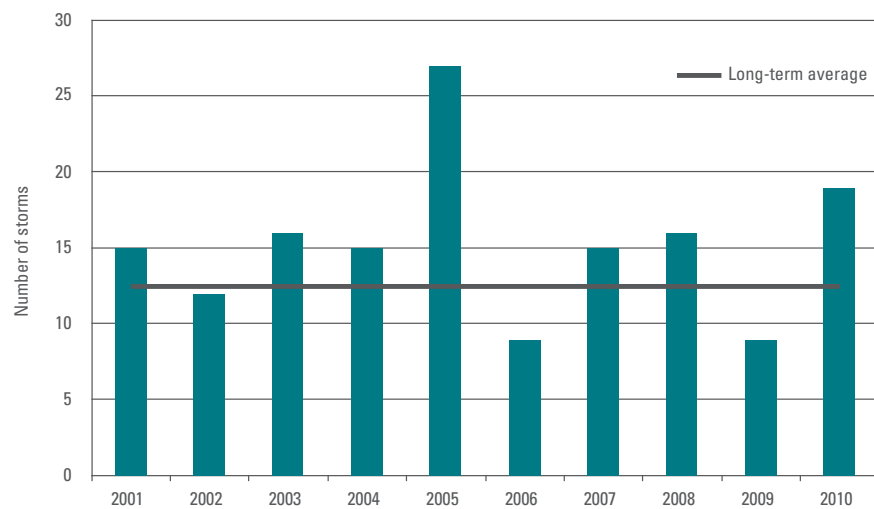


Figure 39. Total storms per year compared to the long-term average of the 1981–2010 base period in the North Atlantic basin (data source: National Hurricane Center (NHC), NOAA); WMO Statements on the Status of the Global Climate).

Note: In the South Atlantic Ocean, SST and atmospheric conditions do not favour the formation of hurricanes. Nevertheless, the first documented hurricane developed in the southern Atlantic Ocean in March 2004. Unofficially named *Catarina*, it made landfall along the southern coast of Brazil and caused significant damage.

had eight major hurricanes. *Katrina*, a Category-5 hurricane, was the most devastating of the decade, making landfall in the southern USA in August 2005. It is also considered the deadliest hurricane to hit the USA since 1928. In the same year, hurricane *Wilma* had the lowest central pressure ever recorded for the Atlantic basin. *Wilma* was a Category-4 hurricane at its landfall in Mexico and Category-3 in Florida.

Year	Category	Name	Places mostly affected	Impact
2001	Tropical storm	<i>Allison</i>	South-eastern Texas, USA	More than 800 mm rainfall; 41 deaths US\$ 5 billion property damage
	Hurricane (4)	<i>Michelle</i>	Cuba, Honduras, Jamaica and Nicaragua	Heavy rain, flooding, 17 deaths
	Hurricane (4)	<i>Iris</i>	Southern Belize, Dominican Republic, Guatemala	Significant flooding and flash floods, 20 deaths confirmed in Belize; damage of US\$ 66.2 million reported
2003	Hurricane (5)	<i>Isabel</i>	Eastern USA	17 deaths, damage estimated at US\$ 3.4 billion
2004	Hurricane (5)	<i>Ivan</i>	Caribbean and south-eastern USA	Flooding; massive destruction; 92 deaths
	Hurricane (3)	<i>Jeanne</i>	Haiti	Flooding; over 3 000 lives lost
2005	Hurricane (5)	<i>Katrina</i>	Louisiana and Mississippi, USA	Storm-surge-induced flooding; more than 1 800 deaths, damage estimated at US\$ 108 billion
	Hurricane (5)	<i>Rita</i>	Texas, USA	Storm surge and floods
	Hurricane (5)	<i>Wilma</i>	South-eastern Mexico and Florida, USA	Major flooding from storm surge
2008	Hurricane (4)	<i>Gustav</i>	Caribbean and Louisiana, USA	341 km/h wind gusts; hundreds of fatalities
	Hurricane (5)	<i>Ike</i>	Caribbean and USA Gulf Coast	Several hundred deaths, one of the most destructive hurricanes ever

Table 8. Some of the most significant tropical cyclones and their impacts in the North Atlantic basin during 2001–2010 (sorted by year)

Case study E1. Hurricane *Katrina*

Katrina was a very powerful hurricane that was responsible for catastrophic damage and a large loss of life. It was the costliest and one of the five deadliest hurricanes to strike the USA. On 25 August 2005, *Katrina* first caused fatalities and damage in southern Florida as a Category-1 hurricane on the Saffir-Simpson Hurricane Scale. After reaching Category-5 intensity over the central Gulf of Mexico, *Katrina* weakened to Category 3 before making landfall on 29 August 2005 on the northern Gulf coast (Figure 40), a part of the USA coastline that is particularly vulnerable to storm surge. The damage and loss of life inflicted by this massive hurricane in Louisiana and Mississippi were staggering, with significant effects extending into the Florida panhandle, Georgia and Alabama. The massive storm surge produced by *Katrina*, even though it had weakened from Category-5 intensity the previous day to Category 3 at landfall in Louisiana, can generally be explained by the huge size of the storm. Precipitation amounts during landfall along the northern Gulf coast were greatest along and just west of the track of the centre. A large precipitation amount of 200–250 mm fell across south-eastern Louisiana and south-western Mississippi, with 250–300 mm over eastern Louisiana. A total of 43 reported tornadoes were spawned by *Katrina*.



Katrina is surpassed by the Galveston (Texas) hurricane in 1900 that claimed at least 8 000 lives, and by the 1928 Lake Okeechobee (Florida) hurricane with over 2 500 fatalities. Based on the recorded fatalities (direct and indirect), *Katrina* ranks as the third deadliest hurricane in the USA since 1900. Thousands of homes and businesses throughout entire neighbourhoods in the New Orleans metropolitan area were destroyed by floods. Strong winds caused significant tree damage throughout much of Mississippi and Alabama. Combining all the areas it impacted, *Katrina* left some three million people without electricity, some for several weeks (source: NOAA-NCDC).

Figure 40. Satellite image of hurricane *Katrina* on 29 August 2005 at 10:15 ETZ (source: NOAA's Geostationary Operational Environmental Satellite (GOES))

Eastern North Pacific basin

A total of 139 named storms were recorded in this basin during the decade 2001–2010, and 65 of them were classified as hurricanes. Compared to the long-term average of 16 storms per year, the activity during the decade was slightly below normal in most years. On a yearly basis (Figure 41), the most active seasons were observed in 2006 and 2009 and the least active in 2007 and 2010. The majority of these tropical cyclones did not make landfall and caused no substantial damage. There were some exceptions, such as hurricane *Kenna* in 2002, which was the third strongest hurricane to strike Mexico from the Pacific and resulted in four deaths and thousands of people

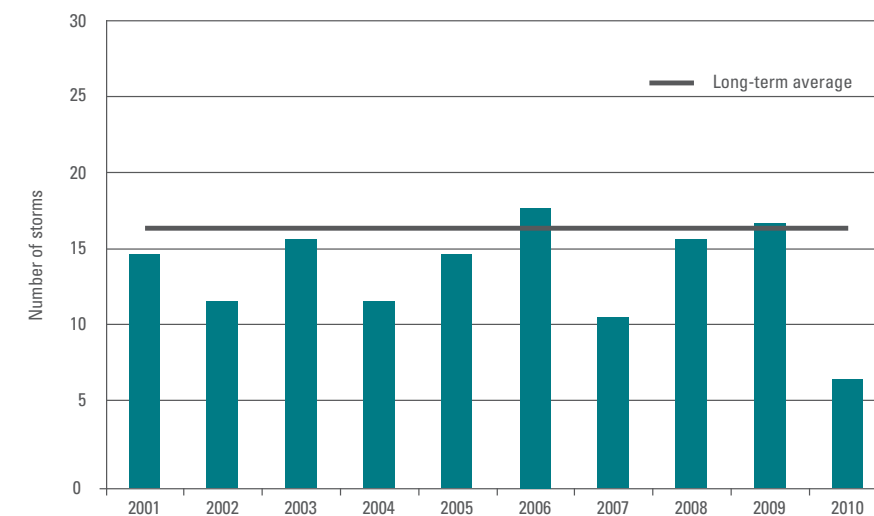


Figure 41. Total storms per year compared to the long-term average of the 1981–2010 base period in the eastern North Pacific basin (data source: NHC, *Statements on the Status of the Global Climate*)

left homeless. Another hurricane to make landfall was *Marty* in 2003, which caused severe damage and deaths in southern Baja California (Mexico). In September 2006, hurricane *Lane* made landfall in western Mexico, recording winds up to 204 km/h and causing flooding and landslides in some parts of the region. *Norbert* made landfall as a Category-2 hurricane on the Baja California Peninsula in October 2008 and later as a Category-1 in mainland Mexico. It caused damage and was blamed for five deaths. In October 2009, with maximum winds of 285 km/h, hurricane *Rick* became the second most intense hurricane on record for this basin, behind *Linda* in 1997.

North-West Pacific basin

In the North-West Pacific a total of 230 tropical cyclones formed during the decade. This is slightly below the long-term average of 260. The 2004 season was the most active of the decade, when 29 tropical cyclones developed, of which 19 were classified as typhoons. The other years of the decade recorded near or less than average tropical cyclone activity (Figure 42). In the least active season in 2010, only 14 named storms formed. Several of these cyclones and typhoons made landfall in south-eastern Asia, causing flooding and associated fatalities and severe damage to infrastructure and people's homes. Some of the most destructive and deadliest cyclones are indicated in Table 9.

Figure 42. Total storms per year compared to the long-term average of the 1981–2010 base period in the North-West Pacific basin (data source: NHC, WMO Statements on the Status of the Global Climate)

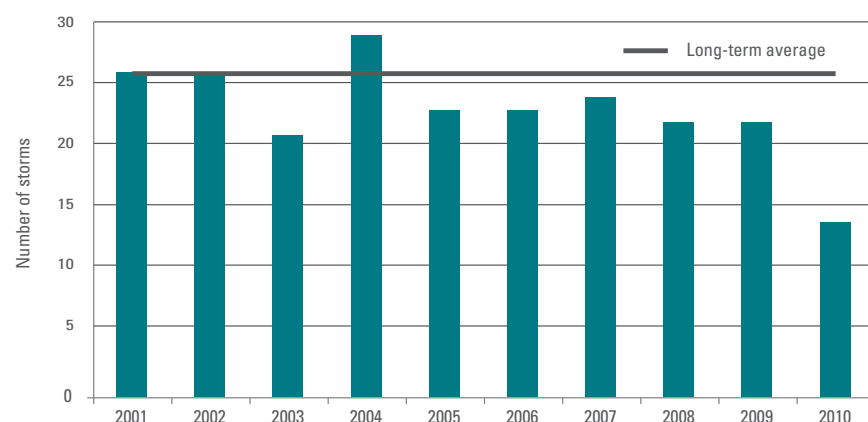


Table 9. Some of the most significant tropical cyclones and their impacts in the North-West Pacific basin during 2001–2010

Year	Category	Name	Places affected	Damage caused
2001	Typhoon	<i>Chebi</i>	Fujian province, China	Flooding; more than 150 deaths
2002	Typhoon	<i>Rusa</i>	Republic of Korea	Flooding; more than 240 deaths
2003	Typhoon	<i>Maemi</i>	Japan, Republic of Korea	Property damage; more than 130 fatalities
2004	Typhoon	<i>Tokage</i>	Japan	Floods; landslides; more than 200 deaths
	Typhoon	<i>Rananim</i>	Zhejiang, China	169 fatalities
2005	Typhoon	<i>Talim</i>	South-eastern China	Flooding; 150 deaths
2006	Typhoon	<i>Durian</i>	Philippines	More than 1 000 deaths; 1.5 million people affected
2007	Typhoon	<i>Lekima</i>	Viet Nam	Worst flooding in 45 years
2008	Typhoon	<i>Fengshen</i>	Philippines	Maritime disaster; winds up to 205 km/h
2009	Typhoon	<i>Morakot</i>	Taiwan Province of China	Severe damage to agriculture and infrastructure; more than 600 deaths
2010	Typhoon	<i>Megi</i>	Northern Philippines, Taiwan Province of China, Fujian Province of China	Widespread damage to infrastructure and agriculture

South-West Indian Ocean

There was near-average tropical storm activity in this region during the 2001–2010 decade. The most active season was observed in 2009 with a total of 16 tropical storms and seven cyclones. On the other hand, 2001 had the least active season with only five tropical storms recorded (Figure 43).

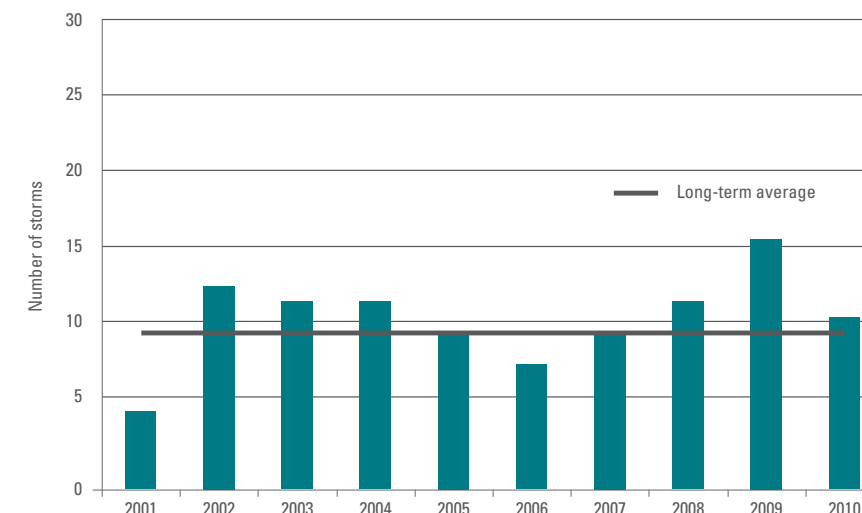


Figure 43. Total storms per year compared to the long-term average of the 1981–2010 base period in the South-West Indian Ocean (data source: NHC, WMO Statements on the Status of the Global Climate)

In 2002, tropical cyclone *Dina* was responsible for a new record of 24-hour precipitation in Mauritius with a total of 745 mm of rain reported. In 2004, tropical cyclone *Gafilo* hit Madagascar, making landfall with winds up to 260 km/h and causing 237 deaths. Tropical cyclone *Gamède* developed in February 2007 and dumped nearly 4 000 mm of rain in a 72-hour period on the French island of La Réunion, resulting in a new worldwide rainfall record.

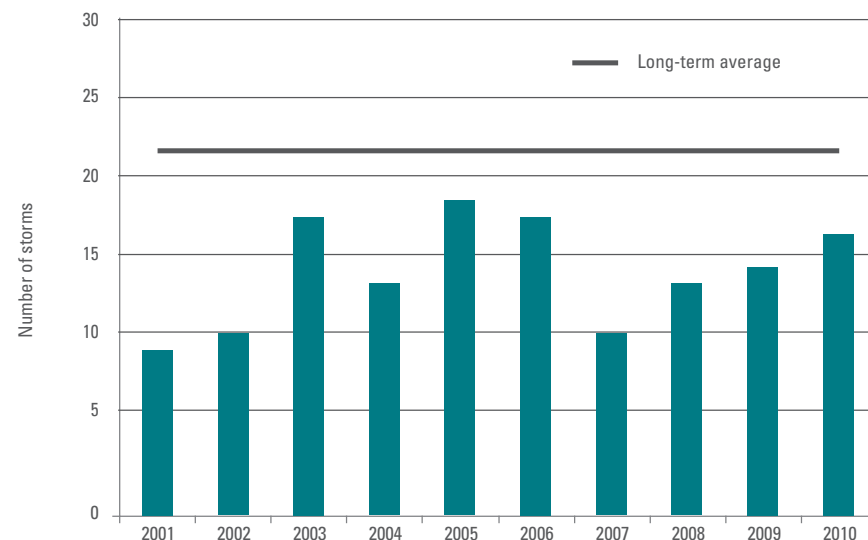
North Indian Ocean

The deadliest tropical cyclone recorded during the 2001–2010 decade was *Nargis*, which developed in the North Indian Ocean and hit Myanmar in early May 2008. More than 138 000 people (EM-DAT/CRED) were reported killed or missing and thousands of homes were destroyed. It was the most devastating cyclone to hit Asia since 1991 and resulted in the worst natural disaster on record for Myanmar. *Nargis* was among the world's deadliest natural disasters of the decade after the Haiti earthquake in 2010, which killed over 220 000 people and the 2004 Indian Ocean tsunami, which caused more than 160 000 fatalities.

In the North Indian Ocean, some other devastating tropical cyclones were observed during the decade, causing damage and deaths. In April 2006, tropical cyclone *Mala* reached maximum winds of more than 200 km/h and hit the coast of Myanmar. In June 2007, tropical cyclone *Gonu* made landfall in Oman, affecting more than 20 000 people before reaching the Islamic Republic of Iran. It was considered the worst tropical cyclone to hit the region since 1945. During the same year, in November, tropical cyclone *Sidr* hit Bangladesh, affecting more than 8 million people and causing more than 3 000 fatalities. Maximum winds of 240 km/h were recorded at landfall. The severe cyclonic storm *Phet* over the Arabian Sea during 2010 had an unusual track, with two landfall points over Oman and Pakistan, and the longest track in recent years for this basin.

Australian and South Pacific Ocean

Tropical cyclone activity was below the long-term average in the 2001-2010 decade¹ in both the Australian and South Pacific regions (Figure 44). There were 88 tropical cyclones during the decade in the Australian region (90°E to 160°E) and 61 in the South Pacific (east of 160°E), compared with the long-term averages of approximately 110 and 80, respectively. The only substantially above-normal season in either region was the 2002/2003 season in the South Pacific, associated with a strong El Niño event, which had 11 cyclones. The most active season in the Australian region was 2005/2006 with 12 cyclones. The least active seasons were 2006/2007 in the Australian region (five cyclones) and 2003/2004 in the South Pacific (three cyclones). Both of these equalled the least active seasons since the beginning of satellite observations.



The decade saw the most intense cyclones on record in both regions. *Zoe* (maximum sustained winds of 245 km/h) hit the Solomon Islands in December 2002, with severe damage on the remote island of Tikopia but no casualties. *Monica* (maximum sustained winds 250 km/h) made landfall in an unpopulated area east of Darwin after tracking along the northern coast of Northern Territory in April 2006, with only minor damage. *Inigo* also reached maximum sustained winds of 245 km/h off the western coast of Australia in 2003 but did not make landfall.

By far the worst tropical cyclone in terms of casualties was *Guba* in November 2007, with at least 150 lives lost in Papua New Guinea as a result of flooding from heavy rains as the system developed. *Larry* (March 2006) was the most intense landfall in Queensland since 1918 and caused an estimated US\$ 470 million damage in the Innisfail area, but no deaths. A sequence of four intense cyclones in five weeks in February and early March 2005, *Meena*, *Nancy*, *Olaf* and *Percy* caused widespread damage in the Cook Islands, American Samoa and Tokelau, while other destructive cyclones in the South Pacific included *Waka* (December 2001, Tonga), *Heta* (January 2004, Niue) and *Oli* (February 2010, French Polynesia).

¹ For the purposes of this report, this is taken to be the tropical cyclone seasons from 2000/2001 to 2009/2010 inclusive, thus including some cyclones in late 2000 and excluding some in late 2010.

Case study E2. Cyclone Nargis

(source: http://www.gfdr.org/gfdr/sites/gfdr.org/files/documents/Myanmar_PDNA_GLANCE.pdf)

Myanmar is the second largest country in mainland South-East Asia with a total land area of 676 578 km², and a population of 51.5 million. About one-third of its total perimeter forms its coastline along the Bay of Bengal and Andaman Sea. It lies in the monsoon region of Asia, with its coastal regions receiving over 5 000 mm of rain annually. The country is prone to cyclones, landslides, and earthquakes.

The Category-3 cyclone *Nargis* struck Myanmar on 2 and 3 May 2008, making landfall in the Ayeyarwady Division, approximately 250 km south-west of Yangon and affecting more than 50 townships. With wind speeds of up to 200 km/h accompanied by heavy rain, the damage was most severe in the delta region, where the effects of the extreme winds were compounded by a 3.6-m storm surge. *Nargis* was the worst natural disaster in the history of Myanmar and one of the most devastating cyclones to strike Asia since 1991.

The official death toll stood at over 84 000 with more than 53 000 people reported missing and nearly 19 000 injured at the time of the Post Disaster Needs Assessment (PDNA). Assessment data shows that some 2.4 million people were severely affected by the cyclone out of an estimated 7.35 million people living in the townships of the area. Estimates suggest that the number of people displaced by the cyclone may have been as high as 800 000 with some 260 000 people living in camps or settlements throughout the delta in the first days after the cyclone.

In addition to the tragic loss of life, the total amount of damage and losses caused by *Nargis* in the affected areas of Myanmar is estimated at more than US\$ 4 billion, of which 43 per cent is damage and 57 per cent is losses.

More remarkably, the value of damage and losses is equivalent to 21 per cent of the country's gross domestic product in the previous fiscal year, providing an additional illustration of the magnitude of the disaster. Worse still, the equivalent magnitudes for the Ayeyarwady and Yangon Divisions are 74 and 57 per cent of their respective gross domestic product: figures that are high in themselves and that are comparable to the magnitude of the 2004 tsunami in different areas of the affected countries. Housing and industry were the two most-affected sectors, followed by agriculture and transport and communication.

According to the report Learning from Cyclone Nargis (UNEP, 2009), the devastating impacts of *Nargis* on the environment and livelihood base of local communities have increased people's vulnerability to future natural hazards. In addition, climate change has the potential to increase disaster vulnerability in the region as a result of rising sea levels, as well as increased frequency and magnitude of natural hazards.

4.5.2 Extra-tropical cyclones and storms

Extra-tropical cyclone activity plays an important role in the atmospheric circulation and in the advection of heat and moisture in mid-latitudes. Extra-tropical cyclones are also responsible for extreme weather conditions leading to natural hazards such as windstorms and flooding. They can be associated with other hazards, e.g. freezing rain and snow, which can cause major impacts such as the disruption of transportation, public services and daily life in general.

Despite the number of different hazards and large geographical scope of extra-tropical cyclones, loss potentials are typically not as severe as those from tropical cyclones. Based on MunichRe data and recent studies, the associated losses over the 10-year period 2002–2011 averaged US\$ 1.8 billion per year in North America. During the same period, losses from tropical cyclones averaged US\$ 15.3 billion and US\$ 9.3 billion from thunderstorms (source: MunichRe).

It is possible to analyse extra-tropical cyclone variability by using the reanalysis datasets that are produced by numerical prediction systems at leading meteorological centres. An important feature of a reanalysis is that it is based on a meteorological data-assimilation system and hence generates a dynamically consistent, continuous dataset of atmospheric state variables. Cyclone activity can be quantified using various numerical tracking algorithms applied to reanalysis datasets.

Figure 45 shows the time series of the number of extra-tropical cyclones with atmospheric pressures at the surface smaller than 980 hPa. They were identified over the North Atlantic and North Pacific in different reanalyses for the respective time periods of their coverage. Cyclones deeper than 980 hPa represent the class of deep and strong ones. For the period 2001–2010, a general decrease of about 3 per cent per decade in the number of deep cyclones in the North Pacific can be detected from the NCEP-NCAR, NCEP-Department of Energy (DOE,NOAA), ERA-Interim and JRA-25 (JMA) reanalyses. The MERRA (NASA) reanalysis, however, does not reveal any robust tendency. For the North Atlantic, the last decade is not characterized by any significant trend in the number of deep cyclones. In the late 1980s, however, a distinct peak with the number of deep cyclones exceeding almost twice the numbers for the most recent decade is notable. It is detected from all reanalyses except the old NCEP-DOE. This preliminary finding needs more investigative studies as some divergence remains among different reanalysis datasets.

Three severe and high impact extra-tropical windstorms that affected Europe during the decade are described in the following case study. These are *Kyrill* (January 2007), *Klaus* (January 2009) and *Xynthia* (February 2010).

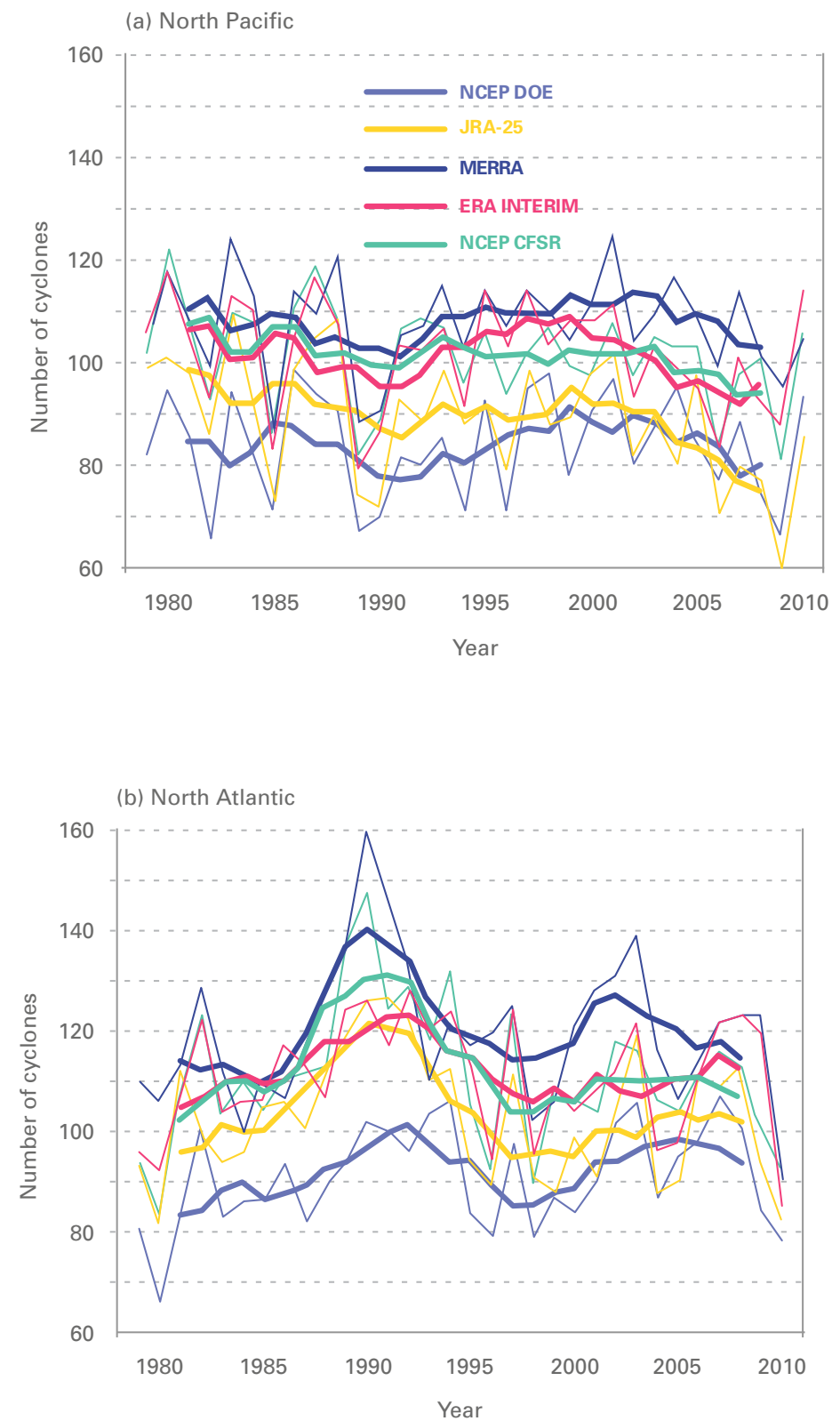


Figure 45. Time series of the number of deep extra-tropical cyclones (atmospheric pressure at the surface smaller than 980 hPa): (a) North Pacific; (b) North Atlantic

Figure 46. Surface vector wind (m/s), 18 January 2007, 12 UTC (source: ECMWF)

Case study F. Extra-tropical windstorms in Europe

Storm *Kyrill*: a cold front passage on 18–19 January 2007 resulted in an extra-tropical storm named *Kyrill*, which affected several countries across central Europe (Figure 46). In Austria, wind gusts up to 160 km/h destroyed power lines, roofs and trees with a total estimated damage of at least 100 million euros.

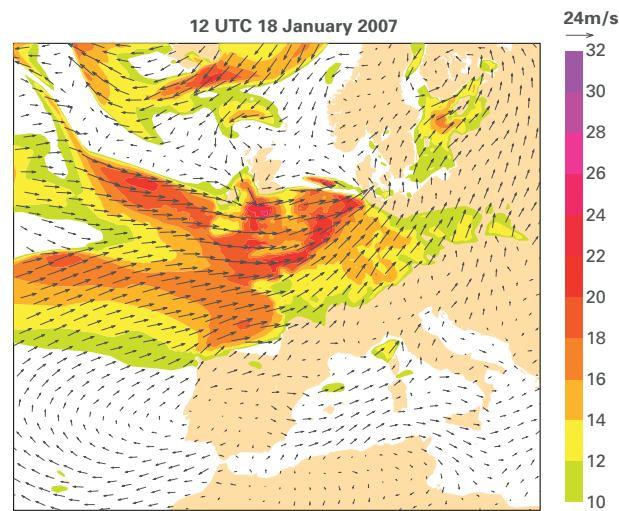
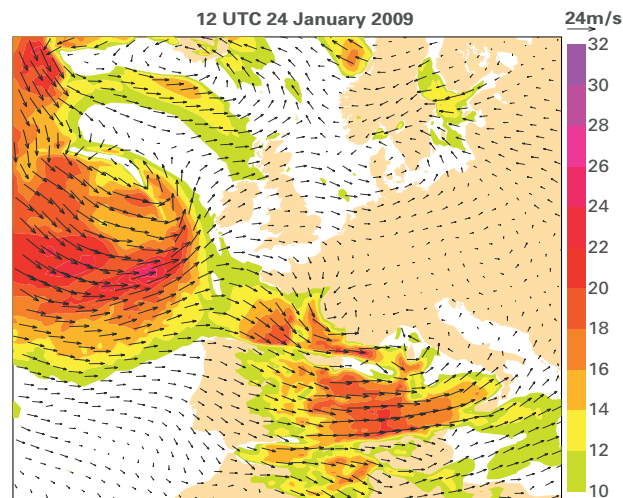


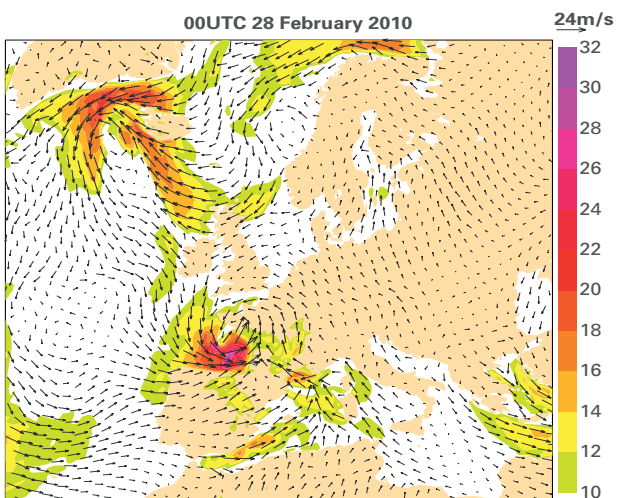
Figure 47. Surface vector wind (m/s), 24 January 2009, 12 UTC (source: ECMWF)



Storm *Klaus*: a destructive extra-tropical storm which affected southern France, Italy and northern Spain (Figure 47) on 23–25 January 2009. The death toll was 31 and economic losses totalled billions of euros. The extreme strength of the wind gusts generated by this storm was the main reason for the damage caused.

Figure 48. Surface vector wind (m/s), 28 February 2010, 00 UTC (source: ECMWF)

Storm *Xynthia*: *Xynthia* crossed north-western Europe on the last two days of February 2010 (Figure 48) with widespread wind and storm-surge damage. More than 60 lives were lost. Insured losses in France and Germany exceeded US\$ 4 billion and there was also substantial damage in Austria, Belgium, the Netherlands, Spain and Switzerland. A wind gust of 238 km/h was recorded on the Pic du Midi in the French Pyrenees and 120–140 km/h gusts were common on low ground in France and Switzerland. It is considered the worst storm of the decade in the region.



Case study G. Sand- and duststorms in the Arabian Peninsula

Sand- and duststorms (SDS), have enormous impact on socio-economic activity in the Arabian Peninsula. The analysis of the observations shows that the frequency of SDS events across Saudi Arabia increased over the decade 2001–2010. This tendency is illustrated by the positive trend of the aerosol optical depth (AOD) (Figure 49).

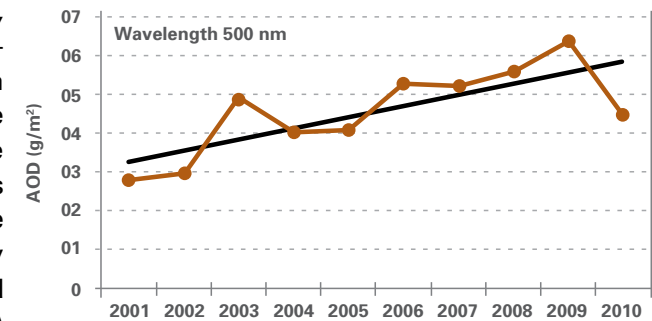


Figure 49. Time series of the AOD (g/m²) obtained at the Solar Village station in Riyadh, Saudi Arabia (latitude 24.91°N, longitude 46.41°E, elevation 650 m). The AOD increase rate is 0.28 g/m² per the decade 2001–2010.

This case study focuses on the SDS which was observed and had been predicted in Saudi Arabia in March 2009 and is a good example of this type of storm. It began as a depression in the Algerian Sahara on 4 March. On 5 March, the SDS was spawned where the cold air coming from Europe met the warm, dry air coming from the Sahara. The storm then moved across the Mediterranean Sea towards the Syrian Arab Republic, Jordan and Iraq, then moved southwards before reaching the west coast of Saudi Arabia on 10 March. The model forecast initiated at 00 UTC on 7 March predicted the SDS event quite well three to five days in advance. This was confirmed by a good agreement with the Meteosat satellite image and visual observations. Figure 50 shows the time series of the forecast dust load and visibility at Riyadh from 06 UTC on 7 March to 00 UTC on 12 March.

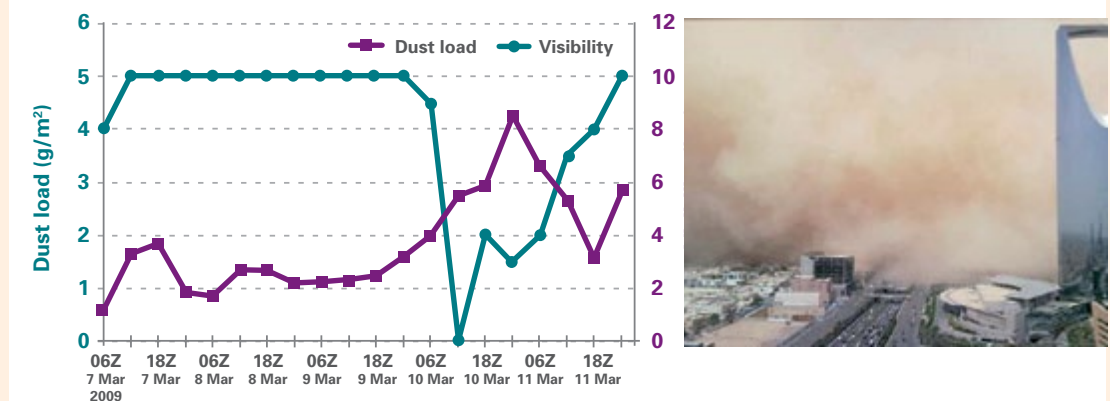


Figure 50 (left). Time series of dust load and visibility forecast as of 06 UTC on 7 March 2009 until 00 UTC on 12 March 2009 at Riyadh, Saudi Arabia (visibility data obtained from the Presidency of Meteorology of Saudi Arabia for station Riyadh (WMO Code 40438) with latitude 24.71°N, longitude 46.73°E, elevation 610 m; dust load data obtained by WRF simulation at the Centre of Excellence for Climate Change Research, King Abdulaziz University)

This intense SDS event caused widespread and heavy dust deposition, reducing visibility to less than 1 km over most cities in the central part of Saudi Arabia. The Kingdom Tower, which is the tallest building in Riyadh (approximately 300 m) and is prominent in Figure 51, provides a clear idea about the extent and height of the SDS event. Riyadh international airport was closed, as were some highway sections. An unusual number of respiratory-related illness (e.g. asthma) were reported by hospitals.

A simulation of dust concentration, using a regional climate model, shows that dust has a significant impact on climate in the Arabian Peninsula. It particularly affects rainfall and temperature, leading to a reduction in temperature and an enhancement of precipitation (Islam and Almazroui, 2012).

Figure 51 (right). A snapshot of the dust event on 10 March 2009 in Riyadh 06 UTC (<http://hopeinthedarkdesert.blogspot.com/>)

4.5.3 Tornadoes

The USA is the only country maintaining detailed and comprehensive long-term tornado statistics. Tornadoes occur elsewhere in the world but, unfortunately, there are no comprehensive datasets for making a comprehensive worldwide tornado assessment. This section will therefore focus extensively on the assessment made in the USA. Nevertheless, brief information on tornado assessment in Europe is provided at the end of the section, based on a few country datasets.

Tornadoes are common in the USA, with over 1 000 cases occurring each year on average. Although tornadoes can occur at any time, they are most common in spring (March–May) as the transition of winter to spring is in full swing and competing cooler air and warmer air masses clash.

While tornadoes have been documented across the entire USA, some areas experience them more frequently than others. There are two regions with a high frequency of tornadoes: Florida, and Tornado Alley, located in south-central USA.

Overall, most tornadoes in the USA are considered weak, based on the Enhanced Fujita (EF, see Table 10) scale (EF0 or EF1) and about 95 per cent of all US tornadoes are below EF3 intensity. The remaining small percentage of tornadoes are categorized as violent (EF3 and above). Of these violent twisters, only a few (0.1 per cent of all tornadoes) achieve EF5 status, with estimated winds more than 320 km/h.

One of the main difficulties with tornado records is that a tornado or evidence of a tornado must have been observed. Unlike precipitation or temperature, which may be measured by a fixed instrument, tornadoes are ephemeral and very unpredictable. If a tornado occurs in a place with few or no people, it is likely that it will remain undocumented.

Today, NOAA's Doppler weather radars cover nearly the entire USA. Even if a tornado is not actually observed, modern damage assessments by NOAA's National Weather Service can discern if a tornado caused the damage and, if so, how strong the tornado may have been. This disparity between tornado records of past and current records contributes a great deal of uncertainty regarding questions about the long-term behaviour or patterns of tornado occurrence.

With increased national Doppler radar coverage, increasing population and greater attention to tornado reporting, there has been an increase in the number of tornado reports over the past several decades (Figure 52(a)). This can create a misleading appearance of an increasing trend in tornado frequency. To better understand the true variability and trend in tornado frequency in the USA, the total number of strong-to-violent tornadoes (EF3 to EF5) can be analysed. These are the tornadoes that would have probably been reported even during the decades before Doppler radar use became widespread. Figure 52(b) indicates that there has been some decrease in the number of the strongest tornadoes in the past three decades from 1981 to 2010, compared to the earlier three decades, 1951–1980. The decrease is particularly significant in the last decade, 2001–2010.

During 2001–2010, some 13 000 tornadoes were reported in the USA, with most being EF0, EF1 or EF2. Nearly 350 tornadoes were documented as major ones (EF3, EF4 or EF5). In annual terms, the highest tornado count – since records began in 1950 – was in 2004

with a total number of 1 818 reported tornadoes (EF0–EF5); a total number of 61 very strong-to-violent tornadoes (EF3 to EF5), the highest strong-to-violent tornadoes count in the decade was recorded in 2008; the least number of EF3 to EF5 tornadoes, with a total of 21, was recorded in 2009.

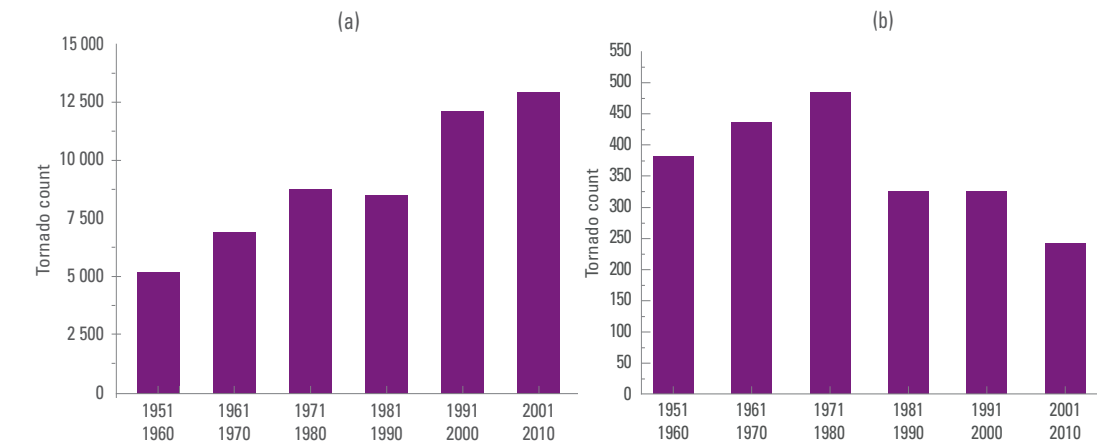


Figure 52. Occurrence of tornadoes across the USA: (a) in all categories; and (b) in the strong-to-violent category (source: NCDC)

Category	Wind intensity	Damage caused
EF0 (gale tornado)	105–137 km/h	Light damage: some damage to chimneys; branches broken off trees; shallow-rooted trees pushed over; damage to signboards
EF1 (moderate tornado)	138–178 km/h	Moderate damage: the lower limit is the beginning of hurricane wind speed; surface peeled off roofs; mobile homes pushed off foundations or overturned; moving cars pushed off roads
EF2 (significant tornado)	179–218 km/h	Considerable damage: roofs torn off frame houses; mobile homes demolished; boxcars pushed over; large trees snapped or uprooted; light-object missiles generated
EF3 (severe tornado)	219–266 km/h	Severe damage: roofs and some walls torn off well-constructed houses; trains overturned; most trees in forest uprooted; heavy cars lifted off ground and hurled
EF4 (devastating tornado)	267–322 km/h	Devastating damage: well-constructed houses levelled; structures with weak foundation blown some distance; cars hurled and large missiles generated
EF5 (incredible tornado)	>322 km/h	Incredible damage: strong frame houses lifted off foundations, carried considerable distance and disintegrating; automobile-sized missiles flying through the air for more than 100 m; trees stripped of their bark; incredible phenomena occur.

Table 10. Enhanced Fujita tornado intensity scale (NOAA switched from the Fujita scale to the Enhanced Fujita scale for rating tornado strength in 2007).

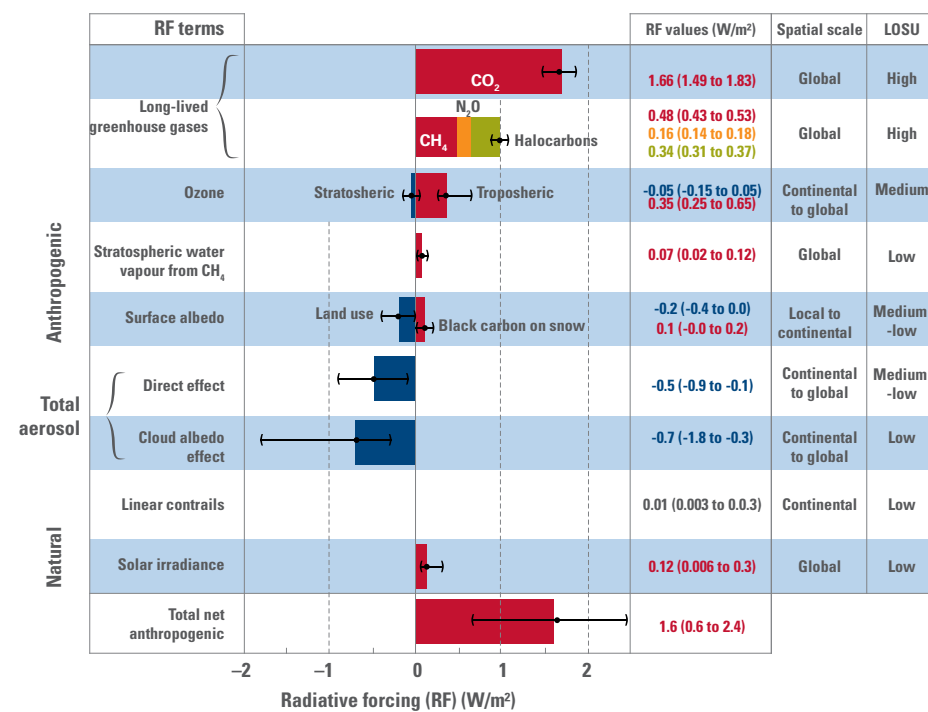
CHAPTER 5. CLIMATE AND COMPOSITION OF THE ATMOSPHERE

5.1 Greenhouse gases and climate

A trace gas is a gas which makes up less than 1 per cent by volume of the Earth's atmosphere, and includes all gases except nitrogen (78.1 per cent) and oxygen (20.9 per cent). The most abundant trace gas at 0.934 per cent is argon. A number of atmospheric trace constituents have an important role in climate forcing and feedbacks. These constituents are listed as essential climate variables (ECVs) by the Global Climate Observing System (GCOS), a WMO co-sponsored programme. They include greenhouse gases (GHGs), ozone and its precursors, and aerosols. Global observations of the atmospheric composition are coordinated through the WMO GAW Programme.

Greenhouse gases are a group of trace gases that impact the radiation budget in the atmosphere. Some gases in this group (minor in amount) have an exclusively anthropogenic origin (chlorofluorocarbons (CFCs)), hydrochlorofluorocarbons (HCFCs), hydrofluorocarbons (HFCs) and sulphur hexafluoride (SF_6) but the major ones (carbon dioxide (CO_2), methane (CH_4) and nitrous oxide (N_2O)) have both anthropogenic and natural sources. Water vapour is the most potent greenhouse gas but, being natural, it is not discussed in this section.

Figure 53. Global average radiative forcing in 2005 (best estimates and 5-95 per cent uncertainty ranges) with respect to 1750 for CO_2 , CH_4 , N_2O and other important agents and mechanisms, together with the typical geographical extent (spatial scale) of the forcing and the assessed level of scientific understanding. Aerosols from explosive volcanic eruptions contribute an additional episodic cooling term for a few years following an eruption. The range for linear contrails does not include other possible effects of aviation on cloudiness (source: IPCC-AR4, Working Group I, Figure SPM.2)



Greenhouse gases let the solar radiation reach the Earth's surface but they absorb and re-emit infra-red radiation and thereby lead to the heating of the surface of the planet. It is necessary to distinguish the natural greenhouse effect from the enhanced greenhouse effect. The natural greenhouse effect is caused by the natural amounts of GHGs and is vital for life. In the absence of the natural greenhouse effect, the surface of the Earth would be approximately 33°C colder.

The enhanced greenhouse effect results from increased concentrations of GHGs induced by human activities. The magnitude of this effect is expressed in terms of radiative forcing. According to the IPCC Fourth Assessment Report (IPCC-AR4), radiative forcing is a measure of the influence a factor has in altering the balance of incoming and outgoing energy in

the Earth-atmosphere system and is an index of the importance of the factor as a potential climate-change mechanism. In IPCC-AR4, the radiative forcing values are provided as changes relative to pre-industrial conditions defined at 1750 and are expressed in watts per square metre (W/m^2). Figure 53 shows different components of radiative forcing in 2005 (related to the change in atmospheric composition since pre-industrial times). Their relative contribution to total increase of radiative forcing changes with time due to the permanent changes of the atmospheric content of greenhouse gases.

The change in annual average total radiative forcing by all the long-lived greenhouse gases (LLGHGs) since the pre-industrial era is used to define the NOAA Annual Greenhouse Gas Index (AGGI), which was introduced in 2004 and has been updated annually since. These calculations are based on the approach recommended by IPCC. The empirical expressions are derived from atmospheric radiative transfer models and generally have an uncertainty of about 10 per cent.

An AGGI is defined as the ratio of the total radiative forcing due to LLGHGs for any year for which adequate global measurements exist, to that of 1990. This index, shown in Figure 54, is a measure of the interannual changes in conditions that affect carbon dioxide emission and uptake, methane and nitrous-oxide sources and sinks and the decline in the atmospheric abundance of ozone-depleting chemicals related to the Montreal Protocol.

The AGGI shows that, from 1990 to 2010, the radiative forcing by LLGHGs increased by 29 per cent (+0.63 W/m^2) with carbon dioxide accounting for nearly 80 per cent of this increase (+0.5 W/m^2). The absolute increase was +0.3 W/m^2 in 1990–2000 and grew to +0.33 W/m^2 in 2000–2010.

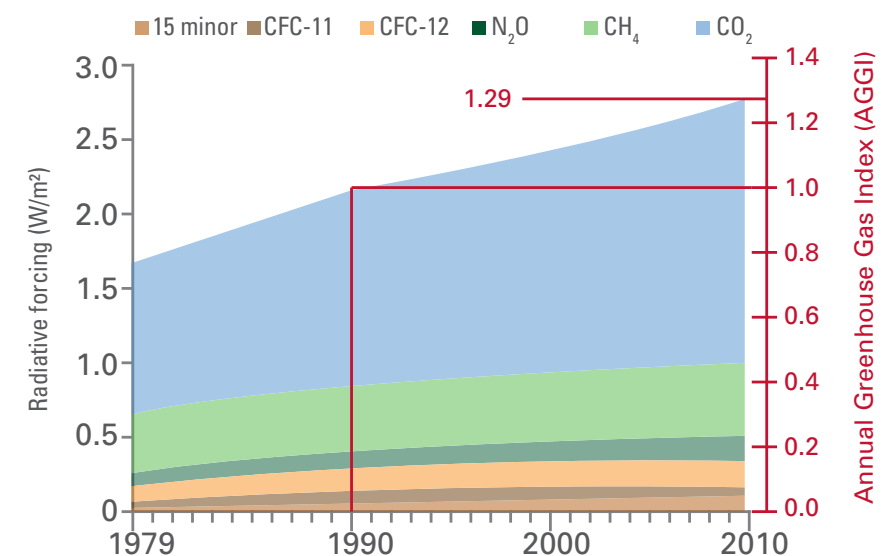


Figure 54. Atmospheric radiative forcing, relative to 1750, of all LLGHGs and the 2010 update of the NOAA AGGI. The reference year for the index is 1990 (AGGI = 1) (source: WMO Greenhouse Gas Bulletin, No.7, 2011)

Carbon dioxide is the single most important anthropogenic GHG in the atmosphere and contributes about 64 per cent of the total increase of overall global radiative forcing by LLGHGs in 2010. It is responsible for 85 per cent of the increase in radiative forcing over the past decade and 81 per cent over the last five years. For about 10 000 years before the start of the industrial era in the mid-18th century, atmospheric carbon dioxide remained almost constant at around 280 ppm (ppm = number of molecules of the gas per million molecules of dry air). Since then, the carbon dioxide mixing ratio has increased by 39 per

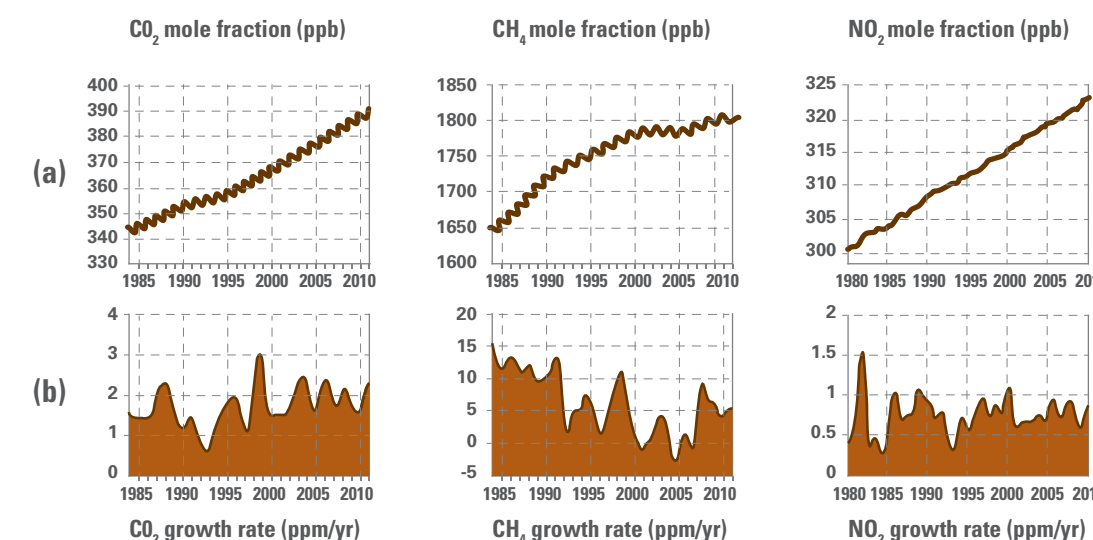
cent by 2010 (389.0 ppm), primarily because of emissions from the combustion of fossil fuels, deforestation and changes in land use. The global average carbon dioxide mixing ratio (Table 11) during 1991–2000 was 361.5 ppm while, in 2001–2010, it rose to 380 ppm. During the same period, the average growth rate increased from 1.5 ppm/yr to 2.0 ppm/yr (Figure 55). The inter-hemispheric difference has also increased from 2.9 ppm in excess of the northern over the southern hemisphere to 3.6 ppm from a decade before, due to faster carbon dioxide mixing ratio growth in the northern hemisphere.

Methane contributes about 18 per cent to the increase in overall global radiative forcing by LLGHGs in 2010 compared to the pre-industrial era and is the second most important GHG after carbon dioxide. Analyses of air trapped in ice cores from the Antarctic and the Arctic revealed that the current atmospheric methane mixing ratio is the highest it has been in the last 650 000 years. Before the industrial era, atmospheric methane was at ~700 ppb (ppb = number of molecules of the gas per billion (10^9) molecules of dry air). Increasing emissions from anthropogenic sources are responsible for the 158 per cent increase in methane by 2010 over pre-industrial times. The globally averaged methane-mixing ratio (Table 11) in the previous decade (1991–2000) was 1 758 ppb, while, in 2001–2010, it reached 1 790 ppb. The growth rate of methane decreased from ~13 ppb/yr during the early 1980s to 5.5 ppb/yr in the 1990s and to 3 ppb/yr in the 2000s (Figure 55). After a brief stabilization phase between 1999 and 2006, the methane mixing ratio started rising again in 2007. Both mixing-ratio averages for the decades 1991–2000 and 2001–2010 in the northern hemisphere exceed those in the southern hemisphere by about 100 ppb. The growth rate during 1991–2000 was slightly higher in the southern hemisphere, while, for the more recent decade, the growth rate is very close for both hemispheres.

Nitrous oxide contributes ~6 per cent to radiative forcing by LLGHGs. It is the third most important contributor to radiative forcing of LLGHGs (surpassing CFC-12 in 2010). It is a potent greenhouse gas as its impact on climate, integrated over 100 years, is 298 times greater than equal emissions of carbon dioxide. Its atmospheric abundance prior to industrialization was 270 ppb. In more recent times, the global average mixing ratio increased from 312.2 ppb (1991–2000) to 319.7 ppb (2001–2010) (Table 11). A main anthropogenic source of nitrous oxide is the use of fertilizers. A consistent inter-hemispheric bias of ~1.2 ppb exists between the northern and southern hemispheres during both periods due to more land being cultivated in the northern hemisphere. The near-linear global growth rate of ~0.8 ppb/yr has remained fairly constant over the past three decades with only a slight increase in recent years.

Other greenhouse gases: sulphur hexafluoride is a potent LLGHG controlled by the Kyoto Protocol. It is produced artificially and used as an electrical insulator in power distribution equipment. Its mixing ratio by 2010 had increased to double that observed in the mid-1990s. The ozone-depleting CFCs, together with minor halogenated gases, contribute some 12 per cent to radiative forcing by LLGHGs. While CFCs and most halons are decreasing, HCFCs and HFCs, which are also potent GHGs, are increasing at rapid rates, although they are still low in abundance. Observations revealed that the differences in the mixing ratios between the two hemispheres were large in the 1980s for CFCs, carbon tetrachloride and methylchloroform but have since narrowed as the emissions have been suppressed and the existing constituents have been mixed across the hemispheres. The mixing ratios of CFC-11, CFC-12 and CFC-113 were higher in 1991–2000 (peaking in the beginning of the 1990s) and were decreasing in the decade 2001–2010 in both hemispheres and globally.

	2010	Increase since pre-industrial times	1991–2000	2001–2010
Carbon dioxide	389.0 ppm	39%	361.5 ppm	380 ppm
Methane	1808 ppb	158%	1 758 ppb	1 790 ppb
Nitrous oxide	323.2 ppb	20%	312.2 ppb	319.7 ppb



The radiative forcing by GHGs is the complex combined effect of all the gases, often expressed as the carbon dioxide equivalent ($\text{CO}_2\text{-eq}$) mixing ratio. Comparison of the decade 1991–2000 with 2001–2010 shows decadal average $\text{CO}_2\text{-eq}$ abundance growth from 430.6 ppm to 457.3 ppm (making it 6 per cent per decade). By 2010, $\text{CO}_2\text{-eq}$ concentration had reached 469.7 ppm.

5.2 Stratospheric ozone depletion

According to Fahey and Hegglin (2011), about 90 per cent of total ozone (O_3) is found in the stratosphere. The gas absorbs UV-B radiation from the Sun and protects life on Earth. Near the surface, excessive (i.e. exceeding natural) concentrations of ozone are generally harmful to life. Stratospheric ozone depletion introduced some negative effects of the total radiative forcing of the climate and a growth of tropospheric ozone increased somewhat the total radiative forcing. All ozone-depleting substances are GHGs and measures to reduce their emissions under the Montreal Protocol have provided the added benefit of reducing the anthropogenic contribution to climate change.

The primary cause of ozone depletion is the presence of chlorine-containing source gases (primarily CFCs, halons and related halocarbons). In the presence of UV light, these gases dissociate, releasing chlorine atoms, which then go on to catalyse ozone destruction. Chlorine-catalysed ozone depletion can take place in the gas phase, but is dramatically enhanced in the presence of polar stratospheric clouds (PSCs). PSCs

Table 11. Mixing ratio of carbon dioxide, methane and nitrous oxide in 2010 and the decadal values for 1991–2000 and 2001–2010

Figure 55. Globally averaged CO_2 (left), CH_4 (centre) and N_2O (right) mole fractions (a) and their growth rates (b) from the 1980s to 2010 (source: WMO Greenhouse Gas Bulletin, No.7, 2011)

Note: Mixing ratio is defined as the abundance of one component of a mixture (for example, a particular GHG) relative to that of all other components (excluding water vapour). Mixing ratio is an equivalent to a more technical term "mole fraction". The following units are used to express mixing ratio: ppm = number of molecules of the gas per million molecules of dry air; ppb = number of molecules of the gas per billion (10^9) molecules of dry air; ppt = number of molecules of the gas per trillion (10^{12}) molecules of dry air.

can convert reservoir gases, such as hydrogen chloride and chlorine nitrate, to active chlorine in the presence of sunlight.

The ozone hole is defined as a region of exceptionally depleted ozone in the stratosphere. It is currently observed over the Antarctic at the beginning of the southern hemisphere spring (August–October). Over the altitude range 14–20 km, all the ozone can be depleted when the ozone hole reaches its maximum around late September or early October. The dynamics of the ozone hole is monitored with satellite instruments which provide daily images of ozone. From the historical record, it is known that total column ozone values of less than 220 Dobson Units (DU) were not observed prior to 1979. For this reason, the level of 220 DU is used as a reference when assessing the boundary of the region representing ozone loss. Aircraft field missions over the Antarctic were used to study the mechanism causing ozone depletion. It was found that a total column ozone level of less than 220 DU is a result of catalysed ozone loss from chlorine and bromine compounds.

The seasonal cycle of the incoming solar radiation is the reason for the maximal Antarctic ozone depletion in spring. During winter, even though PSCs are the most abundant, there is no light over the pole to drive the chemical reactions. During spring, however, the Sun comes out, providing light to drive photochemical reactions. With warming temperatures near the end of spring, the air previously trapped in the circumpolar vortex starts to mix with the air from other stratospheric regions and the warm, ozone-rich air flows in from the lower latitudes, destroying the PSCs. This shuts down the ozone-depletion process and the ozone hole closes.

Over the decade 2001–2010, global total ozone and total ozone in the Arctic and Antarctic regions is no longer decreasing but is not yet increasing. The variation in the size of the ozone hole from one year to another can be explained, to a large extent, by meteorological conditions in the stratosphere, as ozone depletion becomes more severe if the stratosphere is cold. Over the coming years, therefore, the variation in the state of the ozone hole will be governed by interannual changes in the meteorological conditions rather than by changes in ozone-depleting substances, whose decline is quite slow, about 1 per cent per year.

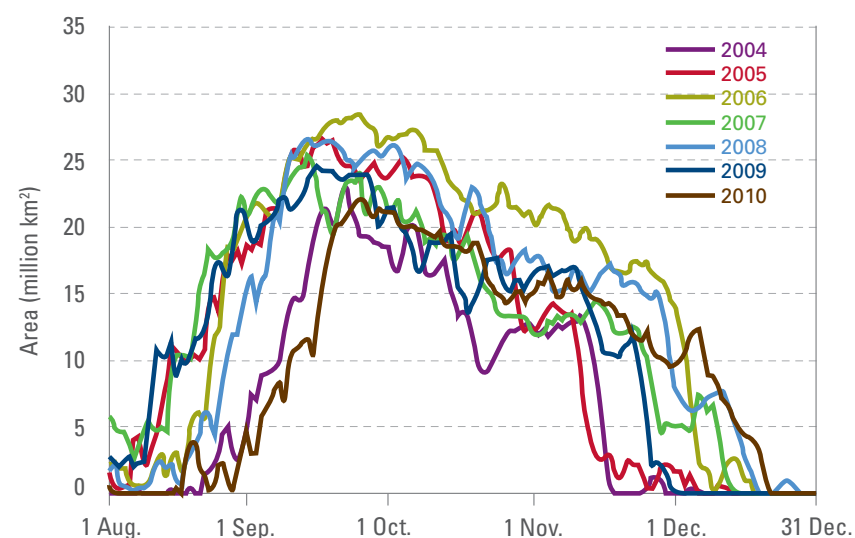


Figure 56. Ozone hole area with respect to 220 DU in the southern hemisphere from August to December for the years 2004–2010; observations made by GOME and SCIAMACHY (source: Royal Netherlands Meteorological Institute and European Space Agency)

The first ozone hole appeared in 1980. During the decade that followed, its size increased more or less gradually from zero to about 25 million km², averaged over the last 10 days of September. Since the early 1990s, the size of the annually recurring ozone hole has remained more or less stable. Several representative time periods are used to calculate the average size of the ozone hole over the course of the season.

The largest ozone hole areas were observed in 2000, 2003 and 2006. Figure 56 presents the evolution of the ozone hole area during 2004–2010. The largest ozone mass deficit occurred in 2000 and 2006, with loss being largest in 2006. One year stands out as different from all other recent years: 2002. During that year, the polar vortex split in two and broke down early in the season and the degree of ozone loss was limited compared with other years.

According to the 2010 issue of the WMO/UNEP Scientific Assessment of Ozone Depletion, the size of the ozone hole is expected to remain high for another decade or so before significant signs of ozone recovery due to the phase-out of ozone-depleting substances under the Montreal Protocol will be seen. Global average mixing ratios of the main ozone-depleting substances are shown in Figure 57. There are still significant amounts of chlorines and bromines in the atmosphere to cause total destruction of ozone in the 14–20 km altitude range, provided the temperature conditions are conducive to ozone destruction.

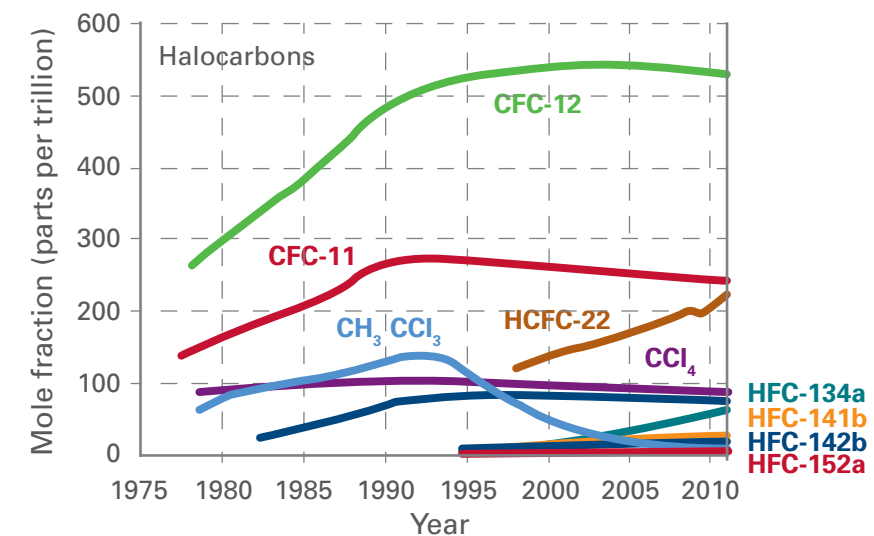


Figure 57. Monthly mean mole fraction of the most important halocarbons from 1977 to 2010 averaged over the network (between seven and 19 stations) (source: WMO Greenhouse Gas Bulletin, No.7, 2011)

At the end of the first decade of the 21st century, unprecedented chemical ozone destruction occurred over the Arctic. In early 2011 it was, as Manny et al. (2011) report, comparable to that in the Antarctic ozone hole, for the first time in the observational record. Unusually long-lasting cold conditions in the Arctic lower stratosphere led to persistent enhancement of ozone-destroying forms of chlorine and to ozone loss, which exceeded 80 per cent at 18–20 km altitude. Manny et al. (2011) have shown that Arctic ozone holes may occur at milder temperatures than those in the Antarctic.

According to Thompson et al. (2011), the influence of the Antarctic ozone hole on surface climate is most pronounced during the austral summer season and strongly resembles the most prominent pattern of large-scale southern hemisphere climate variability, SAM.

The influence of the ozone hole on SAM (see Chapter 3) has led to a range of significant summertime surface climate changes not only over the Antarctic and the Southern Ocean, but also over New Zealand, Patagonia (Argentina) and southern regions of Australia.

5.3 Climate and air quality

Reactive gases, including tropospheric ozone, volatile organic compounds (VOCs), nitrogen oxides (NO_x), carbon monoxide (CO), sulphur dioxide (SO_2) and aerosols characterize air quality at regional and subregional levels. VOCs, NO_x and CO are the primary pollutants and are not greenhouse gases. Nevertheless, they are important for the climate system as they are the precursors of tropospheric ozone, which is a GHG and a highly toxic pollutant. Concentrations of most reactive gases are highly variable in time and space. The current sparse observational network does not allow for assessment of the global trends of SO_2 , VOCs, and NO_x . In most regions of the world – the noteworthy exception being East Asia – surface and free tropospheric ozone mixing ratios have not risen significantly since the year 2000. Prior to the 1990s, almost all records indicate their rise while, during the 1990s, the picture was highly diverse (GAW Report No.199).

Since 1990 global (and especially northern hemispheric) CO mixing ratios (Figure 58) have been decreasing slowly but this tendency was temporarily reversed by the effects of large forest fires during the El Niño events of 1998 and 2003.

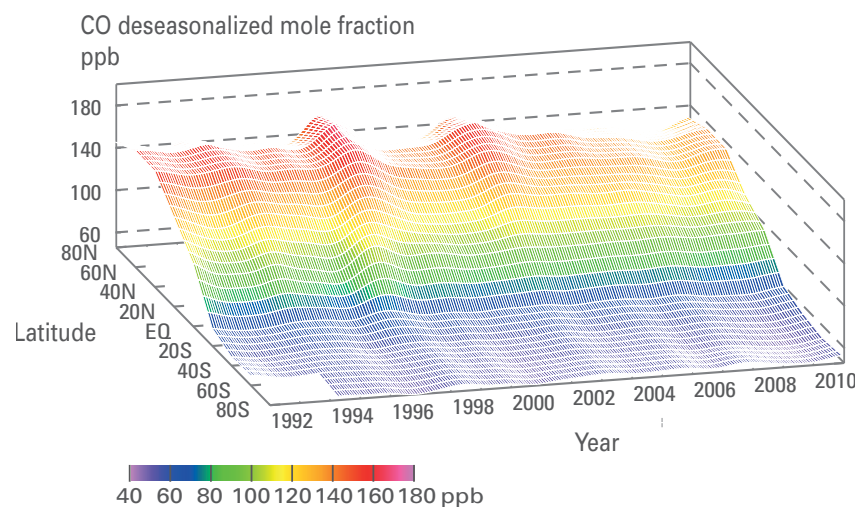


Figure 58. Deseasonalized long-term trends of zonally averaged monthly mean CO mole fractions: the zonally averaged mole fractions are calculated for each 20° zone (source: WDCGG Data Summary No.36, 2011).

The atmospheric content of reactive gases and aerosols depends on the gas emissions from the biosphere and from human activities. It is controlled by a number of physical mechanisms (such as atmospheric transport and deposition) and chemical reactions, which critically depend on temperature, precipitation and atmospheric circulation. Thus, the air quality will probably change appreciably in the future, compounding increases in anthropogenic emissions owing to the necessary increases in industrial activity as we attempt to cope with the Earth's ever increasing population.

- The impact of climate change on the atmospheric abundance of reactive gases and aerosols can occur through different mechanisms (as summarized in Brasseur, 2009):
- Changes in atmospheric temperature affect the rates of chemical reactions;

- Changes in atmospheric humidity affect the production and destruction of chemical species and, specifically, the loss rate of tropospheric ozone;
- Changes in the frequency and intensity of lightning affect the atmospheric production of nitric oxide with direct impact on the ozone budget in the upper troposphere;
- Changes in atmospheric cloudiness affect the atmospheric composition by modifying the penetration of solar radiation and, hence, the photochemical activity in the atmosphere; aqueous and heterogeneous chemistry associated with the presence of clouds is also modified;
- Changes in the frequency and intensity of precipitation resulting from climate change affect the rate of scavenging and removal from the atmosphere of soluble species;
- Changes in surface temperature and precipitation affect the emission and deposition of chemical compounds and the surface deposition by vegetation and soil;
- Changes in ocean temperature affect the atmosphere–ocean exchanges of compounds such as dimethylsulphide, which are a source of sulphate aerosols;
- Changes in the frequency and intensity of prolonged stagnant air conditions affect the dispersion of pollutants and promote the frequency and intensity of pollution events with severe consequence for human health;
- Changes in the general circulation of the atmosphere affect the long-range transport of pollutants from continent to continent;
- Changes in convective activity lead to changes in vertical transport in the chemical composition of the upper troposphere;
- Changes in stratosphere-troposphere exchange affect the abundance of chemical species, including ozone, in the upper troposphere;
- Changes in surface-wind intensity over the continent modify the mobilization of dust particles in arid regions and, therefore, the aerosol burden in the troposphere; and
- Changes in surface-wind intensity over the ocean modify the exchanges of trace gases at the ocean-atmosphere interface and affect the emission of sea-salt particles to the atmospheric boundary layer.

Heatwaves provide a way of estimating how air pollution could evolve under future climate change. In this regard, the heatwaves that took place in western and central Europe in August 2003 and in the Russian Federation in summer 2010 constitute interesting test cases. During the period of exceptionally high temperatures in Europe in 2003, high levels of photochemically produced ozone were observed, especially in the central part of France and south-western Germany. On 8 August 2003, for example, many stations reported ozone concentrations exceeding 90 ppb, which is considerably above air-quality standards. It is believed that about one-third of the deaths reported during this period were associated with health problems caused by these excessive ozone concentrations (Brasseur, 2009).

CHAPTER 6. CRYOSPHERE AND SEA LEVEL

6.1 Cryosphere

According to the definition of the Integrated Global Observing Strategy Cryosphere Theme report, the cryosphere is defined as: “elements of the Earth system containing water in its frozen state”. It includes sea ice, lake (reservoir) and river ice, snow cover and solid precipitation, glaciers, ice caps, ice sheets, ice shelves, permafrost and seasonally frozen ground. The cryosphere is associated with cold climates, which can be found in the polar regions of our planet and also anywhere in high mountains, including those in the tropics and subtropics. The cryosphere thus exists at all latitudes and in 100 countries of the world.

Changes in the cryosphere are associated with processes of melting or freezing. They occur at constant temperatures and involve transfer of heat, often reflecting significant processes in the climate system. This is why cryospheric elements provide valuable indicators of climate change and variability. Like tree rings, annual accumulation of snow is indicative of past climate and ice cores provide highly valuable scientific information about the past climate, making it possible to compare modern climate change with its natural variations up to almost one million years ago.

The presence of frozen water in the atmosphere, on land and on the ocean surface affects energy, moisture, gas and particle fluxes, clouds, total precipitation, hydrological conditions and atmospheric and oceanic circulation. Being frozen water, the cryosphere is an intrinsic part of the global hydrological cycle. In some regions of the world, it contributes to, or even shapes, the availability of freshwater, one of the most valuable commodities for this century.

The following sections of this chapter briefly describe the most important and sometimes dramatic changes observed in the cryosphere in the previous decades, with focus on the first 10 years of this century.

6.1.1 Sea ice

Sea ice is a danger for ships, is a niche of a unique polar marine ecosystem and is an insulator between the ocean and atmosphere, to name but a few of its roles. High reflective ability (albedo) of sea ice is a key factor in the global energy balance of our planet. Sea ice exists in the Arctic Ocean, Southern Ocean and in many so-called “marginal seas” of the world.

The state of sea-ice cover in the 20th century is relatively well documented, largely because of the intensive exploration of the Arctic and existence of routine monitoring services which use, for example, ship observations, aerial reconnaissance and remote-sensing. Since the 1970s, sea ice has been monitored from space. Until the 1960s, Arctic sea ice covered 14–16 million km² in late winter and 7–9 million km² at boreal summer’s end. Since the end of the 1960s, Arctic sea-ice extent has been showing a systematic, marked decline (Figure 59). An even more dramatic reduction in Arctic sea-ice extent was observed more recently. During the last six years of the decade (2005–2010), the lowest five September extents were recorded. Only 2006 was missing and the record minimum extent with 4.28 million km² – 39 per cent below the long-term average – occurred in 2007 (Figure 60). At the end of the decade, the Arctic sea-ice decline rate at the end of the northern summer was estimated as 700 000 km²–800 000 km² per decade.

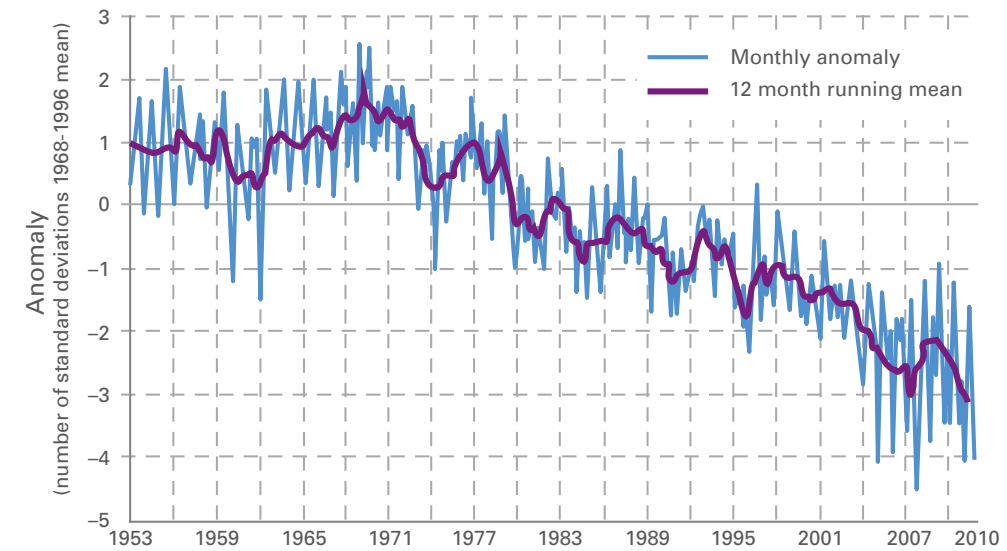


Figure 59. Arctic sea-ice extent standardized anomaly (source: National Snow and Ice Data Center (NSIDC), USA)

On the other hand, the estimated volume of Arctic sea ice has been declining markedly since 2005, with the lowest value on record being reached in 2010. Furthermore, the mean monthly sea-ice volume in the Arctic for 2001–2010 was lower in each month than the corresponding average for the 30-year period 1981–2010 (Figure 61).

The main feature of the sea ice in the Arctic Ocean used to be its stable multi-year character. The continuing observed decline in its volume is the result of both shrinkage of sea-ice cover and a decrease in its average thickness. It is possible to state, therefore, that the decade set the stage for an even more marked future decline in sea-ice extent and volume, ultimately changing the nature of sea ice in the Arctic Ocean from perennial to seasonal. With the reduced ability of sea ice in most of the Arctic Ocean to “survive” the summer, the situation is rapidly changing to one similar to that in the Southern Ocean. Here, the sea ice exhibits a strong annual cycle with considerably smaller trends in the annual averaged extent. This trend towards “seasonality” in the Arctic reduces the differences between the behaviour of sea ice at both poles of the planet. Nevertheless, the average extent of sea ice in the Southern Ocean (or “Antarctic sea ice”) has a small overall positive trend as shown in Figure 62 (despite some regions around the Antarctic exhibiting strong ice losses), contrary to its diminishing northern counterpart.

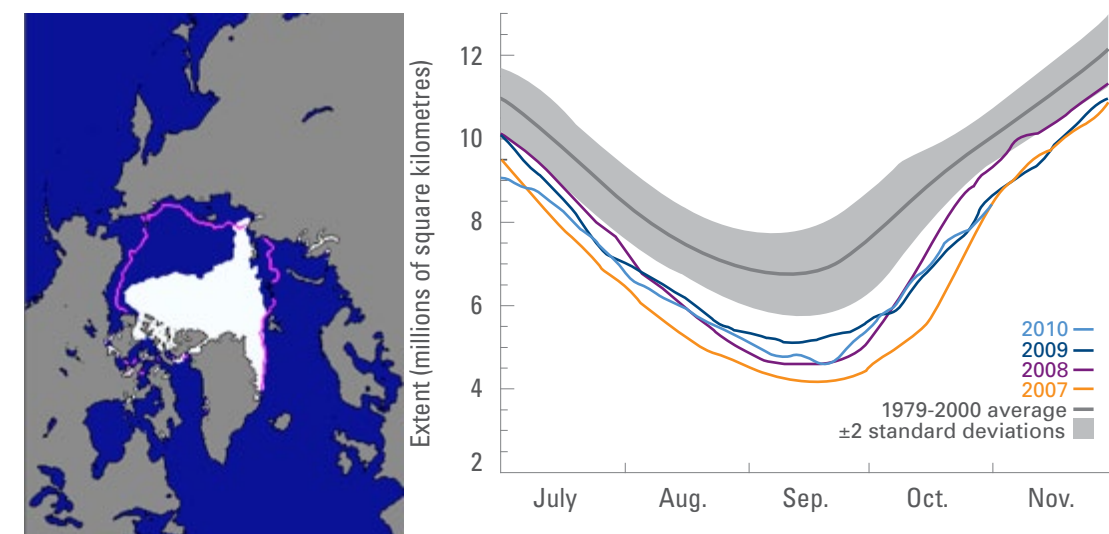


Figure 60. Sea-ice extent for September 2007: the magenta line indicates the long-term median from the 1979–2000 base period (left) and Arctic sea-ice extent at the end of the summer melt season from 2007 to 2010 (right) (source: National Snow and Ice Data Center (NSIDC))

Figure 61. Mean monthly sea-ice volume for the period 1981–2010 (yellow line) and 2001–2010 (blue line) (data source: NSIDC)

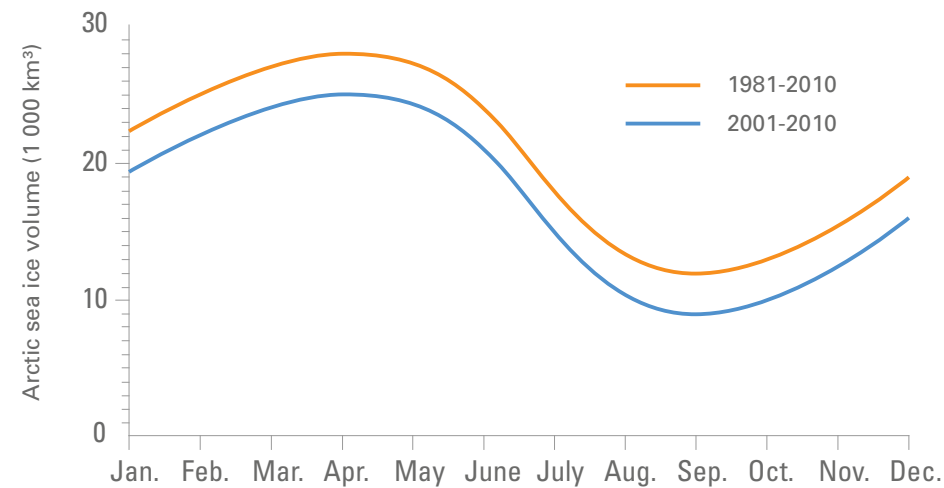
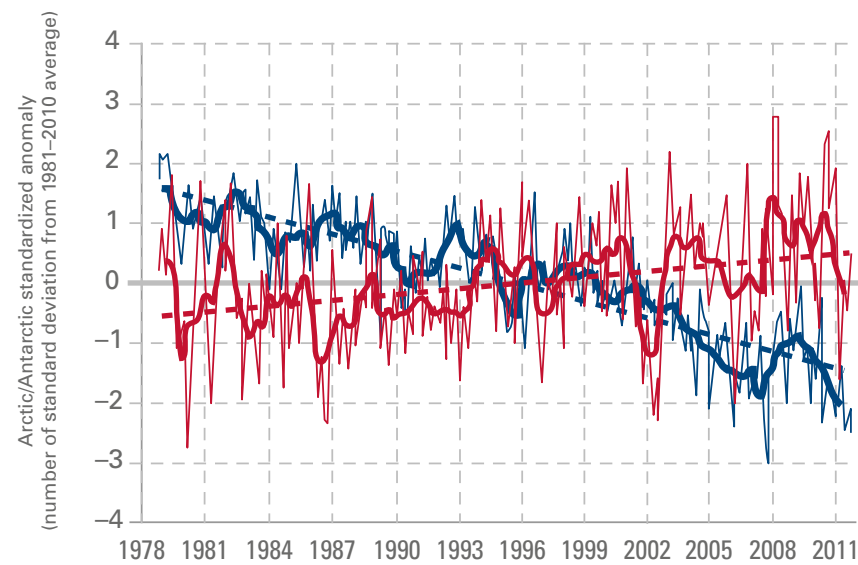


Figure 62. Arctic (blue) and Antarctic (red) standardized anomaly and trend (source: NSIDC)



The decline of sea ice in the Arctic Ocean is largely linked to global warming and its increase in the Arctic that can be partly attributed to the mutual dependence of ice and climate. The reasons for the slight increase in Southern Ocean sea ice are less solidly established. The roles of the strong stratospheric ozone depletion, which has been at its maximum state of development during the first decade of this century, and resultant changes in the atmospheric circulation around the Antarctic, are being vigorously addressed within the scientific community.

6.1.2 Ice sheets

At present, there are two major ice sheets which cover most of the Antarctic and Greenland. They contain more than 99 per cent of the planet's freshwater. During the decade, a significant advance was achieved in the ability to estimate mass balance of the ice sheets using differencing perimeter loss from net accumulation and from satellite gravity measurements. The two techniques are now showing comparable

results, leading to the conclusion that there is an acceleration of the net mass loss from the ice sheets (Figure 63). If this trend continues, ice sheets will contribute to sea-level rise in the 21st century more than any other factor. The first decade of this century can be described as the period in which the trend towards mass loss resulted in consistently negative mass balance for both ice sheets, with the largest losses observed in 2007 and 2008.

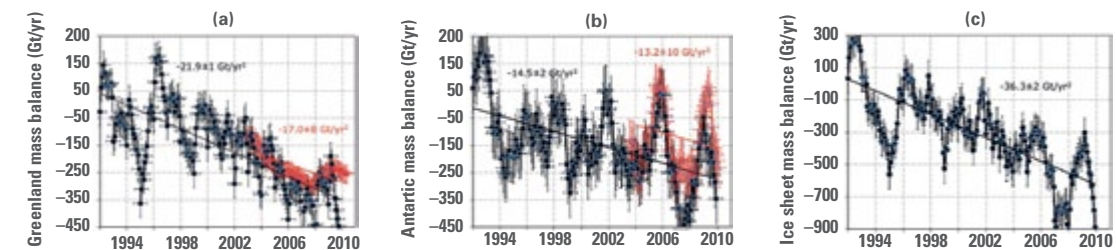


Figure 63. Total ice-sheet mass balance between 1992 and 2009 for (a) Greenland, (b) the Antarctic and (c) the sum of Greenland and the Antarctic in Gt/yr from the Mass Budget Method (solid black circle) and GRACE time variable gravity (solid red triangle) with associated error bars (source: Rignot, 2011)

6.1.3 Glaciers

The World Glacier Monitoring Service (WGMS) reports continuing decreases of mass balance of the 37 "reference" glaciers. The mass loss of glaciers experiences substantial annual variations. Figure 64 shows the mean cumulative specific glacier mass balance since 1945/1946. The mass balance is the difference between ice and snow accumulation and ablation. A negative mass balance shows that the glacier is not in equilibrium with the local climate and is melting. WGMS refers to the observed melt rate and cumulative loss in glacier thickness as "extraordinary" and states that, based on accumulation area rate data, most of the glaciers are in strong and increasing imbalance with the climate and will continue to melt even without further warming. The cumulative mass loss of the world's glaciers was larger in the decade 2001–2010 than in any previous decade since records began.

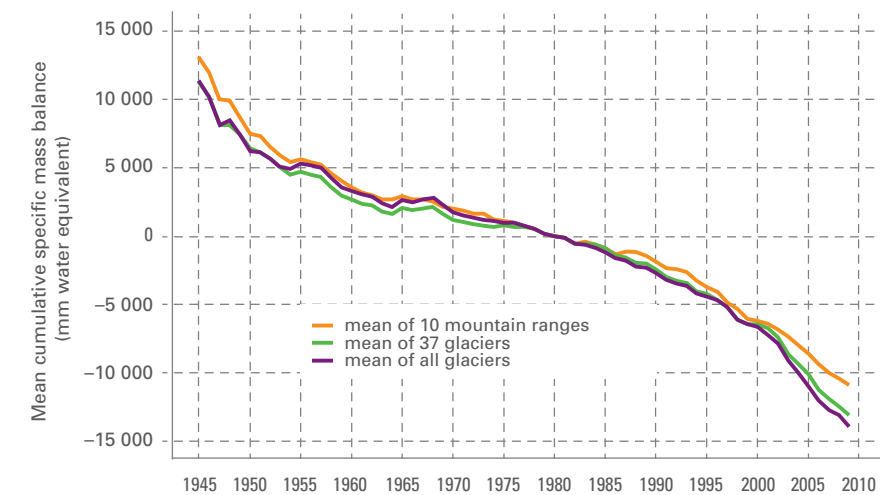
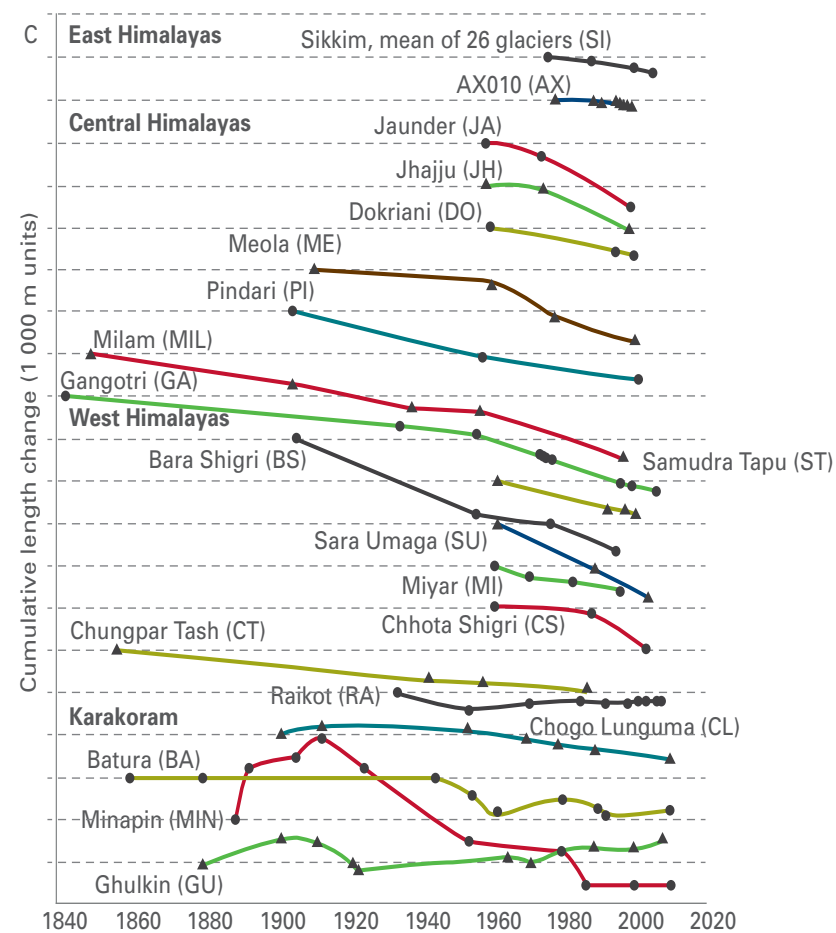


Figure 64. Mean cumulative specific glacier mass balance since 1945/1946 (source: WGMS)

Regional changes in glacier mass mostly reveal similar trends. Figure 65 is taken from Bolch et al. (2012) and shows that most Himalayan glaciers are losing mass at rates similar to glaciers elsewhere, except for emerging indications of stability or mass gain in the Karakoram.

Figure 65. Measured rates of change in glacier cumulative length measurements. The glacier retreat since the mid-19th century is obvious in the Himalayas, with the exception of the glaciers at Nanga Parbat in the north-west (RA, CL). Glaciers in the Karakoram show complex behaviour (source: T. Bolch et al., 2012).



Similar concerns exist for other regions. For example, Willis et al. (2012) report that the southern Patagonian ice field in southern South America is rapidly losing volume at many of the largest outlet glaciers and, in most cases, thinning extends to the highest elevations of the ice field. According to the Bavarian State Ministry of the Environment and Public Health report published in 2012, European glaciers have lost one-third of their volume and half their area since 1850.

Warming temperatures in these regions could preclude ice roads as a major form of northern transportation, thus creating a need for alternatives such as land-based road or rail networks – both enormously expensive in terms of capital costs and risky in terms of longevity, given that warming conditions in these regions are likely also to be affecting the underlying permafrost.

Effects of unseasonably mild conditions on the ice-road network and traditional lifestyles in northern Canada

(Adapted from Arctic Monitoring and Assessment Programme (AMAP), 2011: Snow, Water, Ice and Permafrost in the Arctic (SWIPA): Climate Change and the Cryosphere (Chapter 6). Oslo, Norway. xii + 538 pp.)

Many inhabitants of the Arctic depend on seasonal lake and river ice for access in winter to hunting, fishing and reindeer herding or trapping areas. Ice-based travel

also provides the principal transportation route for some isolated communities and industrial developments in northern latitudes. A winter ice-road network composed of a combination of private and public lake and river crossings, linking all-season road systems, communities and remote industrial and mining complexes, is important for parts of northern Canada, such as the Northwest Territories, where the public road system almost doubles during winter, or the vast territory of Nunavut, where there are no long-distance, all-season highways.

Changes in the duration of lake and river ice, thinner or less stable ice regimes, or mid-winter thaws create uncertainty, can be hazardous to the traveller and reduce the ability to follow traditional harvesting methods. Mild weather in March 2010, for example, caused the province of Manitoba, Canada, to close a 2 200-km winter road network composed of muskeg (bogland), lakes and rivers. The road system had deteriorated to the point of stranding numerous freight haulers and local drivers on thawed winter roads, necessitating emergency evacuations. Typically, the road carries more than 2 500 shipments each year to more than 30 000 First Nations people. In response to dwindling construction supplies, rising food and fuel prices, and a related rise in unemployment, First Nations Chiefs declared a state of emergency in 11 communities. Further, because of deteriorating conditions, approximately 600 km of the winter road system have been relocated to land since 2001 (Government of Manitoba, 2010) and spending on winter roads has tripled since 1999 (Government of Manitoba, 2009).

One winter road, over 600 km long between Tibbitt and Contwoyto in northern Canada includes over 495 km of frozen tundra, lakes and rivers. This road is critical

Figure 66. Ice roads in Canada (AMAP, 2011)

Figure 67. Truck on the ice road (source: BHP Billiton Canada Inc.)

for providing supplies to a number of mining centres and, in the two months per year when it is used (February and March) for a cost of some US\$ 10 million, it carries up to 8 000 truckloads per year, each weighing an average of 30 tonnes, with load capacity rising as the ice thickens and increases in bearing strength. It has been estimated to contribute significantly to the territorial and national annual economies, approximately US\$ 760 million and US\$ 330 million, respectively, in 2001, but rising significantly with enhanced northern development.

6.1.4 Snow cover

Snow and solid precipitation take many forms, e.g. sleet, snow, snowflakes, snow flurries, snow grains, snow pellets, hail and soft hail. Associated phenomena include snowstorms, blowing snow, blizzards and avalanches. Snow is important for climate. Wet snow and icing may affect the safety of constructions and transport, especially road, marine and air traffic.

The Global Snow Lab of Rutgers University, New Jersey, USA, produces climatology of snow cover in the northern hemisphere. There is high variability of this climate variable on decadal and yearly timescales (Figure 68). It is also possible to conclude that the boreal spring and summer snow cover exhibits negative trends from April to September. This negative trend in northern hemisphere snow cover has perhaps been the most prominent feature of its changes in the decade 2001–2010.

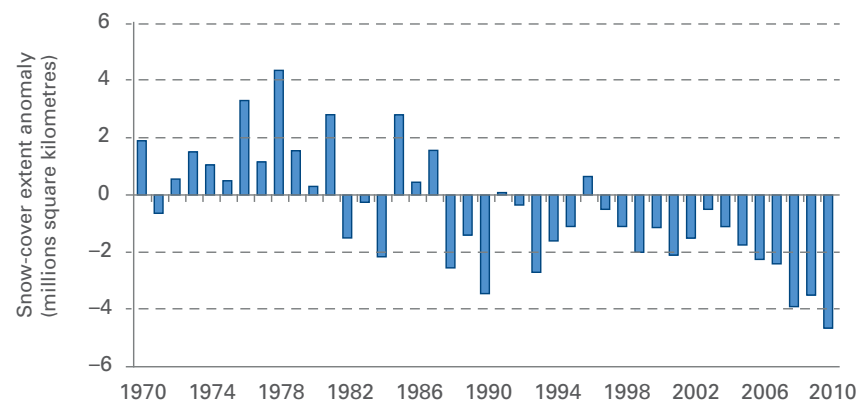


Figure 68. Northern hemisphere snow-cover anomaly for June (1970–2010) (data source: Rutgers University Global Snow Laboratory, USA).

Note: No similar data exist for the southern hemisphere as the land area subject to seasonal snow cover (outside the Antarctic) is very small.

6.1.5 Permafrost and frozen ground

Frozen ground has a temperature below 0°C. If it is frozen for two years or more, it is called permafrost. Permafrost is climatically important because it affects the carbon and hydrological cycles. Constructions on frozen soil and permafrost should take into account the possibility of reducing their bearing capacity. Significant developments in the observing system for permafrost and seasonally frozen ground were achieved during the International Polar Year 2007–2008. As Figure 69 shows, the past three decades have seen widespread increases in permafrost temperatures, with colder boreholes warming more rapidly at Alaskan, Canadian and Russian Federation sites. The 2000s are also characterized by an increase in the thickness of the seasonal thaw layer in the northern European part of the Russian Federation, north-eastern Siberia and Chukotka (Russian Federation), Spitsbergen (Norway) and Greenland.

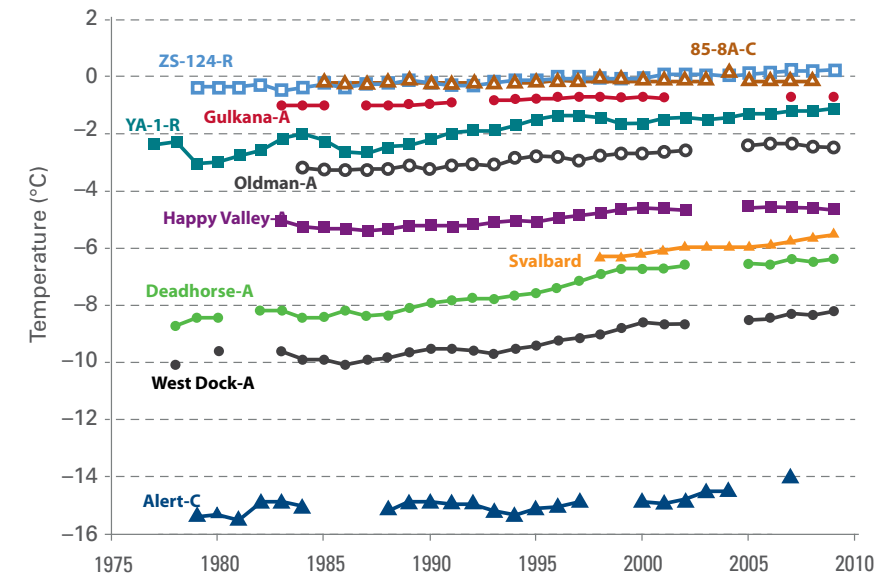


Figure 69. Time series of mean annual ground temperatures at depths between 10 m and 20 m for boreholes throughout the circumpolar northern permafrost regions: C - Canadian site; A - Alaskan site; R - Russian Federation site (source: Romanovskiy et al.)

6.2 Sea level

Global mean sea levels continued to rise over the decade 2001–2010. The observed rate of increase over the decade was about 3 mm/yr year, about double the observed 20th century trend of 1.6 mm/yr. Global sea levels averaged over the decade were about 20 cm higher than those of 1880 (Figure 70). Related to this, it is likely that there has been an increase in coastal high water (IPCC, 2012) owing to anthropogenic influences.

The rising trend in sea level was consistent over most of the decade, but with some short-term fluctuations, largely the result of ENSO and associated variability in global

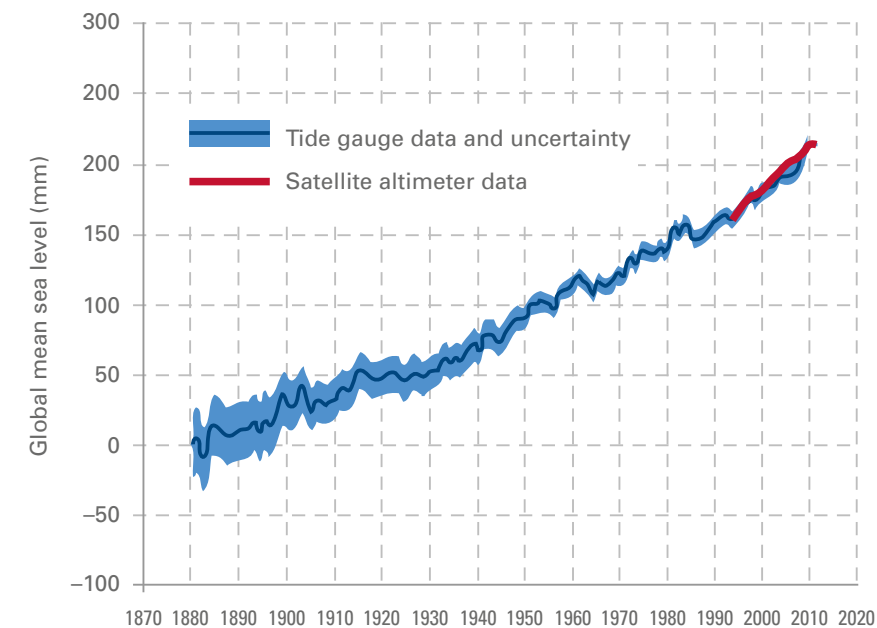
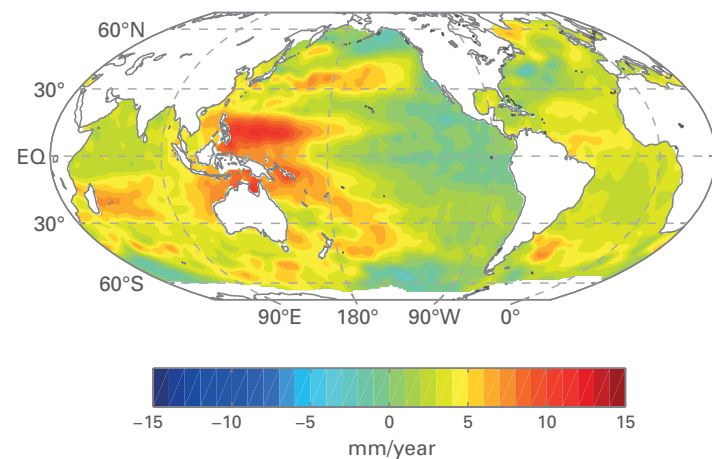


Figure 70. Global time series of sea-level anomalies (mm) from 1880 to 2010, using tide gauges (blue line, with uncertainty in blue shading) and from 1993 to 2011, using satellite altimetry (red line) (source: Commonwealth Scientific and Industrial Research Organisation (CSIRO), Australia: satellite data combined TOPEX/Poseidon, Jason-1 and Jason-2 (CSIRO), tide gauges (Church and White, 2011)).

ocean mass and temperatures. A strong ENSO event can result in global mean sea levels up to 5 mm higher (El Niño) or lower (La Niña) than the long-term trend value. As this equates to 1–2 years of “normal” global sea-level rise, it can result in temporary periods (up to a year or two in length) of weakly decreasing sea level during the transition from El Niño to La Niña (as occurred during 2010) or a strong acceleration of global sea-level rise during the decline of La Niña (as occurred during 2001).

ENSO also has a strong effect on the spatial distribution of sea level. During La Niña years, sea level in the western Pacific can be 10–20 cm above the decadal average, as a result of stronger easterly trade winds pushing warm, low-density water towards the west while, in the eastern Pacific, sea levels are lower than normal. The reverse applies during El Niño years. Trends of sea level over the period 1993–2010 (the period over which comprehensive, satellite-based, records of spatial variations are available) show strong upward trends – more than 10 mm/year in places – in parts of the western Pacific, and little or no trend in parts of the eastern Pacific, a difference which is largely attributable to interannual (El Niño/La Niña) and decadal (for example, the North Pacific Gyre Oscillation and the Pacific Decadal Oscillation) variability over this period (Figure 71).



The data quoted in this section are after removal of the seasonal cycle. There is an annual cycle of about 10 mm in global mean sea level, with the maximum in the northern hemisphere autumn (September–November) and the minimum in the northern hemisphere late winter and spring. This annual cycle exists partly because of the retention of water on land, in the form of snow, over the higher-latitude continents during winter (and its subsequent flowing into the ocean during spring and summer) and partly because of the strong annual cycle of SST (a driver of thermal expansion) in parts of the northern hemisphere oceans. Geological effects, such as post-glacial rebound of the land surface in some regions, are also excluded.

The main contributions to sea-level change in the 20th and 21st centuries are the following:

- Thermal expansion of the oceans (water expands as it warms);
- The addition of mass to the oceans from the melting of glaciers and ice caps in areas such as the Himalayas, Alaska and Patagonia;

- The exchange of mass with the ice sheets of the Antarctic and Greenland;
- The exchange of mass with terrestrial water storages (groundwater, aquifers, dams, lakes).

Since 1960, the thermal expansion of the oceans and the melting of glaciers and ice caps are the largest contributions to sea-level rise. There has also been an increasing contribution from surface melt from the Greenland ice sheet over this period. These contributions are directly related to recent climate change.

Indications of a larger contribution from the movement of outlet glaciers of both the Greenland and West Antarctic ice sheets have, however, been confirmed in the past decade. If this were a sign of acceleration in response to global warming, it would be a major concern, as the ice sheets contain enough water to raise sea level by 7 m and 6 m, respectively, and any such dynamic response could raise sea level significantly faster than surface melting alone. The impacts of sea-level rise will be felt through an increase in both mean sea level and the frequency of extreme sea-level events, for example, storm surges, of a given level. Impacts include increased flooding – both in severity and frequency – of low-lying areas, erosion of beaches, and damage to infrastructure and the environment, including wetlands, intertidal zones and mangroves, with significant impacts on biodiversity and ecosystem function.

Millions of people in low-lying nations such as Bangladesh, in the Mekong and other deltas, and Pacific islands such as Tuvalu, will have to respond to rising sea levels during the 21st century and beyond. Improved sea-level rise projections will contribute to more effective coastal planning and management. Adaptation measures include, for example, enhanced building codes, restrictions on where to build and developing infrastructure better able to cope with flooding.

Figure 71. Mean sea-level trend over the period 1993–2010 (mm/year), derived from satellite altimeter data (source: CSIRO)

CONCLUSION

This report summarizes the main climate features during the decade 2001–2010, combining the most up-to-date knowledge derived from global datasets, the findings in the WMO Annual Statements on the Status of the Global Climate and the results of a special WMO survey to which a large majority, 139 of the 191 Member States provided summaries which were used to assess the changing climate conditions and perform comparisons of temperature anomalies and their long-term behaviour in various regions. Important climate features are described in the six chapters of this report.

Temperature assessment shows most prominently the continued warming during 2001–2010, in particular the fact that it was the warmest decade starting with the digit 1 since the beginning of instrumental records, and it ended with the warmest year on record. Except for the year 2008, the remaining years, together with 1998, constitute the top 10 warmest years on record since 1850, the start of modern meteorological measurements. The decade was also the warmest on land, ocean and in the two hemispheres when taken separately in the assessment. Global annual surface temperature reached 14.54°C in 2010, +0.54°C above the 1961–1990 average. In terms of the magnitude of the warming relative to the beginning of the past 20th century, the global average temperature increased by 0.88°C during the decade.

The decade 2001–2010 was nearly 0.21°C warmer than the decade 1991–2000 which was 0.14°C warmer than 1981–1990, while the previous four decades in the period 1931–1970 showed nearly constant global decadal surface temperatures. This indicates that modern warming accelerated in the past four decades, 1971 to 2010.

Regional assessments provided, albeit at varying magnitudes, a predominant warming over all land areas on the continental scale. Europe (Greenland included) had the greatest warming, with a decadal temperature anomaly exceeding +1°C in 2001–2010. Another prominent result of the regional temperature assessment was that the coldest years of the decade were still above average in all continents except Australia, which recorded a negative temperature anomaly in a single year: 2001.

The WMO survey proposed a common approach to report on the state of the climate at national level during the decade and previously in order to reflect local climate-change reality with particular emphasis on temperature, precipitation and extreme events.

A prominent feature of the past global climate is that the decade 2001–2010 was the warmest globally since the beginning of instrumental records. At national level, this is reflected in a different way in terms of the number of countries reporting the decade as the warmest compared to previous decades. It shows that 2001–2010 was reported at the highest rate in the country datasets as the warmest decade compared with previous decades.

The WMO survey was also useful in assessing the nation-wide record values of maximum temperature, minimum temperature and 24-hour precipitation. The influence of global temperature increase on daily weather extremes at national level was reflected in the assessment of these record values, especially for the absolute daily maximum temperature and minimum temperature. The result of this assessment fits well with the IPCC findings (IPCC, 2012) on the upward tendency of hot days and downward tendency of cold nights.

A great part of the report was dedicated to extremes, covering their impacts on lives and goods and providing through statistics and case studies substantial information on extremes which were recorded worldwide. Disaster-related databases were useful in mapping by

disaster event and by region the type and impact of weather and climate extremes. It is still not yet possible to make a definite link between the increase in the observed losses with an increase in the frequency and intensity of extreme events. Other factors come into play, such as increased vulnerability and exposure of populations and the increase in the number of reports of disasters. Nevertheless, it is worthwhile to note a large increase of loss of life from heat conditions, particularly in two unprecedented extreme heatwaves that affected Europe in summer 2003 and the Russian Federation in summer 2010.

On the other hand, there were fewer deaths due to storms and floods in 2001–2010 compared with 1991–2000 figures, with a decrease of 16 per cent and 43 per cent, respectively. This is an encouraging indicator of the importance of weather warning systems against extreme meteorological and hydrological events which continuously improved over the decade.

There is a significant amount of data relevant to tropical cyclones which allowed some statistical analysis to be performed on long-term variations. In this respect, the report indicates below- to near-average cyclonic activity in 2001–2010 in all oceanic basins except the tropical Atlantic Basin, where the number of tropical cyclones was above average, and in the Australian and South Pacific Basin, where the number was significantly below average.

Due to the lack of complete datasets on several other types of extreme events, it was not possible to perform robust trend analysis. The lack of these datasets is currently being addressed by the WMO Commission for Climatology Expert Team on Definitions of Extreme Weather and Climate Events. The Team is working on a harmonized approach worldwide for better identification and assessment of these events.

Moreover, the Expert Team on Climate Change Detection and Indices has been working for several years on developing simple climate indices that can be derived from daily data to analyse the changes in the distribution characteristics related to key climate variables, i.e. temperature and precipitation (WCDMP No. 72).

Some climate conditions have been identified to be a consequence of large atmospheric and/or oceanic fluctuations such as ENSO (drought and floods in Australia and East Africa), AO and NAO (e.g. extreme conditions during the northern hemisphere winter 2009/2010). The report summarizes the past variation of these fluctuations and refers to their possible influence on extreme climate conditions in some of the case studies.

The highest value of the carbon dioxide mixing ratio recorded for at least the last 10 000 years was observed with a globally averaged value of 389 ppm by the end of the decade. The alarming increase in CO₂ concentration in the atmosphere indicates that human influence on the climate and its observed warming continued at an accelerated pace and contributed to the observed high-impact extremes by making some of them more devastating than they would have been had they occurred naturally. This conclusion has been recently supported by studies on the attribution of climate extremes.

The size of the Antarctic ozone hole has remained more or less stable since the early 1990s. Depending on the averaging period, the largest ozone holes during the decade were observed in 2000, 2003 and 2006. Reactive gases reached their highest levels at many stations in heatwave conditions. Atmospheric composition and climate data demonstrated two-way interactions: in the future, increasing temperatures, driven by an increase in the atmospheric content of greenhouse gases, could lead to the worsening of air quality in many regions of the world.

This report provides an analysis of the status of the cryosphere, including sea ice, ice sheets, glacier, snow cover and permafrost. Except for the southern hemisphere, where the causes of the observed slight increase in sea-ice extent have not yet been well established, the other components of the cryosphere, including Arctic sea ice, ice-sheet mass, snow cover and glaciers, indicated a clear, long-term downward trend, which was particularly pronounced in the northern hemisphere. The five lowest minimum Arctic sea-ice extents at the end of the melting season were all recorded in the second half of the decade with the record set in 2007. Consistent with these observations, the rate of temperature increase was particularly high in the northern latitudes of the northern hemisphere, with Greenland recording the largest decadal mean temperature anomaly of +1.71°C.

Sea-level rise was also addressed in this report. An average of 3 mm/yr of global sea-level rise is one of the main features of the decadal assessment. Averaged over the decade, global sea levels were about 20 cm higher than those of 1880. There were short-term, sea-level fluctuations, mainly owing to ENSO episodes.

Millions of people in low-lying nations such as Bangladesh, those in the Mekong and other deltas, and Pacific islands, such as Tuvalu, will have to respond to rising sea levels during the 21st century and beyond.

A way forward

Assessment of global warming is founded on multiple-year data analysis. A decade is the minimum possible time frame to detect temperature changes. Assessing the changes in the behaviour of extreme weather and climate events requires an even longer-term time frame because these events, by definition, do not happen frequently. It is important, therefore, to develop a more complete understanding of these events through enhanced data collection, data management and research. In this regard, the development of coherent and long-term, high-quality databases on extreme weather and climate events is one of the urgent requirements to which NMHSs need to pay increased attention.

Long-term cryosphere monitoring emerges as an urgent matter from both the science and application points of view. There are still uncertainties with respect to ice-sheet melting and how it will evolve. Understanding cryosphere variability will help improve sea-level rise projections, which will contribute to more effective coastal planning and management. Adaptation measures include, for example, enhanced building codes, restrictions on where to build and developing infrastructure better able to cope with flooding.

A promising new research area on the attribution of individual extreme events based on observational and model data is emerging. The aim of this research is to develop robust scientific knowledge and understanding of the extent to which natural climate variability and climate change are responsible for triggering or strengthening the individually observed high-impact extreme weather and climate events. It is therefore important to develop this area and use the outcomes of the research in the application world and it will be even more necessary as the Global Framework for Climate Services evolves into its operational phase in the next few years.

Acknowledgements

This publication was issued in collaboration with WMO Members and several international climate and meteorological institutions. Useful information was obtained from EM-DAT/CRED, FEWS-NET, UNISDR, OCHA and MunichRe. The scientific content was developed and reviewed by a number of international experts:

Enric Aguilar	University of Rovira i Virgili, Spain
Mansour Almazroui	Centre of Excellence for Climate Change Research King Abdulaziz University, Saudi Arabia
Peter Bissolli	Deutscher Wetterdienst, Germany
Stephan Bojinski	WMO
Geir Braathen	WMO
Manola Brunet	University of Rovira i Virgili, Spain
Jean-Louis Fellous	Committee on Space Research (International Council for Science (ICSU))
Barry Goodison	WMO
Sergey Gulev	Sea-Atmosphere Interaction and Climate Laboratory of the Russian Ac. Sci. Institute of Oceanology, Russian Federation
David Hargitt	CRED, Université catholique de Louvain, Belgium
Peer Hechler	WMO
Anahit Hovsepian	Armenian State Hydrometeorological and Monitoring Service
Hama Kontongomde	WMO
John Kennedy	Met Office, United Kingdom
Leslie Malone	WMO
Antonio Mestre	Agencia Estatal de Meteorología, Spain
D.R. Pattanaik	Indian Meteorological Department, India
Vladimir Ryabinin	World Climate Research Programme, WMO
Ahira Sanchez Lugo	NOAA-NCDC, USA
Serhat Sensoy	Turkish State Meteorological Service, Turkey
Julio Serje	UNISDR
Adrian Simmons	ECMWF
Robert Stefanski	WMO
José Luis Stella (input coordinator)	Servicio Meteorológico Nacional, Argentina
Peter Stott	Met Office, United Kingdom
Oksana Tarasova	WMO
Natalia Tilinina	Sea-Atmosphere Interaction and Climate Laboratory of the Russian Ac. Sci. Institute of Oceanology
Blair Trewin (scientific review leader)	Bureau of Meteorology, Australia
Sachiko Tsuji	FAO
Axel von Engel	EUMETSAT
Angelika Wirtz	Geo Risks Research/Corporate Climate Centre, MunichRe, Germany

WMO Secretariat coordination:
 Observing and Information System Department, WMO, Geneva, Switzerland
 Omar Baddour, Chief of Division, WMO
 Karolin Eichler, Professional Officer, WMO

References and bibliography

Almazroui M., 2013: Simulation of Present and Future Climate of Saudi Arabia Using a Regional Climate Model (PRECIS). *International Journal of Climatology*, DOI: 10.1002/joc.3721.

AMAP, 2011: *Snow, Water, Ice and Permafrost in the Arctic (SWIPA): Climate Change and the Cryosphere*. Arctic Monitoring and Assessment Programme, Oslo, Norway. xii + 538 pp.

Antarctic Climate Change and the Environment, SCAR, 2009:
<http://www.scar.org/publications/occasional/acce.html>

Bayerische Gletscher im Klimawandel – ein Statusbericht, Bavarian State Ministry of the Environment and Public Health.

Bolch, T., A., Kulkarni, A., Kääh, C. Huggel, F. Paul, J.G. Cogley, H. Frey, J.S. Kargel, K. Fujita, M. Scheel, S. Bajracharya, M. Stoffel, 2012: The State and Fate of Himalayan Glaciers. *Science*, 336, 310 (2012), DOI: 10.1126/science.1215828.

Brasseur, G.P., 2009: Implications of climate change for air quality, *WMO Bulletin*, 58(1), 10-15.

Butler, R.A., 2012: Climate Change and the Amazon Rainforest. *Mongabay.com/A Place Out of Time: Tropical Rainforests and the Perils They Face*. 7 November 2012. http://http://rainforests.mongabay.com/amazon/amazon_climate_change.html

Chhetri, P., A. Hashemi, F. Basic, A. Manzoni and G. Jayatilleke, 2012: Bushfire, Heat Wave and Flooding – Case Studies from Australia. Report from the International Panel of the WEATHER project funded by the European Commission's 7th framework programme. Melbourne.

Church, J.A. and N.J. White, 2011: Sea-level rise from the late 19th to the early 21st century. *Surveys in Geophysics*, 32, 585-602, doi:10.1007/s10712-011-9119-1

Climate Change Monitoring Report 2010. Japan Meteorological Agency, 2011.

Climate Sense, 2009, WMO

Derksen, C. and R. Brown, 2011: *Snow, Arctic Report Card: Update for 2011*

Fahey, D.W. and M.I. Hegglin, (coordinating lead authors), 2011: *Twenty Questions and Answers About the Ozone Layer: 2010 Update, Scientific Assessment of Ozone Depletion: 2010*, WMO, Geneva, Switzerland, 72 pp.

GAR, 2011: *Global Assessment Report on Disaster Risk Reduction 2011: Revealing Risk, Redefining Development*, UNISDR.

GAW Report No.199

Global Observing Strategy Cryosphere Theme report, August 2007, WMO/TD-No. 1405

IPCC, 2012: *Managing the Risks of Extreme Events and Disasters to Advance Climate Change Adaptation. A Special Report of Working Groups I and II of the Intergovernmental Panel on Climate Change*. C.B. Field, V. Barros, T.F. Stocker, D. Qin, D.J. Dokken, K.L. Ebi, M.D. Mastrandrea, K.J. Mach, G.-K. Plattner, S.K. Allen, M. Tignor and P.M. Midgley (eds.). Cambridge University

Press, Cambridge, United Kingdom and New York, NY, USA, 582 pp.

IPCC Fourth Assessment Report (IPCC-AR4)

Islam, M.N. and M. Almazroui, 2012: Direct effects and feedback of desert dust on the climate of the Arabian Peninsula during the wet season: a regional climate model study. *Climate Dynamics*, 39(9-10): 2239-2250, DOI: 10.1007/s00382-012-1293-4.

Joughin, I. and R.B. Alley, 2011: Stability of the West Antarctic ice sheet in a warming world, *Nature Geoscience*, 4, 506–513 (2011), doi:10.1038/ngeo1194.

Kunkel, K.E., R.A. Pielke Jr. and S.A. Changnon, 1999: Temporal fluctuations in weather and climate extremes that cause economic and human health impacts: A review. *BAMS*, 80:1077–1098.

Manny, G.L., M. Santee et al., 2011: Unprecedented Arctic ozone loss in 2011. *Nature*, 478, 469–475, doi:10.1038/nature10556.

Milojevic A. et al., January 2012: Health effects of flooding in rural Bangladesh. *Epidemiology*.

Ordóñez, C., N. Elguindi, O. Stein, V. Huijnen, J. Flemming, A. Inness, H. Flentje, E. Katragkou, P. Moinat, V.-H. Peuch, A. Segers, V. Thouret, G. Athier, M. van Weele, C.S. Zerefos, J.-P. Cammas and M.G. Schultz, 2010: Global model simulations of air pollution during the 2003 European heatwave. *Atmos. Chem. Phys.*, 10, 789–815.

Perkins, S. and L. Alexander, 2013: On the measurement of heatwaves. *Journal of Climate* (in press).

Peterson et al., July 2012: Explaining Extreme Events of 2011 from a Climate Perspective, *BAMS*, July 2012

PONJA, 2008: *Post-Nargis Joint Assessment Report* http://www.mm.undp.org/UNDP_Publication_PDF/PONJA%20full_report.pdf

Queensland University of Technology (QUT), 2010: *Impacts and adaptation response of infrastructure and communities to heatwaves: the southern Australian experience of 2009*. Report for the National Climate Change Adaptation Research Facility.

Richter-Menge, J. and J.E. Overland (eds.), 2010: *Arctic Report Card 2010*.

Rignot, E., I. Velicogna, M.R. van den Broeke, A. Monaghan and J. Lenaerts, 2011: Acceleration of the contribution of the Greenland and Antarctic ice sheets to sea level rise. *Geophysical Research Letters*, 38, L05503, doi:10.1029/2011GL046583.

Rodriguez-Llanes, J.M. et al., November 2011: Child malnutrition and recurrent flooding in rural eastern India: a community-based survey. *BMJ Open*.

Romanovsky, V.E., S.L. Smith, H.H. Christiansen, N.I. Shiklomanov, D.S. Drozdov, N.G. Oberman, A.L. Kholodov and S.S. Marchenko, 2011: *Permafrost, Snow, Arctic Report Card: Update for 2011*, NOAA.

Romanovsky, V.E., S.L. Smith and H.H. Christiansen, 2010: Permafrost Thermal State in the Polar Northern Hemisphere during the International Polar Year 2007–2009: a Synthesis. *Permafrost and Periglacial Processes*, 21: 106–116, Wiley online Inter Science(www.interscience.wiley.com) DOI: 10.1002/ppp.689

Second Report on the Adequacy of the Global Observing Systems for Climate in support of the UNFCCC, 2003. WMO/TD No. 1143

State of the Climate in 2010: Special supplement to BAMS, 92, 6, June 2011.

Stott et al., 2012: Attribution of Weather and Climate-related Events, <http://www.wcrp-climate.org/conference2011/documents/Stott.pdf>

Thompson, D.W.J., S. Solomon et al., 2011: Signatures of the Antarctic ozone hole in Southern Hemisphere surface climate change. *Nature Geoscience*, 4, 741–749, doi:10.1038/ngeo1296

UNEP, 2009: Learning from Cyclone Nargis: A Case Study.

Willis, M.J., A.K. Melkonian, M.E. Pritchard and A.Rivera, 2012: Ice loss from the Southern Patagonian Ice Field, South America, between 2000 and 2012. *Geophysical Research Letters*, 39, L17501, doi:10.1029/2012GL053136.

World Data Centre for Greenhouse Gases (WDCGG) Data Summary No.36, 2011.

WGMS, 2011: Zemp, M., S.U. Nussbaumer, I. Gärtner-Roer, M. Hoelzle, F. Paul, and W. Haeberli, (eds.): *Glacier Mass Balance Bulletin No. 11 (2008–2009)*. ICSU(WDS)/IUGG(IACS)/UNEP/UNESCO/WMO, World Glacier Monitoring Service, Zurich, Switzerland, 102 pp.

WMO, 2009: Guidelines on analysis of extremes in a changing climate in support of informed decisions for adaptation. WCDMP No. 72.

WMO, 2006: Drought monitoring and early warning: concepts, progress and future challenges (WMO-No. 1006).

WMO Greenhouse Gas Bulletin, No.7, 2011

WMO Statements on the Status of the Global Climate (<http://www.wmo.int/wcdmp>)

WMO, 2010: Assessment of the observed extreme conditions during the 2009/2010 boreal winter. WMO/TD-No. 1550.

WMO, 2012: Atlas of health and climate (WHO/WMO)

Global surface temperature datasets were obtained from:

Met Office Hadley Centre and Climatic Research Unit, University of East Anglia, United Kingdom: www.hadobs.org and www.cru.uea.ac.uk

NOAA-National Climatic Data Center, USA: www.ncdc.noaa.gov

NASA-Goddard Institute for Space Studies, USA: <http://data.giss.nasa.gov/gistemp/>
Country climate summaries from the National Meteorological and Hydrological Services responding to a WMO Survey

Global annual climate reports, WMO Statements on the Status of the Global Climate (2001–2010 series)

Other data were obtained from:

Bulletin of the American Meteorological Society (BAMS) <http://www.ametsoc.org/pubs/bams/>

Climate Prediction Center, USA (El Niño/La Niña, Arctic Oscillation, North Atlantic Oscillation): www.cpc.ncep.noaa.gov

Commonwealth Scientific and Industrial Research Organization, Australia <http://www.csiro.au/>

ECMWF ERA-Interim reanalysis

EM-DAT: OFDA/CRED International Disaster Database – www.emdat.be – Université catholique de Louvain – Brussels, Belgium.

FEWS-NET: Famine Early Warning System Network (USAID)

Global Precipitation Climatology Centre, Deutscher Wetterdienst, Germany: <http://gpcc.dwd.de>
(For detailed information on the generation of these products, please visit: http://www.dwd.de/bvbw/generator/DWDWWW/Content/Oeffentlichkeit/KU/KU4/KU42/en/Reports_Publications/GPCC_intro_products_2011,templateId=raw,property=publicationFile.pdf/GPCC_intro_products_2011.pdf)

<http://climate.rutgers.edu/snowcover/index.php> (snow-cover data)

National Climate Centre, Australian Bureau of Meteorology (El Niño/La Niña, Indian Ocean Dipole): www.bom.gov.au/climate

NOAA Earth System Research Laboratory, Physical Sciences Division (NCEP/NCAR Reanalysis Project) <http://www.esrl.noaa.gov/psd/data/reanalysis/reanalysis.html>

NOAA-NCDC, USA: www.ncdc.noaa.gov

The global gridded precipitation anomalies (Chapter 2) were computed on a station-by-station basis and then averaged into a 5°x 5° grid. The global precipitation average was computed by averaging the grid boxes across the globe using cosine weighting. Additional info can be found at: <http://www.ncdc.noaa.gov/temp-and-precip/ghcn-gridded-products.php>

National Snow and Ice Data Center, USA (sea ice): www.nsidc.org

UNISDR: <http://www.unisdr.org/>

WMO Global Atmosphere Watch Programme

Acronyms

AAO	Antarctic Oscillation	LOSU	level of scientific understanding
AGGI	Annual Greenhouse Gas Index (NOAA), USA	MERRA	Modern-Era Retrospective Analysis for Research and Applications (NASA-GSFC)
AMAP	Arctic Monitoring and Assessment Programme	MunichRe	Munich Reinsurance Company (www.munichre.com)
AO	Arctic Oscillation	NAO	North Atlantic Oscillation
AOD	aerosol optical depth	NASA	National Aeronautics and Space Administration (USA)
BAMS	Bulletin of the American Meteorological Society	NCAR	National Center for Atmospheric Research (NOAA)
CCI	Commission for Climatology (WMO)	NCDC	National Climatic Data Center (NOAA)
CFC	chlorofluorocarbon	NCEP	National Centers for Environmental Prediction (NOAA)
CFSR	Climate Forecast System Reanalysis (NCEP)	NHC	National Hurricane Center (NOAA)
CRED	Centre for Research on the Epidemiology of Disasters	NMHS	National Meteorological and Hydrological Service (WMO)
CSIRO	Commonwealth Scientific and Industrial Research Organization	NOAA	National Oceanic and Atmospheric Administration (USA)
CSM	Climate System Monitoring	NSIDC	National Snow and Ice Data Center, USA
DLR	German Aerospace Centre	OCHA	United Nations Office for the Coordination of Humanitarian Affairs
DMI	Danish Meteorological Institute	OECD	Organization for Economic Cooperation and Development
DOE	Department of Energy (USA)	OFDA	Office of Foreign Disaster Assistance (USA)
DU	Dobson Unit	PDNA	Post Disaster Needs Assessment
DWD	Deutscher Wetterdienst (Germany)	PONJA	Post Nargis Joint Assessment
ECMWF	European Centre for Medium-Range Weather Forecasts	ppb	parts per billion
ECVs	essential climate variables (GCOS)	ppm	parts per million
EF	Enhanced Fujita (Scale)	ppt	parts per trillion
EM-DAT	Emergency Events Database	PSC	polar stratospheric cloud
ENSO	El Niño/Southern Oscillation	PSD	Physical Sciences Division (ESRL)
ESRL	Earth System Research Laboratory (NOAA)	RF	radiative forcing
ETD	expected time of departure	SAM	Southern Annular Mode
FAO	Food and Agriculture Organization of the United Nations	SCIAMACHY	Scanning Imaging Absorption Spectrometer for Atmospheric Chartography
FEWS-NET	Famine Early Warning System Network (USAID)	SOI	Southern Oscillation Index
GAR	Global Assessment Report on Disaster Risk Reduction (UNISDR)	SST	sea-surface temperature
GAW	Global Atmosphere Watch (WMO)	UNEP	United Nations Environment Programme
GCOS	Global Climate Observing System	UNISDR	United Nations Strategy for Disaster Risk Reduction
GCW	Global Cryosphere Watch (WMO)	USAID	United States Agency for International Development
GDP	Gross Domestic Product	USGS	US Geological Survey
GFCs	Global Framework for Climate Services	WCDMP	World Climate Data and Monitoring Programme (WMO)
GFDRR	Global Facility for Disaster Reduction and Recovery	WDCGG	World Data Centre for Greenhouse Gases
GHG	greenhouse gas	WGMS	World Glacier Monitoring Service
GISS	Goddard Institute for Space Studies (NASA)	WHO	World Health Organization
GOME	Global Ozone Monitoring Experiment	WMO	World Meteorological Organization
GPCC	Global Precipitation Climatology Centre, Germany	WRF	Weather research and forecasting model
GRACE	Gravity Recovery and Climate Experiment (NASA-DLR)		
GSFC	Goddard Space Flight Center		
HCFC	hydrochlorofluorocarbon		
HFC	hydrofluorocarbon		
IBTraCS	International Best Track Archive for Climate Stewardship (NOAA), USA		
IDMC	Internal Displacement Monitoring Centre, Switzerland		
IOD	Indian Ocean Dipole		
IPCC	Intergovernmental Panel on Climate Change (WMO-UNEP)		
JAMASTECC	Japan Agency for Marine-Earth Science and Technology		
JMA	Japan Meteorological Agency		
LASG	State Key Laboratory of Numerical Modeling for Atmospheric Sciences and Geophysical Fluid Dynamics, China		
LLGHG	long-lived greenhouse gas		

Glossary

“Hurricane”, “cyclone” and “typhoon” are different terms for the same weather phenomenon which is accompanied by torrential rain and maximum sustained wind speeds (near centre) exceeding 119 km/h.

In the western North Atlantic, central and eastern North Pacific, Caribbean Sea and Gulf of Mexico, such a weather phenomenon is called a “hurricane”. In the western North Pacific, it is called a “typhoon”. In the Bay of Bengal and Arabian Sea, it is called a “cyclone”. In the western South Pacific and south-east Indian Ocean, it is called a “severe tropical cyclone”. In the south-west Indian Ocean, it is called a “tropical cyclone”.
(source: WMO fact sheet)

There is no one definition for a heatwave. An example is given in Kunkel et al., 1999: “Heatwaves are defined as warm periods of at least four days with an average temperature exceeding the threshold for a one-in-ten-year occurrence.”

WMO climatological standard normals are averages of climatological data computed for the following consecutive periods of 30 years: 1 January 1901 to 31 December 1930, 1 January 1931 to 31 December 1960, etc. (WMO Technical Regulations). WMO publishes the climatological standard normals which are computed by Members for their observing stations. The latest updates of the WMO standard normals consist of averages computed over 1961–1990 period (Climatological Normals (CLINO), WMO-No. 847).

Definitions (UNISDR)

Climatological disasters: heatwave, cold wave, wildfire, drought

Hydrological disasters: river flood, flash flood, storm surge, mass movement wet (landslide)

Meteorological disasters: tropical storm, winter storm, local storm, severe weather, hail, tornado

Geophysical disasters: earthquake, volcanic eruption

A **hazard** is a physical event, phenomenon or human activity that can cause the loss of life or injury, property damage, social and economic disruption or environmental degradation. Hazards have different origins: natural (geological, hydrological, meteorological and biological) or due to human actions (environmental or technological).

Disasters are a combination of hazards, conditions of vulnerability and insufficient capacity or measures to reduce the negative consequences of risk. A hazard becomes a disaster when it coincides with a vulnerable situation, when societies or communities are unable to cope with it with their own resources and capacities.

Vulnerability is the degree to which someone or something can be affected by a particular hazard and depends on a number of factors and processes:

- Physical (unstable locations; closer proximity to hazards; fragile, unprotected houses);

- Economic (no productive assets, limited income-earning opportunities, poor pay, single income revenue, no savings or insurance);
- Social (low status in society, gender relations, fewer decision-making possibilities, oppressive formal and informal institutional structures, and political, economic and social hierarchies);
- Psychological (fears instigated by religious and other belief systems, ideologies, political pressures, mental illness);
- Physiological (status in life – young, old, adolescent, pregnant, lactating mothers, chronic illness, disability, exposure to sexual violence and harassment, HIV/Aids and other infections).

Risk is the probability of harmful consequences or expected losses (deaths, injuries, property, livelihoods, economic activity disrupted or environment damaged) resulting from interactions between natural or human-induced hazards and vulnerable populations.

Annex 1. Source and methodology for global surface-temperature assessment

Global average temperature records are essential to help understand how the climate is changing. To understand changes and variations in the climate, it is essential to know how the surface temperature changes – from month to month up to decade to decade. Global average temperature records provide this vital information. From these records it can be seen how warm specific months, years or decades are, and trends can be discerned in the climate system over longer periods of time. The global surface temperature assessment is based on the instrumental records of the air temperature measured at 1.25 to 2 m above the surface level on the land. Sea-surface temperature measurements are recorded by various observation platforms, including ships and buoys. The annual assessment is based on these measurements after they have been quality-controlled to filter data errors and homogenized. Data from the following four centres, which maintain global climate datasets and calculate global average temperature and related anomalies on monthly and annual timescales were used:

- Met Office, United Kingdom, in collaboration with the Climatic Research Unit at the University of East Anglia, United Kingdom;
- National Climatic Data Center, NOAA, USA;
- Goddard Institute for Space Studies, NASA, USA;
- European Centre for Medium-Range Weather Forecasts.

The development of climate datasets is based on the following:

- Routinely disseminated daily and monthly weather and climate observations by the National Meteorological and Hydrological Services of WMO's 191 Members following:
- WMO standards for data collection, quality control and exchange;
- Historical climate records dating back to 1850, including those available from marine climate summaries;
- Recovered old climate records worldwide as part of continuous data-rescue efforts promoted by WMO and its Members;
- Peer-reviewed scientific methods for quality-control, homogenization and interpolation to constitute high-quality global climate datasets.

Temperature anomalies

Absolute temperatures are not used directly to calculate the global average temperature. They are first converted into anomalies, which are the difference in temperature from the normal level. The normal level is calculated for each observation location by taking the long-term average for that area over a base period. One of the main reasons for using anomalies is that they remain fairly constant over large areas. The anomaly method also helps to avoid biases. For example, if actual temperatures were used and information from an Arctic observation station were missing for that month, the global temperature record would seem warmer. When anomalies are used, such missing data will not bias the temperature record.

Accuracy of the observations

Each observation station follows international standards for taking observations set out by WMO. Each National Meteorological Service provides reports on how its data are collected and processed to ensure consistency. This includes recording information about the local environment around the observation station and any changes to that environment. This is important for ensuring the required data accuracy and performing homogeneity tests and adjustments. There are additional uncertainties because temperatures over large areas of the Earth are not observed as a matter of routine. These elements are taken into account by factoring the uncertainty into global average temperature calculations, thereby producing a temperature range rather than one definite figure.

Annex 2. Country survey – general information

For this publication a survey was made by WMO. It was sent out to all its 191 Members and contained the request for the following data:

- The highest national decadal maximum temperature for the last decade and, if available, for the decades before
- The highest national decadal minimum temperature for the last decade and, if available, for the decades before
- The lowest national decadal maximum temperature for the last decade and, if available, for the decades before
- The lowest national decadal minimum temperature for the last decade and, if available, for the decades before
- The highest national decadal 24-h precipitation for the last decade and, if available, for the decades before
- The decadal mean temperature and its anomaly with respect to 1961–1990 for the last decade and, if available, for the decades before
- The annual mean temperature of each of the last 10 years (2001–2010) and its anomaly with respect to 1961–1990
- The three most severe extreme events which occurred during the last decade and their impact

To complete the survey, it was suggested that the following recommendations be taken into account:

1. To use stations with the same period of observations and a good geographical distribution;
2. To compute from these stations the annual series of mean temperature and their anomaly with respect to the 1961–1990 reference period, which is the period used for computing the current WMO standard normals;
3. To calculate the decadal averages of these two quantities for each station;
4. To include the averages over the stations of the result found in 3. above.

If another method was used to compute these averages, Members were requested to indicate and explain.

A total of 139 of WMO's 191 Members responded to the survey. A list is given in Annex 3. As not every Member was able to provide all the requested information, the actual sample size used is provided with each assessment.

Regional averages were calculated with respect to geographical regions.

Annex 3: Country data submission to the WMO survey

Algeria	Office National de la Météorologie
Angola	Instituto Nacional de Hidrometeorología e Geofísica
Argentina	Servicio Meteorológico Nacional
Armenia	Armenian State Hydrometeorological and Monitoring Service
Australia	Bureau of Meteorology
Austria	Central Institute for Meteorology and Geodynamics
Azerbaijan	National Hydrometeorological Department
Bahrain	Bahrain Meteorological Service
Bangladesh	Bangladesh Meteorological Department
Belarus	Department of Hydrometeorology
Belgium	Royal Meteorological Institute of Belgium
Benin	Service Météorologique National
Bhutan	Department of Hydromet Services
Bolivia,	Servicio Nacional de Meteorología e Hidrología
Plurinational State of	
Bosnia	Federal Hydrometeorological Institute
and Herzegovina	
Botswana	Botswana Meteorological Services
Brazil	Instituto Nacional de Meteorologia
British	Cayman National Weather Service
Caribbean Territories	
Burkina Faso	Direction de la Météorologie
Burundi	Institut Géographique du Burundi
Canada	Environment Canada
Chad	Direction de la Météorologie Nationale
Chile	Dirección Meteorológica de Chile
China	China Meteorological Administration
Colombia	Instituto de Hidrología, Meteorología y Estudios Ambientales
Congo	Direction de la Météorologie
Costa Rica	Instituto Meteorológico Nacional
Côte d'Ivoire	SODEXAM / Direction de la Météorologie Nationale
Croatia	Meteorological and Hydrological Service
Cyprus	Meteorological Service
Czech Republic	Czech Hydrometeorological Institute
Democratic Republic	Agence Nationale de Météorologie et de Télédétection par Satellite
of the Congo	
Denmark	Danish Meteorological Institute
Dominican Republic	Oficina Nacional de Meteorología
Ecuador	Instituto Nacional de Meteorología e Hidrología
Egypt	The Egyptian Meteorological Authority
El Salvador	Ministerio de Medio Ambiente y Recursos Naturales, Observatorio Ambiental
Estonia	Estonian Meteorological and Hydrological Institute
Ethiopia	National Meteorological Agency
Finland	Finnish Meteorological Institute
France	Météo-France
French Polynesia	Météo-France
Gabon	Direction de la Météorologie Nationale
Gambia (the)	Department of Water Resources
Georgia	The National Environmental Agency

Germany	Deutscher Wetterdienst
Greece	Hellenic National Meteorological Service
Guinea	Direction Nationale de la Météorologie
Guinea-Bissau	Instituto Nacional de la Meteorología
Guyana	Hydrometeorological Service
Hong Kong, China	Hong Kong Observatory
Hungary	Országos Meteorológiai Szolgálat (Hungarian Meteorological Service)
Iceland	Icelandic Meteorological Office
India	India Meteorological Department
Indonesia	Meteorological, Climatological and Geophysical Agency
Iran, Islamic Republic of	Islamic Republic of Iran Meteorological Organization
Iraq	Iraqi Meteorological Organization
Ireland	The Irish Meteorological Service
Israel	Israel Meteorological Service
Italy	USAM - CNMCA
Japan	Japan Meteorological Agency
Jordan	Jordan Meteorological Department
Kazakhstan	Kazhydromet
Kenya	Kenya Meteorological Department
Kuwait	Department of Meteorology
Kyrgyzstan	Agency on Hydrometeorology (Ministry of Emergency situations of the Kyrgyz Republic)
Latvia	Latvian Environment, Geology and Meteorology Agency
Lebanon	Département de la Météorologie (Direction Générale de l'Aviation Civile)
Lesotho	Lesotho Meteorological Service
Libya	Libyan National Meteorological Center
Lithuania	Lithuanian Hydrometeorological Service
Luxembourg	Service de la météorologie et de l'hydrologie
Macao, China	Macao Meteorological and Geophysical Bureau
Madagascar	Direction de la Météorologie et de l'Hydrologie
Malawi	Malawi Meteorological Service
Malaysia	Malaysian Meteorological Department
Maldives	Maldives Meteorological Service
Mali	Direction Nationale de la Météorologie
Malta	Malta Airport Met Office
Mauritius	Mauritius Meteorological Services
Mexico	Servicio Meteorológico Nacional
Monaco	Direction de l'environnement
Mongolia	Institute of Meteorology, Hydrology and Environment
Montenegro	Hydrometeorological Institute
Morocco	Direction de la Météorologie Nationale
Mozambique	Instituto Nacional de Meteorologia
Namibia	Namibia Meteorological Services
Netherlands (the)	Royal Netherlands Meteorological Institute
New Caledonia	Météo-France NC
New Zealand	National Institute of Water and Atmospheric Research
Niger	Direction de la Météorologie Nationale

Nigeria	Nigerian Meteorological Agency
Niue	Niue Meteorological Service
Norway	Norwegian Meteorological Institute
Oman	Directorate General of Meteorology and Air Navigation
Pakistan	Pakistan Meteorological Department
Peru	National Service of Meteorology and Hydrology of Peru
Poland	Institute of Meteorology and Water Management
Portugal	Instituto de Meteorologia
Qatar	Department of Meteorology, Civil Aviation Authority
Republic of Korea	Korea Meteorological Administration
Republic of Moldova	State Hydrometeorological Service
Romania	National Meteorological Administration
Russian Federation	Russian Research Institute of Hydrometeorological Information
Rwanda	Rwanda Meteorological Service
Saudi Arabia	Presidency of Meteorology and Environment and Centre of Excellence for Climate Change Research, King Abdul-Aziz University
Senegal	Direction de la Météorologie Nationale
Serbia	Republic Hydrometeorological Service
Seychelles	Seychelles Meteorological Service
Singapore	Meteorological Services Division (National Environment Agency)
Slovakia	Slovak Hydrometeorological Institute
Slovenia	Environmental Agency of the Republic of Slovenia
South Africa	South African Weather Service
South Sudan	South Sudan Meteorological Department
Spain	Agencia Estatal de Meteorología
Sri Lanka	Department of Meteorology
Sudan	Sudan Meteorological Authority
Swaziland	Swaziland Meteorological Service
Sweden	Swedish Meteorological and Hydrological Institute
Switzerland	Federal Office of Meteorology and Climatology
Thailand	Meteorological Department
The former Yugoslav Republic of Macedonia	Hydrometeorological Institute
Tonga	Tonga Meteorological Service
Trinidad and Tobago	Trinidad and Tobago Meteorological Services
Tunisia	Institut National de la Météorologie
Turkey	Turkish State Meteorological Service
Turkmenistan	Administration of Hydrometeorology
Uganda	Department of Meteorology
Ukraine	Ukrainian Hydrometeorological Centre
United Arab Emirates	National Centre of Meteorology and Seismology
United Kingdom	MetOffice
United Republic of Tanzania	Tanzania Meteorological Agency
Uruguay	Dirección Nacional de Meteorología
USA	National Oceanic and Atmospheric Administration
Uzbekistan	Uzhydromet
Venezuela, Bolivarian Republic of	Servicio de Meteorología de la Aviación

Yemen
Zambia
Zimbabwe

Yemen Meteorological Service
Zambia Meteorological Department
Zimbabwe Meteorological Services Department

For more information, please contact:
World Meteorological Organization

Observing and Information Systems Department
Tel.: +41 (0) 22 730 82 14 – Fax: +41 (0) 22 730 80 21
E-mail: wcdmp@wmo.int – Website: www.wmo.int

7 bis, avenue de la Paix – P.O. Box 2300 – CH 1211 Geneva 2 – Switzerland

JN 13657